AGARD-CP-488

AGARD-CP-488

AGARD

ADVISORY GROUP FOR AEROSPACE RESEARCH & DEVELOPMENT

7 RUE ANCELLE 92200 NEUILLY SUR SEINE FRANCE

AGARD CONFERENCE PROCEEDINGS No.488

Electronic Counter-Counter Measures for Avionics Sensors and Communication Systems

(Les Contre-Contremesures Electroniques pour les Capteurs d'Avionique et les Systèmes de Télécommunications)

NORTH ATLANTIC TREATY ORGANIZATION

DISTRIBUTION AND AVAILABILITY ON BACK COVER

NORTH ATLANTIC TREATY ORGANIZATION

ADVISORY GROUP FOR AEROSPACE RESEARCH AND DEVELOPMENT

(ORGANISATION DU TRAITE DE L'ATLANTIQUE NORD)

AGARD Conference Proceedings No.488

Electronic Counter-Counter Measures for Avionics Sensors and Communication Systems

(Les Contre-Contremesures Electroniques pour les Capteurs d'Avionique et les Systèmes de Télécommunications)

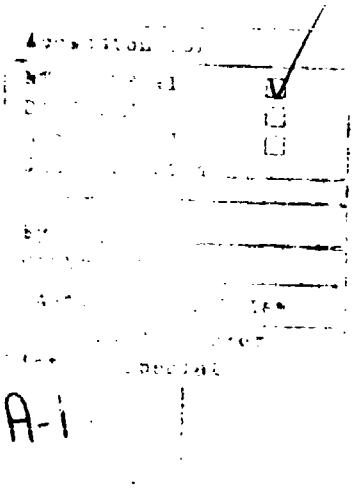

Papers presented at the Avionics Panel Symposium held in Ottobrunn, Germany, from 1st to 5th October 1990.

The Mission of AGARD

According to its Charter, the mission of AGARD is to bring together the leading personalities of the NATO nations in the fields of science and technology relating to aerospace for the following purposes:

- Recommending effective ways for the member nations to use their research and development capabilities for the common benefit of the NATO community;
- Providing scientific and technical advice and assistance to the Military Committee in the field of aerospace research and development (with particular regard to its military application);
- Continuously stimulating advances in the aerospace sciences relevant to strengthening the common defence posture;
- Improving the co-operation among member nations in aerospace research and development;
- Exchange of scientific and technical information;
- Providing assistance to member nations for the purpose of increasing their scientific and technical potential;
- Rendering scientific and technical assistance, as requested, to other NATO bodies and to member nations in connection with research and development problems in the aerospace field.

The highest authority within AGARD is the National Delegates Board consisting of officially appointed senior representatives from each member nation. The mission of AGARD is carried out through the Panels which are composed of experts appointed by the National Delegates, the Consultant and Exchange Programme and the Aerospace Applications Studies Programme. The results of AGARD work are reported to the member nations and the NATO Authorities through the AGARD series of publications of which this is one.

Participation in AGARD activities is by invitation only and is normally limited to citizens of the NATO nations.

Published February 1991

ISBN 92-835-0605-7

Printed by Specialised Printing Services Limited
40 Chigwell Lane, Loughton, Essex IG10 3TZ

Theme

The performance of sensor and communication systems can be limited significantly by hostile Electronic Counter Measures (ECM). These include passive measures such as radar and laser warning receivers, interception, emitter location systems as well as active measures such as jammers in various roles using different techniques and deception devices. The Warsaw Pact nations are known to possess a large number of different Electronic Warfare (EW) systems covering the entire frequency spectrum. These EW systems and techniques were the subjects of the 52nd Avionics Panel (AVP) Symposium which was held in Florence, Italy in 1986.

The symposium follows up and complements the 52nd AVP Meeting and concentrates on Electronic Counter-Counter Measures (ECCM) which may be designed into sensor and communications systems, and procedures to alleviate the adverse effects of the expected electronic threat. The symposium covers ECCM ranging from frequency agility to spread spectrum and data fusion techniques for both sensor and communications systems and will encourage cross-fertilization between the users, engineers and scientists working in the two disciplines thus stimulating new ideas and/or new applications of the known techniques. As far as terrestrial and satellite communications systems are concerned, we have to provide not only for protection against ECM but also for compatibility and interoperability of the radio systems used by different forces participating in joint operations and for systems shared by member nations of NATO.

Thème

Les performances des systèmes de détection et de télécommunications peuvent être limitées de façon sensible par les contremesures électroniques hostiles (ECM). Celles-ci comprennent les mesures passives, telles que les récepteurs d'alerte radar et laser, l'interception, et les ensembles de repérage des émetteurs, ainsi que les mesures actives telles que les brouilleurs employés dans divers rôles à l'aide de différentes techniques et de différents systèmes de déception.

Les pays du Pacte de Varsovie possèdent un grand nombre de systèmes différents de guerre électronique (EW) qui couvrent tout le spectre de fréquences. Ces systèmes et techniques EW ont fait l'objet du 52ème symposium du Panel AGARD d'avionique, organisé en 1986 à Florence en Italie.

Ce symposium suit et complète les travaux de la 52ème réunion du Panel. Il concerne principalement les contre-contremesures électroniques (ECCM) susceptibles d'être intégrées aux systèmes de détection et de télécommunications, ainsi que les procédures qui seraient à suivre afin de contrer les effets néfastes de la menace électronique escomptée.

Le symposium couvre tout l'éventail des techniques ECCM, de l'agilité de fréquences à l'étalement du spectre, sans oublier les techniques de fusion des données pour les systèmes de détection et de télécommunications, et doit permettre une certaine osmose entre les utilisateurs, les ingénieurs et les scientifiques qui travaillent dans les deux disciplines, sollicitant ainsi des idées nouvelles et/ou des applications novatrices pour ces techniques connues.

En ce qui concerne les systèmes de télécommunications terrestres et les systèmes spatiaux, nous nous devons d'assurer non seulement la protection contre l'ECM, mais aussi la compatibilité et l'interopérabilité des systèmes radio et des systèmes répartis entre les pays membres de l'OTAN et utilisés par les différentes forces participant aux opérations combinées.

Avionics Panel

Chairman: Dr Richard Klemm
FFM—FGAN
Neuenahrer Strasse 20
D-5307 Wachtberg 7
Germany

Deputy Chairman: Eng. Jose M.B.G.Mascarenhas
C-924
c/o Cinciberlant Hq
2780 Oeiras
Portugal

TECHNICAL PROGRAMME COMMITTEE

Chairman: Prof. Dr A.Nejat INCE
Burumcuk Sokak 7/10
Cankaya 06550
Ankara
Turkey

Ing. L.Crovella
Aeritalia—SAIpA
Gruppo Sistemi Avionics Equipaggiam
10072 Caselle Torinese (Torino)
Italy

Mr J.Dorey
Directeur Technique Adjoint
Thomson-CSF Branche Equipments
Aéronautiques
Cedex 67
92045 Paris la Défense
France

Mr Manfred Jacobsen
Director, Airborne EW System Div
Telefunken Systemtechnik
Sedanstrasse 10
7900 Ulm/Donau
Germany

Dr R.Klemm
FGAN — FFM
Neuenahrer Strasse 20
D-5307 Wachtberg
Germany

Dr K.Krucker
FGAN — FHP
Neuenahrer Strasse 20
D-5307 Wachtberg
Germany

Dr C.H.Krueger, Jr
WRDC/AAA
Wright Patterson AFB, OH 45433
United States

Dr R.Voles
Chief Scientist
Thorn EMI Electronics Ltd
120 Blythe Road
Hayes, Middx UB3 1DL
United Kingdom

PANEL EXECUTIVE

Lt Colonel James E.Clay

Mail from Europe:
AGARD—OTAN
Attn: AVP Executive
7, rue Ancelle
92200 Neuilly sur Seine
France

Mail from US and Canada:
AGARD—NATO
Attn: AVP Executive
APO New York 09777

Tel: 33(1)47 38 57 65
Telex: 610176 (France)
Telefax: 33(1)47 38 57 99

Contents

* Printed in classified publication CP 488 (Supplement)

* Printed in classified publication CP 488 (Supplement)

SESSION V – MEASURES OF EFFECTIVENESS

* Printed in classified publication CP 488 (Supplement)

KEYNOTE ADDRESS

by

Dr-Ing. Hans-Werner Fieweger
Head of the Electronics and Communications Division
Federal Office of Defense Technology and Procurement
5400 Koblenz
Germany

It's an honour and a pleasure for me to respond to your invitation and present the Keynote Address to this AGARD Avionics Panel Symposium.

I'm also delighted to welcome you to Germany. Surely, your choice of Munich as venue for this Symposium is not pure coincidence. For many Germans Munich is the so-called "secret" capital of the Republic and this is unlikely to be changed by the unification of Germany, regardless which city may then become the official capital.

Of course I'm also certain that your timing of this Symposium is not a coincidence either. The natives of Munich contend that their Oktoberfest is the largest carnival in the world. They are probably right, because six to seven million visitors who consume five million litres of beer — that's hard to beat. I would assume that you also will not be oblivious to the attraction of the Oktoberfest which — by the way — celebrates its 180th anniversary.

The theme you have chosen for this Symposium is "Electronic Counter-Counter Measures for Avionics Sensors and Communication Systems". This is a subject which is not only of high technical interest, but in my view it is also totally independent of the political developments and thus always current.

In brief the present political situation can be described as follows:

- The systems of the NATO Alliance and the Warsaw Pact are revising their policies and strategies.
- East and West will reduce their force levels both, in terms of manpower and material. This means cuts in the defence budgets and thus in expenditures for hardware.
- As a consequence of German unification Germany is faced with the problem of integrating in some fashion the remants of the East German Army in the Bundeswehr. You are aware that our Chancellor has offered a reduction of the German Federal Armed Forces to a force level of 370,000 troops.

I believe, it is true to say that the priority policy objectives in East and West at present are to create more peace with fewer arms. Let's hope, it works!

An immediate consequence of arms reductions is the need to further enhance our command & control and intelligence collection capability in order to ensure continuity of our defence posture at an agreed lower level. For this reason reconnaissance and C-cube systems, and I'm talking about sensors and communications, have been assigned a very high priority at NATO level and by the German Federal Armed Forces.

However, such command & control and intelligence collection capability can only be ensured if the equipment and the systems designed for this mission have adequate ECCM properties. There are two fundamentally different approaches to achieve this objective:

- by electronic "armor" — which ensures that hostile ECM cannot penetrate, and thus retain the functioning of equipment and systems, or
- by electronic "concealment and deception" — which impairs or denies reconnaissance by an adversary.

Since the Vienna arms reduction talks and/or subsequent negotiations will not restrict electronic warfare the technology for ECM and ECCM will continue to be advanced commensurate with progress in the state of the art. And as far as I am concerned this is a field which does not lend itself to effective verification anyway.

Therefore, the objective of electronic warfare will continue to be to achieve superiority in the total electromagnetic spectrum, to aim for electronic "suppression" of the adversary and thus retain the command & control and reconnaissance capability of the friendly forces while denying the adversary's capability to the maximum extent possible. That makes electronic warfare, and in particular the robustness of friendly systems against hostile ECM, a genuine force multiplier.

Electronic warfare fits well into the defensive structures which are appropriate to the present political situation. This increases their relative priority in armament planning and it is particularly true for all ECCM. It would certainly not apply to the same degree to SIGINT and ELINT and ECM in general.

Moreover, NATO introduced the term "Electronic Protective Measures" for the purely defensive part of electronic warfare which, in addition to ECM also includes active electronic masking against hostile SIGINT and ELINT, but no ECM against other reconnaissance sensors and communication facilities. So, further development of electronic protective measures will likely be an important task for the near future.

However, this task won't be all that easy to accomplish, since – hopefully – we will not have such a clearly defined threat scenario in the future. It will require the development of scenarios based on available technologies and the products which are offered on the world market. My very personal opinion is that, because of the process of detente and the treaties envisaged with the USSR, we will have to develop a new concept of electronic warfare in the years to come.

One of the items on the agenda that the AGARD Symposium will address in detail over the next few days is *technical* issues of ECCM for sensors and communications systems. Initially, when electronic warfare started in World War II it was limited primarily to the radar sector. To this day there are no effective techniques to protect analog radio systems against hostile ECM. This is why for a long time the radio community focussed their attention on the protection of transmissions against eavesdropping, in other words, COMSEC. Only the advent of digital radio transmission introduced effective ECCM in this field and in many cases good protection against detection was achieved as well.

However, the advances in ECCM technology have brought about a situation, where man is more and more excluded from the operational processes. At best he will switch modes and some systems do that automatically already.

Generally speaking the ECM robustness of reconnaissance and communication systems is increasingly determined by the configuration, that is to say by the overall system design, rather than by the individual piece of hardware. Because of the extensive use of the entire electromagnetic spectrum and the many different types of interference signals – also including man-made noise – the ECCM capabilities contribute already in peacetime to the performance of the sensors and communications systems. I think, this can be regarded as a bona fide "spin-off".

A major problem in particular for defence electronic equipment is the discrepancy between the life cycle of more than 20 years on the one hand, the changes in operational conditions within shorter time spans, and the technological advances which have a shorter time constant still, on the other. This is of course the reason why we go for the growth potential approach for major systems which is mostly true for weapon systems and their electronics.

My impression is that we have somewhat neglected the option of subsequent performance improvement potential of reconnaissance and communications systems during the development of these systems. Since the scope of data processing for sophisticated systems is steadily increasing, our options for adjusting to changes in operational requirements are in essence the modification of the software. In my opinion we must make considerably more use of these options. Otherwise we run the risk of falling behind in this vital field of command & control and intelligence collection. And in the light of diminishing defence budgets the life cycles of defence equipment will likely be extended, even with reduced force levels.

A special aspect of electronic warfare is simulation, not only to demonstrate the performance of the system during development, but also during its service life and for the training of the operators. The more complex ECM and ECCM techniques become, the less can their capabilities be demonstrated without the tool of simulation and the weak points of the system be identified at the same time. I believe this is an aspect that considerably more effort must be devoted to in the future.

Ultimately all considerations are dictated by political developments. These developments will determine the scope of future armament planning and acquisition. But, be that as it may, the performance of reconnaissance and communications systems will be materially a function of their ECCM capability, and we all know that such capabilities are not just an add-on feature – they are major criteria of the system design. Like testability ECCM robustness cannot be integrated in a system afterwards.

Let me conclude my presentation by summarizing the key statements:

- With decreasing force levels command & control and intelligence collection will be even more important in the future.
- Therefore, the performance of reconnaissance and communications systems must meet very special demands.
- Their performance is materially a function of their ECCM capability.
- The ECCM capability has a major impact on system design; it cannot be integrated afterwards.
- The options for growth potential must be taken account of during development in order to permit adaption to changes in operational requirements.
- Because of the use of data processing these options will be based more and more on modification of the software.

This AGARD Symposium addresses ECCM for reconnaissance and communications in the frequency spectrum up to cm- and mm-waves. In the light of the growing significance of electro-optics, especially in the sensor field, it is obvious that EOCCM will be a very relevant subject to be dealt with in the future.

It has been a privilege to present the Keynote Address to this Symposium. I hope that you will have a fruitful session and wish you a pleasant stay in Munich, Germany's "secret" capital, and a good time with lots of fun at the Oktoberfest.

A method to enhance azimuth accuracy by the use of the a priori knowledge of the antenna pattern.

by
W.E. Hoekstra
SHAPE Technical Centre
p/o Box 174, 2501 CD The Hague, The Netherlands

This paper presents a method to remove sidelobe contamination in antenna measurements for a circular scan antenna. Although the approach described is in principle only applicable to situations where the jamming is constant over one scan of data and requires perfect knowledge of the own antenna pattern, it is shown that the method provides a substantial enhancement if these conditions are weakened. The mathematics used are not new, but this particular application might be.

Introduction

Passive tracking from moving platforms requires precise knowledge of own position and orientation and accurate measurements of emitter bearings. In the near future, we expect that moving platforms will be equipped with precise positional navigation systems such as GPS and/or JTIDS Relative Navigation, and then one of the current impediments, a precisely known own location and orientation at any moment of time, will be removed. The other impediment, accurate location of jammer strobes is the subject of this paper.

In this paper the basic mathematics supporting the method are reviewed. Analysis of the operational behavior and influences of non-stationarity of the sensor or rapid changes in the environment on the quality of the solution are discussed.

Azimuth accuracy

To illustrate the problem, consider the results of a simple least squares approach to determine the position of an emitting target at a range of 200 nm. The own platform direction crosses the bearing to the target at angles between -90° and 90° and has a straight line, uniform speed. The geometry is shown in figure 1. The importance of the accuracy of the bearing for achieving fast convergence even in geometrically advantageous situations is shown in figure 2. Convergence was assumed when 3 successive scans were within 3 nm from each other. More complex algorithms could provide better solutions, but that is not the subject of this paper.

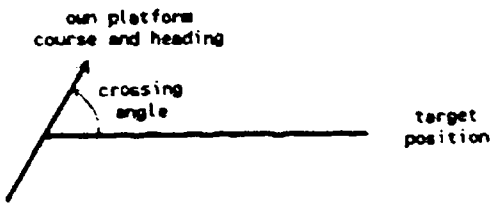

Figure 1. Geometry

Azimuth measurements

In active and passive tracking, sidelobe contamination can cause faulty measurements and even ghost strobes or tracks. This is illustrated in figures 3 and 4. In figure 3, we have a synthetized antenna pattern and we assume that the antenna points towards a target. A jamming strobe enters the measurement via the sidelobes of the antenna and its

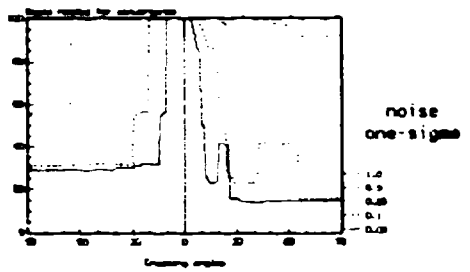

Figure 2. Simple Least Squares

effect on the coverage is shown in figure 4. The sidelobe contamination is tied to the direction of the main lobe of the antenna, thus generating ghost strobes or false alarms in the case of active radar emissions in the direction of the main lobe.

Many systems use guard antennas or adaptive sidelobe cancelling to prevent this type of contamination and then additional antennas are required to monitor each jammer. In the approach, described in this paper, only the signal from the main antenna is used.

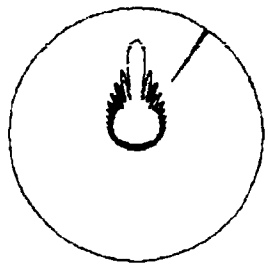

Figure 3. Synthetized antenna diagram and jammer strobe

The method

The method presented below, seems to be perfectly suited for real time applications, especially when special purpose hardware (a commercially available array processor or a programmable spectrum analyzer) is used. A complete enhancement of one scan of measurements could take less than 200 milliseconds, and because this can be done by special hardware it does not need to constitute an additional burden to existing processing capability.

The method requires $O(6N\log_2 N)$ operations, with N the number of azimuth resolution cells. A system with a 12 bits azimuth resolution has 2^{12}=4096 azimuth resolution cells. Conventional methods to perform the same result would use standard matrix inversion techniques requiring $O(N^2)$ to $O(N^3)$ operations to obtain the same result.

Knowledge of the pattern of the own antenna is a prerequisite. We assume that this knowledge is available as a discretised pattern defined by the N-tupie $\underline{c}_N$ of the antenna gains for each azimuth resolution cell.

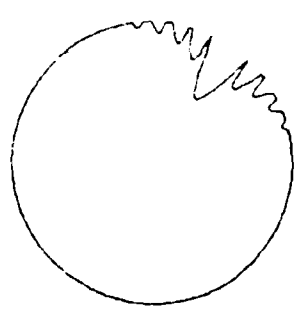

Figure 4. Coverage reduction

Mathematical background

An antenna measurement v_m (see figure 3) is the result of an inner product of the antenna with the actual environment. It is associated to the direction of the main lobe of the antenna, here indicated by the index m. The actual environment is supposed to be discretised as an N-tuple $\underline{u}_N$. It is this vector $\underline{u}_N$ (outer circle in figure 3) that we want to determine.

A complete scan is the N-tuple $\underline{v}_N$ consisting of N measurements in the N azimuth directions. This N-tuple is the circular convolution of the antenna characteristics with the environment and it can be represented by the matrix-vector product:

$$\underline{v}_N = \underline{C}_N \underline{u}_N \quad \text{---------- (1)}$$

The formal solution of (1) is then given as:

$$\underline{u}_N = \underline{C}_N^{-1} \underline{v}_N =$$

$$= \underline{W}_N \underline{D}_N^{-1} \underline{W}_N^{-1} \underline{v}_N =$$

$$= \underline{W}_N \underline{D}_N^{-1} \underline{P}_N \underline{W}_N \underline{v}_N \quad \text{---------- (2)}$$

where the matrix $\underline{W}_N$ is defined below, $\underline{W}_N^*$ is its complex conjugate, and w is defined by $w = \exp(2\pi i/N)$:

$$\underline{W}_N = (1/\sqrt{N}) \begin{vmatrix} 1 & 1 & .. & 1 \\ 1 & w & .. & w^{N-1} \\ 1 & w^2 & .. & w^{2(N-1)} \\ . & . & .. & . \\ 1 & w^{N-1} & .. & w^{(N-1)(N-1)} \end{vmatrix} \quad \text{----- (3)}$$

The evaluation of (2) can be done by two consecutive DFTs and some vector multiplications, in total $6N\log_2 N$ operations. A detailed derivation is provided in Appendix A to this paper.

The matrix $\underline{D}_N$ in (2) is a diagonal matrix with $c^n{}_{w^{(n-1)(N-1)}}$ in the n-th row, and $\underline{P}_N$ is the persymmetric matrix (see appendix A, equation 15.4).

Should one of the eigen-values of D_N be 0, then one could substitute any value for its inverse. This means that the corresponding eigenvector of $\underline{W}_N$ has a weight equal to zero in the Discrete Fourier Transform of the antenna pattern. Then the DFT of the measurement $\underline{v}_N$ will have a weighting equal to zero as well for this eigen-vector, because it is the result of a convolution of the antenna pattern and the environment (see(1)). In general an antenna is used within a certain bandwidth and this means that the nulls in the antenna pattern are filled up. Also the antenna is rotating and thus the gain in one particular direction is the average gain over the time period needed to rotate over one azimuth resolution cell.

Hardware requirements

For 4096 azimuth resolution cells, i.e. N=4096, this approach is about 60 times faster than when the inverse was computed with other methods [2,3]. Thus solution of (2) becomes feasible as a real time operation. Moreover, fast efficient and relatively cheap hardware for DFT's and inner products exists.

An estimate, based on the specified computing times for the Magnavox-MAP, gives a total computing time for y_N of less than 200 msecs.

The technique, described above would require knowledge of the far-side lobes and the backlobes of an antenna. A well designed antenna could have its first sidelobes below -40 dB and the backlobes will be substantially lower. Measuring these is difficult; using them for pattern matching could be cumbersome. However, if we restrict ourselves to the area around the main beam of the antenna, then the circulant behavior of the matrix is lost and we are stuck with the Toeplitz behavior which means that although the matrix to be inverted becomes smaller, the inversion procedure becomes more complicated.

In principle it is possible to use a transversal filter matched to the main beam and near side-lobes of the antenna pattern in a kind of monopulse mode. Then one cannot reject strong jammers which still influence the measurement but are beyond the azimuth coverage of the matched filter.

The method described is, subject to stationarity requirements, able to resolve up to N jammers.

A/D converters, working at sufficiently high update rates, with sufficient resolution to cover the whole antenna pattern in detail are at the edge of technology. Further resolution could be obtained by using attenuators for saturated signals and by keeping track when these attenuators are switched on and off so that the dynamic range of the signal can be restored for subsequent floating point processing, or by sharing the A/D converter between two receivers differing in gain.

Results

The method, described above, was simulated using the NATO standard scenario. This is a scenario developed at STC to analyze tracking performance. This scenario consists of 50 targets flying into a surveillance area where they perform dogleg manoeuvres until they reach a manoeuvre area where they turn 180 degrees. On their way back they perform dogleg manoeuvres again. An overview of this scenario is presented in figure 5.

All targets are assumed to have detectable reflections or emissions. The method was tested with one out of the 50 A/C jamming and with 7 A/C jamming. Jamming was defined as 100 dB above normal detection level.

The results in figures 6 and 7 show the unprocessed returns and the processed returns of the case with one jamming target. In the unprocessed returns other targets are than the jammer are completely masked. The processed returns reconstruct the bearings as they would look without jamming.

Imperfect knowledge of the antenna pattern

In a live environment, one cannot expect a perfect knowledge of the own antenna pattern. To investigate this effect, the reference antenna pattern was disturbed and the results of the same tests are displayed. Although the detection of non-jamming targets in the close neighbourhood of jammers is still cumbersome, the jamming impact is substantially reduced and the bearing to the jammers themselves is improved. Results obtained with imperfect antenna knowledge before and after processing are shown in figures 8 and 9.

Non-stationarity of the environment

Until now , it was tacitly assumed that the environment is stationary. In real life, this will not be the case. To investigate these effects, the environment was randomly perturbed from slant to slant Rather than performing the algorithm once each scan of 360° it could be performed once every 20° and the results of this process show that the algorithm can handle weakly non-stationary jammers. Because the azimuth resolution of jammers is enhanced, the process described in this paper, could also be used as a first step to improve adaptive sidelobe cancelling methods to handle strongly non-stationary jammers.

Additional benefits

The algorithm described above could be modified to calibrate the knowledge of the own antenna pattern. Rather than measuring an unknown environment, one measures a known emitter and uses these measurements to determine the antenna pattern. Such a measurement could be performed in flight and the improved knowledge of the own antenna pattern would greatly support the azimuth enhancement process described above and could be used to monitor system performance.

The method could also be used to improve the azimuth resolution of simple radar systems, for instance navigational systems, in a non-jamming environment.

Literature:

[1] Levinson N. "The Wiener (root mean square) error criteria in filter design and prediction", J. Math. Phil., Vol 25, 1947, pp261-278.

[2] Trench W.F. "An algorithm for the inversion of finite Toeplitz matrices", J. SIAM, 12, 3 Sept. 1964, pp 515-527.

[3] Zohar S. "Toeplitz matrix inversion : The algorithm of W.F. Trench", J. ACM, 16, 4 Oct. 1969, pp 592-601.

[4] LU-decomposition. See for instance: "Handbook of Automatic Computation, Volume II, Linear Algebra", by Wilkinson J.H. and Reinsch C., Springer-Verlag, 1971, pp 93-110.

[5] Merz G. "Fast Fourier Transform algorithms and applications", In: "Computational aspects of complex analysis", H. Werner a.o. (Eds), Reidel, Dordrecht, 1983, pp 249-272.

Appendix A: Mathematical background

A complete measurement is the N-tuple $\underline{v}_N$ consisting of N measurements in the N azimuth directions. This N-tuple is the circular convolution of the antenna characteristics with the environment and it can be represented by the matrix-vector product:

$$\underline{v}_N = \underline{C}_N \underline{u}_N \quad \text{---------- (1)}$$

The formal solution of (1) is then given as:

$$\underline{u}_N = \underline{C}_N^{-1} \underline{v}_N \quad \text{---------- (2)}$$

The sheer size of $\underline{C}_N$ (16 N elements typically) requires special inversion techniques. Moreover, even if the inverse matrix $\underline{C}_N^{-1}$ is known, computing (2) requires again 16 N operations. (M means 10^6).

The matrix $\underline{C}$ used in (1) is a so-called circulant. A circulant is a matrix in which each next row is the previous row with its last element passed over to the first place. So each next row is the previous one, circularly shifted one place to the right. One place corresponds here to one azimuth resolution cell. Such a circulant is illustrated in (3) below.

$$\underline{C}_N = \begin{vmatrix} c_0 & c_1 & \cdot & \cdot & c_{N-1} \\ c_{N-1} & c_0 & \cdot & \cdot & c_{N-2} \\ \cdot & \cdot & \cdot & \cdot & \cdot \\ \cdot & \cdot & \cdot & \cdot & \cdot \\ c_1 & c_2 & \cdot & \cdot & c_0 \end{vmatrix} \quad \text{------(3)}$$

This matrix has a special structure. Each diagonal contains the same elements, which makes it a so-called Toeplitz matrix and it has only N different elements, which is a further refinement in the class of Toeplitz matrices. The general approach to invert a matrix, for instance with LU decomposition [1] would require $O(N^3)$ operations. An algorithm for symmetric Toeplitz matrices was proposed by Levinson [2]. This algorithm was modified for general matrices by Trench [3], see also Zohar [4]. With their algorithm the inversion would require $O(N^2)$ operations. Merz [5] gives an algorithm to solve (2) by means of discrete Fourier transforms (DFT), using the eigenvalues and eigenvectors of a circulant. It is this approach that we want to describe here in more detail.

The circulant $\underline{C}_N$ can be written as a weighted sum of shift operators, this is illustrated below for N=5:

$$\underline{C}_N = c0 \begin{vmatrix} 1 & \cdot & \cdot & \cdot & \cdot \\ \cdot & 1 & \cdot & \cdot & \cdot \\ \cdot & \cdot & 1 & \cdot & \cdot \\ \cdot & \cdot & \cdot & 1 & \cdot \\ \cdot & \cdot & \cdot & \cdot & 1 \end{vmatrix} + c1 \begin{vmatrix} \cdot & 1 & \cdot & \cdot & \cdot \\ \cdot & \cdot & 1 & \cdot & \cdot \\ \cdot & \cdot & \cdot & 1 & \cdot \\ \cdot & \cdot & \cdot & \cdot & 1 \\ 1 & \cdot & \cdot & \cdot & \cdot \end{vmatrix} +$$

$$+ \ldots + c_{N-1} \begin{vmatrix} \cdot & \cdot & \cdot & \cdot & 1 \\ 1 & \cdot & \cdot & \cdot & \cdot \\ \cdot & 1 & \cdot & \cdot & \cdot \\ \cdot & \cdot & 1 & \cdot & \cdot \\ \cdot & \cdot & \cdot & 1 & \cdot \end{vmatrix}$$

$$= c_0 \underline{I}_N + c_1 \underline{K}_1 + \ldots + c_{N-1} \underline{K}_{N-1} \quad \text{---------- (4)}$$

Observe that $\underline{K}_1 * \underline{K}_1 = \underline{K}_2$, and for shift operators $\underline{K}_i * \underline{K}_j = \underline{K}_k$, where k=i+j modulo N. Thus we can write (4) as:

$$\underline{C}_N = c_0 \underline{K}_1^0 + c_1 \underline{K}_1^1 + \ldots c_{N-1} \underline{K}_1^{N-1} =$$

$$= \sum_{n=0}^{N-1} c_n \underline{K}_1^n \quad \text{---------- (5)}$$

The eigen-values of $\underline{K}_1$ are given by the μ's which solve the characteristic equation

$$|\underline{K}_1 - \mu \underline{I}_N| = 0.$$

Expansion of this equation yields:

$$\begin{vmatrix} -\mu & 1 & \cdot & \cdot & 0 \\ 0 & -\mu & \cdot & \cdot & 0 \\ \cdot & \cdot & \cdot & \cdot & \cdot \\ \cdot & \cdot & \cdot & -\mu & 1 \\ 1 & \cdot & \cdot & \cdot & -\mu \end{vmatrix} = 1 + (-\mu)^N = 0 \quad \text{---------- (6)}$$

Thus the eigen-values μ_m of $\underline{K}_1$ are the N-roots of 1 and are defined by:

$$\mu_m = \exp(2\pi i m/N), \; m=0(1)N \quad \text{---------- (7)}$$

The eigen-vectors of $\underline{K}_1$ are then given by the solutions $\underline{q}_m$, m=0(1)N-1 of $\underline{K}_1 \underline{q}_m = \mu_m \underline{q}_m$:

$$\begin{vmatrix} 0 & 1 & 0 & . & 0 \\ 0 & 0 & 1 & . & . \\ . & & & . & . \\ 0 & & & . & 1 \\ 1 & 0 & & . & 0 \end{vmatrix} \begin{vmatrix} q_{m,0} \\ . \\ . \\ . \\ q_{m,N-1} \end{vmatrix} = \mu_m \begin{vmatrix} q_{m,0} \\ . \\ . \\ . \\ q_{m,N-1} \end{vmatrix} \quad \text{--- (8)}$$

Take $q_{m,0} = 1/N$ then:

$$q_{m,n} = \mu_m^n/N, \quad n=0(1)N-1 \quad \text{---------- (9)}$$

Knowing the eigenvalues and a set of orthonormal eigenvectors of $\underline{K}_1$, one can bring $\underline{C}_N$ to its diagonal form $\underline{D}_N$ using orthonormal transformations.

$$\underline{D}_N = \underline{U}_N^* \underline{C}_N \underline{U}_N =$$

$$= \underline{U}_N^* \left(\sum_{n=1}^{N-1} c_n \underline{K}_1^n \right) \underline{U}_N =$$

$$= \sum_{n=0}^{N-1} (c_n \underline{U}_N^* \underline{K}_1 \underline{U}_N) \quad \text{---------- (10)}$$

where the matrix $\underline{U}_N$ consists of the eigenvectors of $\underline{K}_1$ and its complex conjugate is $\underline{U}_N^*$. Setting $w = \exp(2\pi i/N)$ one gets:

$$\underline{U}_N = (1/\sqrt{N}) \begin{vmatrix} 1 & 1 & .. & 1 \\ 1 & w & .. & w^{N-1} \\ 1 & w^2 & .. & w^{2(N-1)} \\ . & . & .. & . \\ 1 & w^{N-1} & .. & w^{(N-1)(N-1)} \end{vmatrix} \quad \text{----- (11)}$$

Observe that this matrix $\underline{U}_N$ is the same as one would get for a Discrete Fourier Transform over N points. We define the matrix $\underline{Q}_n$, which is the diagonal form of $\underline{K}_1^n$, n=0(1)N-1.

$$\underline{Q}_n = \underline{U}_N^* \underline{K}_1 \underline{U}_N = \begin{vmatrix} 1 & 0 & .. & 0 \\ 0 & w^n & .. & 0 \\ 0 & 0 & .. & 0 \\ . & . & .. & . \\ 0 & . & .. & w^{(N-1)n} \end{vmatrix} \quad \text{------ (12)}$$

We can now express $\underline{D}_N$ in terms of the matrices $\underline{Q}_n$:

$$\underline{D}_N = \sum_{n=0}^{N-1} c_n \underline{Q}_n \quad \text{---------- (13)}$$

This gives the general expression of the m-th eigen-value l_m:

$$l_m = \sum_{n=0}^{N-1} c_n w^{mn} \quad \text{---------- (14)}$$

and thus the main diagonal of $\underline{D}_N$ (see 9) can be computed by a Discrete Fourier Transform (DFT).

$$l_N = \sqrt{N}\, \underline{U}_N \underline{c}_N \quad \text{---------- (15)}$$

So apparently the eigenvalues of a circulant matrix are defined by the Fourier transform of any row of this matrix. For completeness sake some properties of the DFT matrix $\underline{U}_N$ are mentioned. These properties are given below:

(i) $\underline{U}_N = \underline{U}_N^T$ ---------- (16.1)

(ii) $\underline{U}_N^* \underline{U}_N = \underline{I}_N$ ---------- (16.2)

(iii) $\underline{U}_N^2 = \underline{P}_N$ ---------- (16.3)

where $\underline{P}_N$ is the so-called persymmetric transformation matrix, given by:

$$\underline{P}_N = \begin{vmatrix} 1 & 0 & ..... & 0 & 0 \\ 0 & . & ..... & 0 & 1 \\ 0 & . & ..... & 1 & 0 \\ . & . & ..... & . & . \\ 0 & 1 & ..... & 0 & 0 \end{vmatrix} \quad \text{---------- (16.4)}$$

(iv) $\underline{U}_N^4 = \underline{I}_N$ ---------- (16.5)

(v) $\underline{Q}_1 \underline{U}_N = \underline{U}_N \underline{K}_{N-1}$ ---------- (16.6)

(vi) $\underline{U}_N^{-1} = \underline{U}_N^3 = \underline{P}_N \underline{U}_N$ ---------- (16.7)

Using (12), the original measurement equation (1) can now be written as:

$$\underline{v}_N = \underline{C}_N \underline{u}_N = \underline{U}_N^* \underline{D}_N \underline{U}_N \underline{u}_N \quad \text{---------- (17)}$$

Hence with (ii) and (vi), the solution $\underline{u}_N$ of (2) becomes:

$$\underline{u}_N = \underline{C}_N^{-1} \underline{v}_N = \underline{U}_N \underline{D}_N^{-1} \underline{U}_N^{-1} \underline{v}_N =$$

$$\underline{U}_N \underline{D}_N^{-1} \underline{P}_N \underline{U}_N \underline{v}_N \quad \text{---------- (18)}$$

which can be done by two consecutive DFTs and some vector multiplications, in total $6N\log_2 N$ operations are required.

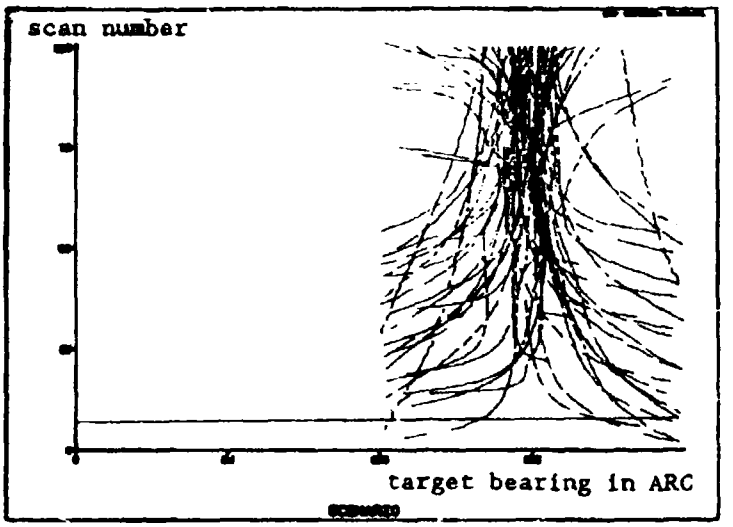

Figure 5. Scenario

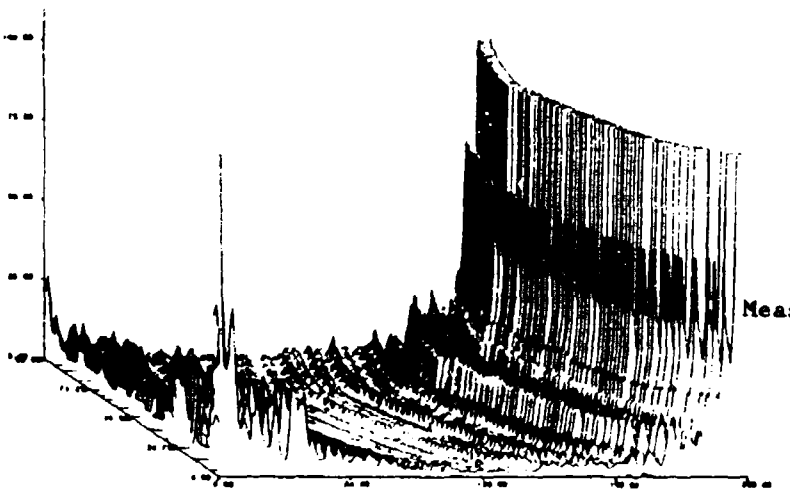

Figure 6.
Measurement, 50 targets, 1 jammer

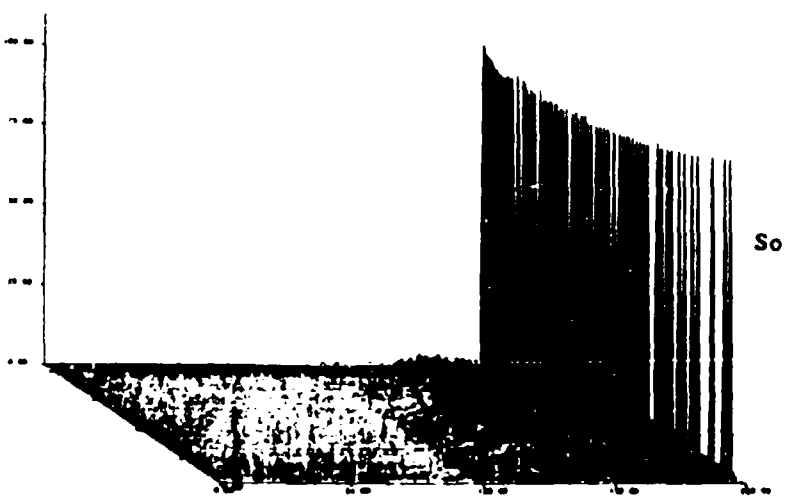

Figure 7.
Solution, 50 targets, 1 jammer

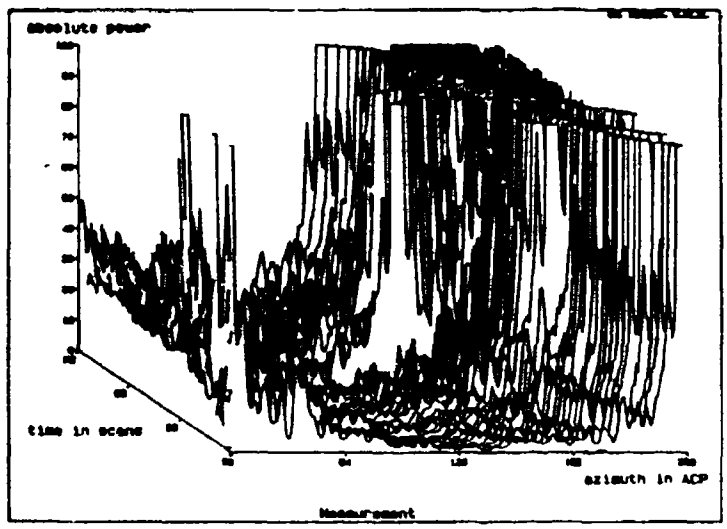

Figure 8. Measurement, 50 targets, 5 jammers

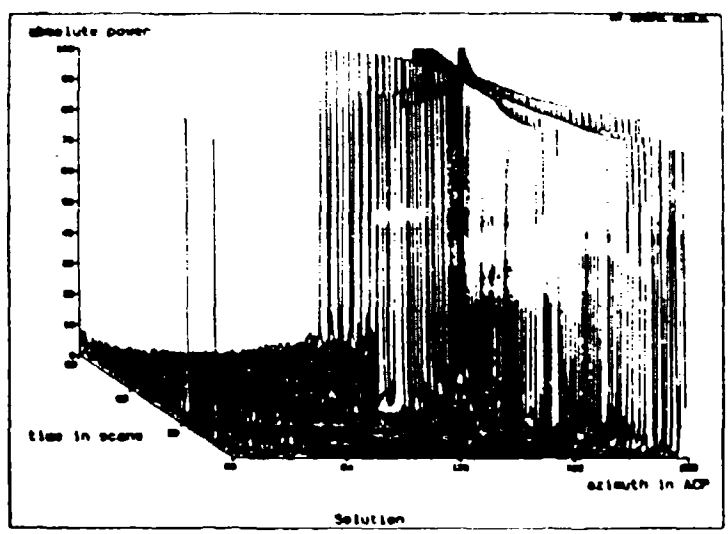

Figure 9. Solution, 50 targets, 5 jammers

Discussion

C.Kayserilioglu, MBB, Ge

If you have a strong jammer and saturation in your system, what is the effect on your azimuth accuracy enhancement?

Author's Reply

(In the example shown), the power was clipped at 100 dB. So really, information at the top of the antenna pattern was not used and that is essentially the same as what you would have with saturation. But the trick of the whole method is that there is still information in the form of the pattern next to the elements that are saturated.

ECCM ADVANTAGES OF ADAPTIVE DIGITAL PULSE COMPRESSION

GUY R. PAINCHAUD AND MARTIN BLANCHETTE

Radar Division, Defence Research Establishment Ottawa,
3701 Carling Avenue, Ottawa, Ontario, Canada K1A 0Z4

SUMMARY

The ECCM advantages of an experimental adaptive digital pulse compression (DPC) system are described. This pulse compression system is implemented by a complex correlation between the transmitted waveform and the signal received by the radar. Central to the adaptability of this unit is the use of high speed VLSI digital ICs which permit bandwidths of up to 10 MHz, along with the ability to use a different waveform or pulse code on each transmission. The DPC unit is intended to be used in a multi-function radar (MFR) which would employ many different waveforms.

The objective of this paper is to describe how waveform adaptability can be used as an ECCM technique. Examples of its use as a counter-measure against both ESM and ECM systems are given. Both denial and deceptive ECM are considered.

INTRODUCTION

Pulse compression systems have traditionally used surface acoustic wave (SAW) filters as both pulse expanders and compressors. The impulse response of these analogue components is coded into the device at the time of manufacture and cannot be changed. As the SAW device is matched to a single waveform, a separate device is required for each code. The recent availability of high speed multi-bit digital correlators implemented in VLSI IC form has made it possible to build compact digital pulse compression filters[1].

Among the advantages offered by a digital implementation, the ability to change waveforms on a pulse by pulse basis makes this device very attractive for use in an MFR. This permits a single DPC unit to handle all the different waveforms required by the radar to perform its various functions. Emphasis will be given in this paper to the use of pulse compression as an ECCM technique, with emphasis on the pulse to pulse adaptability provided by a digital implementation.

The ECCM advantages provided by DPC can counter the effects of both ESM and ECM systems. Examples of both of these counters will be given.

ECCM ADVANTAGES

The benefits provided by DPC can be used to counter both ESM and ECM systems. The low peak power/high duty cycle waveforms used by solid state transmitters normally use pulse compression to provide good detectability and acceptable range resolution. This type of waveform also provides an ECCM advantage as the low peak power inherent in the waveform yields a shorter ESM intercept range.

Another ECCM advantage of DPC is provided by waveform agility. By changing the code on a pulse to pulse or coherent processing interval (CPI) basis, it is harder for the ESM system to identify the various codes and associate them with a given emitter. This identification problem is compounded when the received signal is weak and not all of the codes are detected. Waveform agility can also be used to make a particular radar emulate a mode of another radar, or to make it look like more then one radar. The purpose of this tactic would be to make a radar, and its associated platform, look less threatening or simply to confuse the identification algorithms.

Adaptive DPC can also be used to counter various forms of ECM. Generically, ECM can be classified as either denial or deceptive[2]. The purpose of denial is to prevent the radar from detecting one or more targets . Deceptive ECM tries to generate a number of false returns so that the radar has difficulty in distinguishing the real targets from the false ones. The real targets are not necessarily masked by the false returns, although they can be.

In general, denial ECM is usually implemented by transmitting a noise waveform about the carrier frequency of the target radar. Deception ECM evolves transmitting a waveform similar to that emitted by the radar. In order to generate false targets whose range is controllable, the deceptive waveform must be synchronised to the radar. For the case of a simple pulse radar, the deceptive waveform is relatively easy to generate. This is especially true if one neglects the coupling between the range rate as calculated by range updates and that calculated from the doppler of the false targets.

It is more difficult to generate false targets when the radar uses pulse compression. The ECM waveform must be matched to the pulse compression filter or it will not be compressed into a target like return by the radar. It is usually not feasible for the ECM set to generate the required waveform. Instead, a replica of the radar transmission is stored in a suitable memory[2] and this waveform is emitted back at the radar.

In general, a pulse compression radar will be more robust in noise ECM then a conventional pulse radar. A pulse compression filter performs a coherent integration of a number of sub-pulses in the code. This processing can provide significant improvement in the signal to noise ratio (SNR). For example, the value of the SNR might be -5 dB for the uncompressed waveform and 15 dB for the peak of the compressed pulse. This coding is essential in low peak power/high duty cycle transmitters.

PERFORMANCE IN INTERFERENCE

The performance of DPC in the presence of three different types of interference is

illustrated in Figures 1-6. Although some of this interference could be generated by other radar sets, in the present context it is assumed to represent various types of ECM. Figures 1 and 2 apply to uncorrelated Gaussian noise for SNRs of 10 dB and 0 dB. It is noted that although the expanded waveform is completely buried in the noise for the 0 dB case, the peak of the compressed waveform is clearly detectable.

The effect of pulse interference on the same P3 code[3,4] is shown in Figures 3 and 4. A train of 200 ns rectangular pulses with a 10% duty cycle is assumed and results are given for SNRs of 10 dB and 0 dB. Again, the peak of the compressed pulse is clearly detectable.

Lastly, Figures 5 and 6 present the effect of an interfering P4 code[3,4] of the same length as the desired P3 code. The PDC

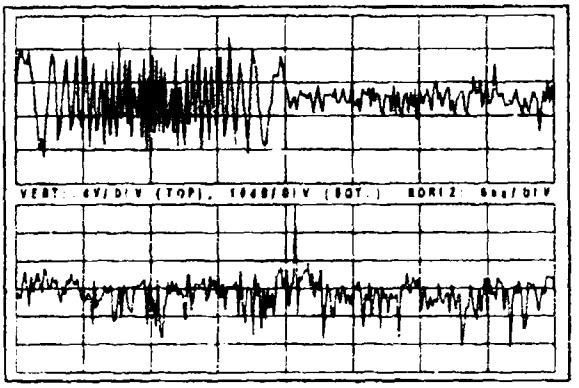

Figure 1. Expanded and compressed waveforms for a P3 code of length 128 imbedded in Gaussian noise. SNR=10 dB.

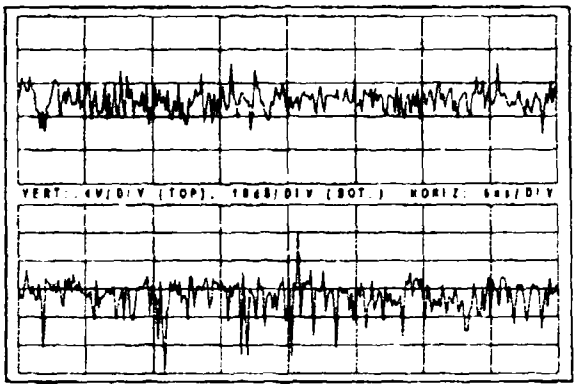

Figure 2. Expanded and compressed waveforms for a P3 code of length 128 imbedded in Gaussian noise. SNR=0 dB.

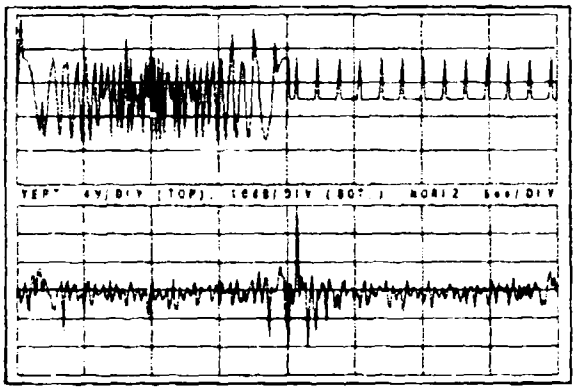

Figure 3. Expanded and compressed waveforms for a P3 code of length 128 imbedded in pulse interference. The interference has a 10% duty cycle and SNR=10 dB.

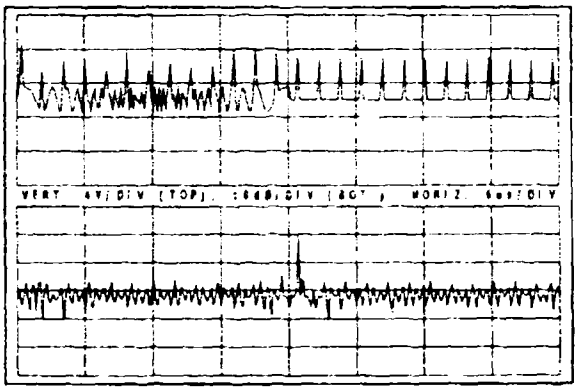

Figure 4. Expanded and compressed waveforms for a P3 code of length 128 imbedded in pulse interference. The interference has a 10% duty cycle and SNR=0 dB.

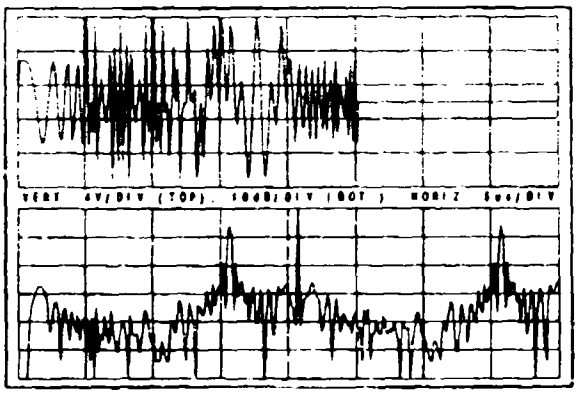

Figure 5. Expanded and compressed waveforms for a P3 code of length 128 in the presence of an interfering P4 code of equal length. SNR=0 dB.

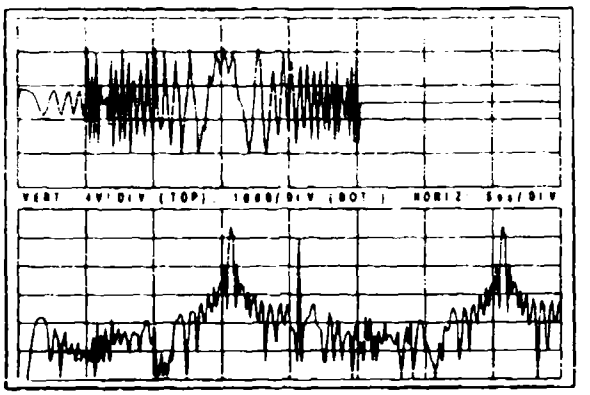

Figure 6. Expanded and compressed waveforms for a P3 code of length 128 in the presence of an interfering P4 code of equal length. SNR=-10 dB.

filter coefficients are matched to the P3 code and plots are shown for SNRs of 0 dB and -10 dB. The P4 code is not as well suppressed as were the Gaussian and pulse interferences for the same values of SNR. This is because the P4 and P3 codes are partially correlated. The response due to the P4 code consists of two peaks which occur ±12.8 us from the trailing edge of the P4 waveform.

In the ECM context, Figures 1 and 2 are representative of using Gaussian noise as denial ECM. The second figure illustrates that even when the SNR=0 and the transmitted waveform is buried in noise, the peak of the compressed pulse is 15 dB or more above the peak sidelobe level.

The pulse train interference considered in Figures 3 and 4 is characteristic of using a pulse train to perform denial ECM (by trying to raise adaptive thresholds in the radar). It is also representative of using a pulse train as deceptive ECM by trying to generate false targets. The DPC filter is also quite effective in reducing this type of interference.

The P4 code interference presented in Figures 5 and 6 is characteristic of deceptive ECM in which a waveform similar to that emitted by the radar is repeated in order to generate false targets. Since such a code will be partially matched to the DPC filter, it will still generate a detectable output. However, it is noted that this output can have more then one main peak and that these peaks will occur at false ranges. It will be shown later that this fact can be used to help eliminate false targets.

The results presented in the previous figures were for a single transmission of a particular code. In practice, a radar would employ several transmissions to detect a target. If these returns are coherently integrated, the depth of interference suppression will be increased. A longer code can also be used.

PERFORMANCE IN DECEPTIVE ECM

It will be shown that adaptive DPC can be used to counter the effects of repeater jammers. The scenario considered is that of a repeater jammer which stores a replica of the radar's waveform and emits it in order to generate false targets. This is illustrated in Figure 7.

The repeater jammer contains a digital radio frequency memory (DRFM)[5] which can store an accurate replica of the radar waveform. This code is then emitted by the jammer at controlled intervals in an attempt to generate false targets in the victim radar. To negate this, the radar selects a different code on each transmission. On the n^{th} pulse repetition interval (PRI), the radar receives the current code from skin returns and an amplified version of the $(n-1)^{th}$ code from the repeater jammer. The technique is to select codes that minimise detection when a code is received to which the DPC filter is not currently matched.

This technique will only prevent the jammer from generating false targets at ranges between itself and the radar. It is felt that this scenario is of interest from an operational viewpoint. Consider an aircraft which fires one or more missiles at a target. The generation of false missile targets in conjunction with the attack would make it more difficult to identify the threat.

Waveform Optimisation

A burst of pulses is transmitted and a different code is used for each pulse. The returns from each pulse are then combined and compared to a threshold. It is desired to select codes which minimise the detection of false targets in the combined output.

A rigorous formulation of this problem would be to write an expression for the output of the DPC filter in which the parameter(s) of the code are varied from pulse to pulse. The individual output for each pulse in the burst is then combined. An optimisation procedure would then be used to maximise the signal to interference ratio (SIR) by varying the code parameter(s).

The above methodology is unwieldy. Instead, an ad hoc solution is used. Two different coding techniques are evaluated to generate the required waveforms. The first consists of a series of "V" chirps where the ratio of the up and down chirp portions is varied randomly from pulse to pulse. The other method is to generate a set of chirps in which the start frequency is varied randomly from pulse to pulse. The frequency versus time characteristics of the two schemes is shown in Figure 8.

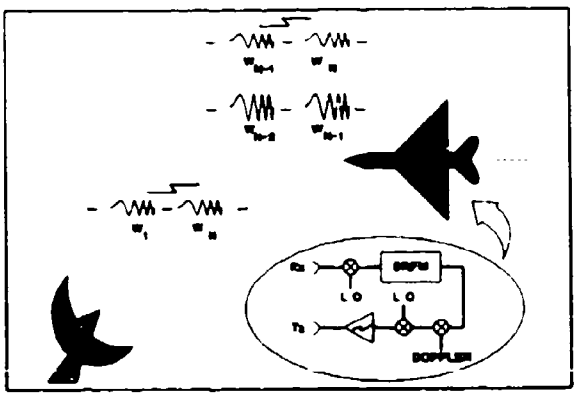

Figure 7. Illustration of a DRFM based repeater jammer attempting to generate false targets against adaptive DPC.

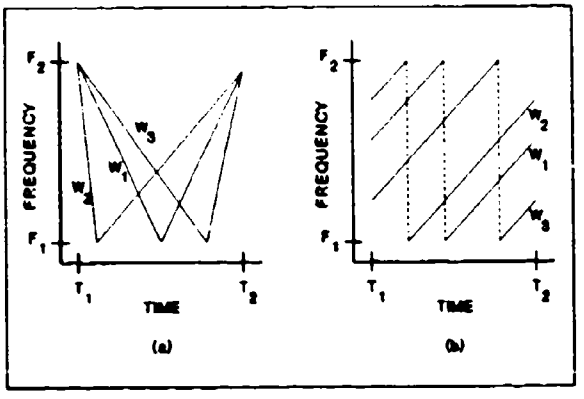

Figure 8. Frequency versus time relation for the sets of "V" chirps (a) and linear chirps (b) that were evaluated.

A computer simulation was performed to evaluate the two techniques. It was assumed for the simulation that two waveforms are simultaneously received. The first waveform represents a skin return from a target; the DPC filter is matched to this code. The other return is an amplified replica of the previous code and represents the ECM. The filter is not matched to this code. This is illustrated in Figure 7 by the waveforms W_{n-1} and W_{n-2}.

The output of the DPC filter is plotted in Figures 9 and 10 for the two techniques. In each case, three different snapshots of the output are shown, each corresponding to a different (random) relationship between the current and previous code. The true target is located at delay unit 128 and the ECM or interference was assumed to be 20 dB stronger then the skin return.

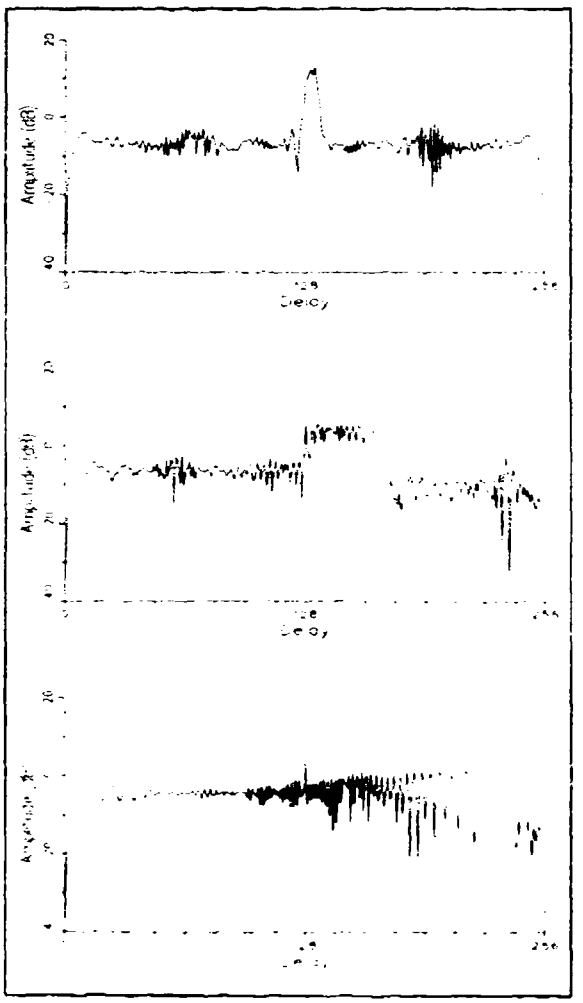

Figure 9. Output of DPC filter for three successive pulses. The signal to interference ratio is -20 dB. A different "V" chirp waveform of length 128 is randomly selected for each transmission.

It is noted that the compressed waveforms for the two schemes exhibit different characteristics. In general, the sidelobe level for the "V" chirps appear to form broad plateau(s) which sometimes tend to mask the peak due to the true target. The sidelobe level for the linear chirps are more characteristic of those for a single chirp with the response to the interfering code usually showing up as two broader spurious peaks. These characteristics are due to the different frequency versus time relationships for the two schemes. For the "V" chirp, Figure 8 illustrates that the slopes of this relation for the matched and interfering waveforms are never parallel. In contrast, these slopes are parallel for the linear chirps. This characteristic gives rise to the dual peak response for the interfering code in this case.

The peak due to the true target always occurs at the same delay in the output of the DPC filter, while those due to the interference are randomly distributed. This fact is exploited by coherently integrating the output over a batch of pulses.

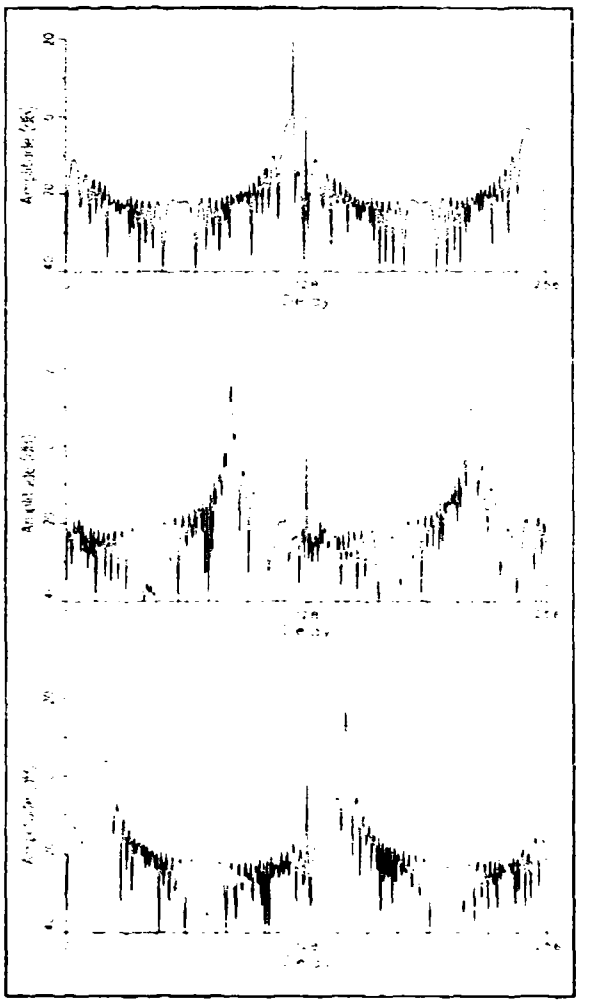

Figure 10. Output of DPC filter for three successive pulses. The signal to interference ratio is -20 dB. A different linear chirp waveform of length 128 is randomly selected for each transmission.

Coherent integration causes the weaker returns due to the skin return to integrate to a strong peak, while spreading out the energy due to the ECM. The improvement required in SIR for target detection is obtained by using an appropriate batch size.

In order to compare the relative performance of the two waveforms, the output of the DPC filter was coherently integrated. A batch of 100 pulses was assumed and the simulation was run for SIR values of 0 dB, -10 dB, -20 dB and -30 dB. The output of the DPC filter after integration of these pulses is plotted in Figure 11 for the set of "V" chirps and in Figure 12 for the set of linear chirps.

It can be seen from these two figures that the true target can still be detected by both methods when the ECM is 30 dB stronger than the skin return (SIR = -30 dB for a single pulse). However, the probability of detection is less than .85 for this value of SIR as the corresponding SIR after integration is only 18 dB for the linear chirp. For a single pulse SIR of -20 dB, the integrated SIR is 25 dB.

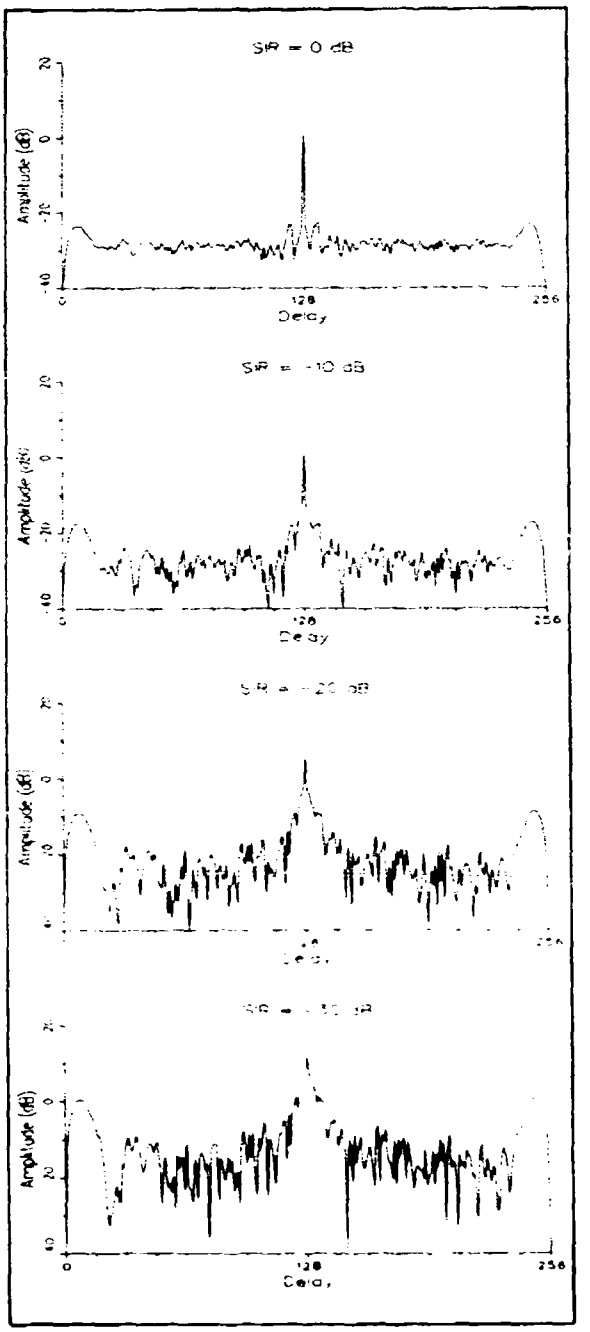

Figure 11. Coherent integration of a burst of 100 pulses at the output of the DPC filter. The results are plotted for SIR values of 0 dB, -10 dB, -20 dB and -30 dB. A set of randomly selected "V" chirps of length 128 is used.

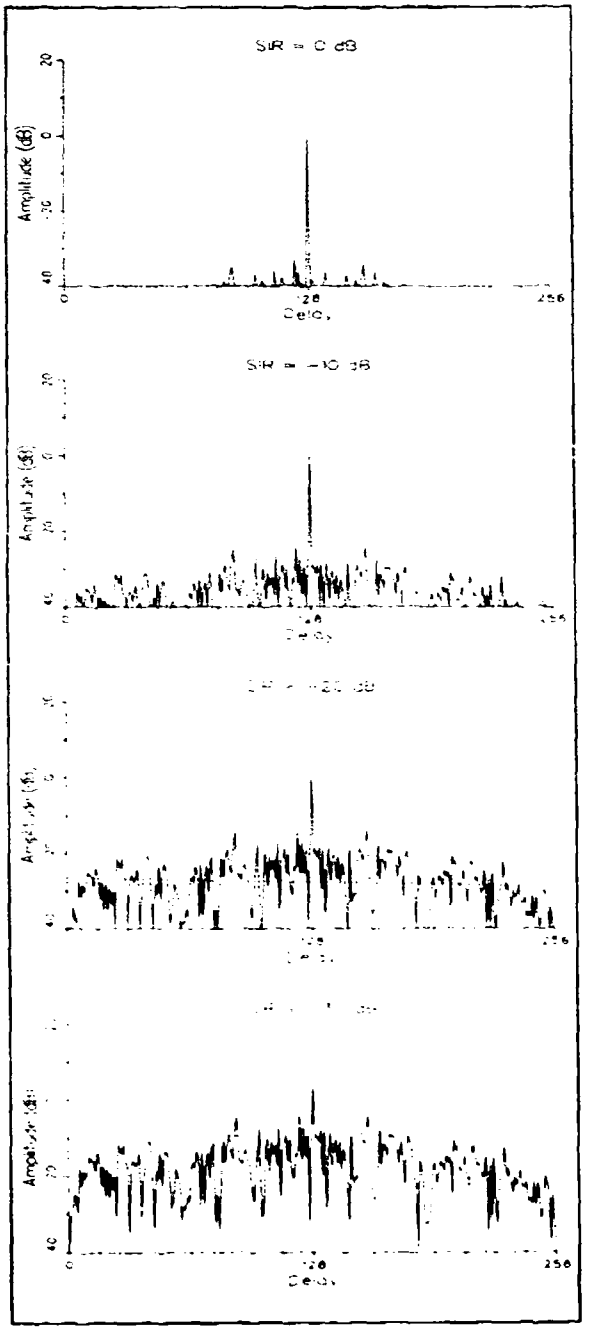

Figure 12. Coherent integration of a burst of 100 pulses at the output of the DPC filter. The results are plotted for SIR values of 0 dB, -10 dB, -20 dB and -30 dB. A set of randomly selected linear chirps of length 128 is used.

This yields a probability of detection in excess of .95 for a Swerling 1-2 target at a false alarm probability of 10^{-6}. The above calculation assumes that the ECM energy has a normal probability distribution. This is probably justified if their are enough pulses in the burst.

If the cross section of the false targets is made much larger than that of real targets, the element of deception is lost. It is thus unlikely that values of SIR less than -20 dB would be encountered.

The peak tends to have a broad pedestal for the "V" chirp waveforms when the SIR is less than 0 dB. In contrast, the peak for the linear chirp waveforms remains narrow right down to the sidelobe level. This characteristic might be more suitable for use with an automatic detection algorithm.

DPC IMPLEMENTATION

Implementation consists of both waveform generation and compression. The desired code must first be generated in digital format and converted to an analogue signal suitable for subsequent up-conversion. On reception, the digitised radar returns must be processed in a digital matched filter which compresses the transmitted waveform.

The desired waveforms are calculated off line and are stored in a PROM whose address lines are connected to a counter. The waveform is clocked into a digital to analogue converter (DAC) whose output is up-converted to IF. Control lines are provided to select one of several waveforms stored in the PROM. A limiting amplifier along with appropriate filters ensure a constant amplitude signal of good spectral purity. The time-bandwidth product of the code is a function of the number of stored samples and the clock rate. This is illustrated in Figure 13.

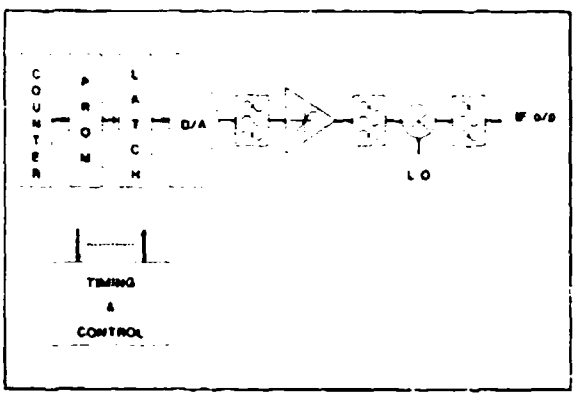

Figure 13. Conceptual diagram of the DPC waveform generation circuitry.

On reception, the radar returns are digitised into I and Q channels for processing by the pulse compression filter. The present implementation of the filter consists of sixteen digital correlator VLSI ICs configured into four parallel channels to processes real, imaginary and cross term products[8]. A micro-processor based controller provides the means for changing the filter coefficients on a pulse by pulse basis, along with providing a BITE function. This architecture yields a filter which is highly adaptable. A conceptual diagram of the DPC filter is shown in Figure 14.

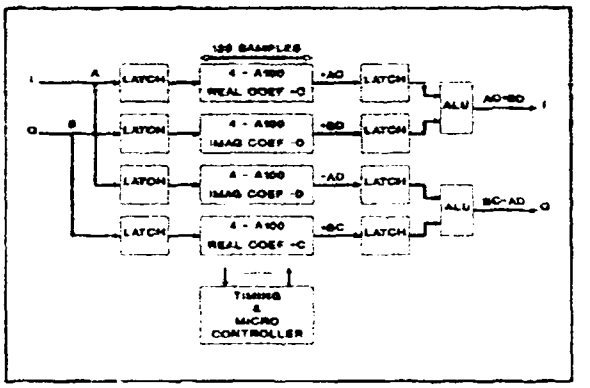

Figure 14. Conceptual diagram of the pulse compression filter and control circuitry.

An actual radar digital signal processor would contain additional circuitry to implement functions such as doppler processing, adaptive thresholding, etc. These functions are not illustrated in Figure 14. A photograph of the pulse compressor hardware is shown in Figure 15.

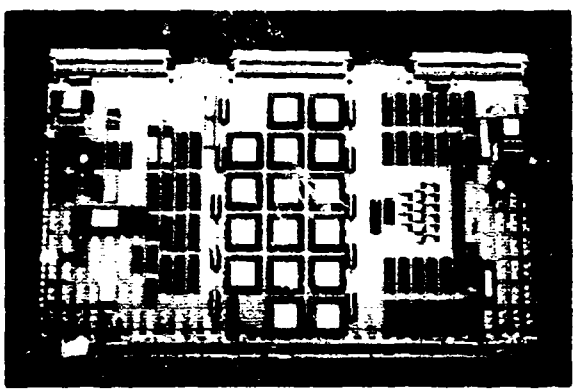

Figure 15. Photograph of the pulse compression filter and control circuitry.

CONCLUSIONS

The ECCM advantages of adaptive DPC were discussed. Examples of this type of waveform agility as a counter to both ESM and ECM systems were given. In the case of ECM, both denial and deceptive ECM tactics were considered. It was demonstrated that adaptive DPC can be used as an effective counter-counter measure against repeater jammers which store an accurate replica of the radar signal.

An experimental digital pulse compressor has been built and used to evaluate some of the techniques discussed above. The use of VLSI digital correlator ICs permits a compact implementation of the DPC filter. This implementation makes it now feasible to use adaptive DPC in an airborne MPR where space is at a premium.

At present, experimental evaluation has consisted of injecting digitised waveforms into the DPC filter in real time. An IF section and digital demodulator is presently under construction. Once completed, this

unit will be used to study the effects of imperfections in the analogue path on the performance of the DPC waveforms. It is also proposed to implement a two dimensional filter which would simultaneously perform pulse compression and doppler processing.

REFERENCES

[1] G.R. Painchaud, J.A.H. McKenzie, M. Blanchette and A. Voy, "An Experimental Adaptive Digital Pulse Compression Subsystem For Multi-Function Radar Applications", Proc. IEEE International Radar Conference, pp. 153-158, May 1990.

[2] L.B. Van Brunt, "Applied ECM", vol. 1, Dunn Loring, Va.: EW Engineering Inc., July 1980.

[3] B.L. Lewis and F.F. Kretschmer, "A New Class of Polyphase Pulse Compression Codes and Techniques", IEEE Trans. on Aerospace and Electronic Systems, vol. AES-17, no. 3, pp. 364-372, May 1981.

[4] B.L. Lewis and F.F. Kretschmer, "Linear Frequency Modulation Derived Polyphase Pulse Compression Codes", IEEE Trans. on Aerospace and Electronic Systems, vol. AES-18, no. 5, pp. 637-641, September 1982.

[5] E. Koos, "Digital RF Memories Enter Second Decade", Journal of Electronic Defense, pp. 49-51, August 1985.

[6] H. Yassaie, "Correlation and Convolution with the IMS A100", INMOS Corporation IMS A100 Application Note 3, June 1986.

ACKNOWLEDGEMENT

The experimental DPC filter described in this paper was constructed by the Radar Division of the Canadian Marconi Company in cooperation with the Defence Research Establishment Ottawa.

Discussion

Mr Buering, Ge

Obviously one uses the same code on many pulses to be able to suppress clutter and to use Doppler filtering. Did you take these things into account in your simulation?

Author's Reply

No, we did not carry out such analysis. But what we shall do later on (is to)... get rid of the Doppler effect and maybe we shall use also a two-dimensional filter so that we can do both at the same time — that is, the pulse compression and Doppler effect supression.

Prof. P.W.Baier

The question is related to the presented digital impulse compression circuit. What is the resolution of the A/D converters (bits for input and reference signals)? What is the clock frequency?

Author's Reply

The circuits can carry out actuations of 16-bits with the radar signals and also 16 bits for the coefficients with 2.5 MHz frequency. Now for 10 MHz frequency we shall use only 4 bits for the filter coefficients. The analogue output — I think it is 10 bits. It's just to give you an idea of the type of calculation...It is not always necessary to carry out such calculations.

Mr Weis

Is the correlator a special-purpose computer or is it procured from the shelf?

Author's Reply

It has been built by INMAS. It is a correlator for 32 bits for carrying out complex operations. It is one of (its) applications — Digital pulse compression is one of the uses of such a computer.

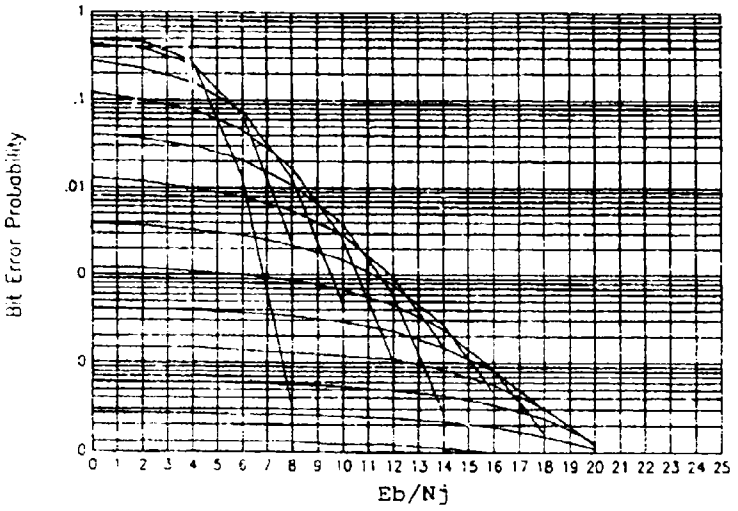

Figure 3. DPSK Rate 1/2, K = 7, Hard Decision, L = 16, M = 384

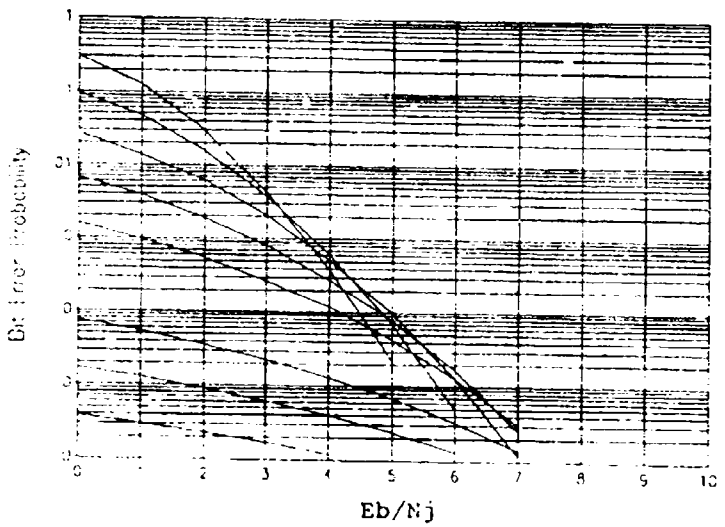

Figure 4. BPSK Rate 1/4, Soft Decision, L = 16, M = 384

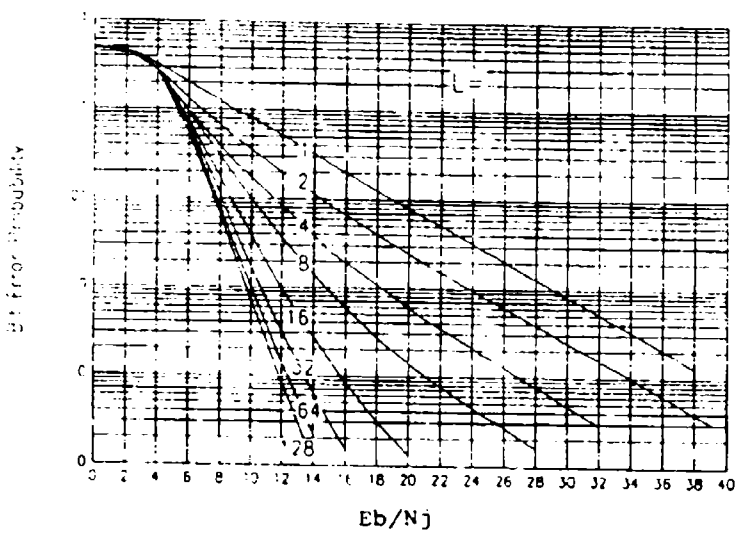

Figure 5. DPSK Rate 1/2, K = 7, Hard Decision, M = 384

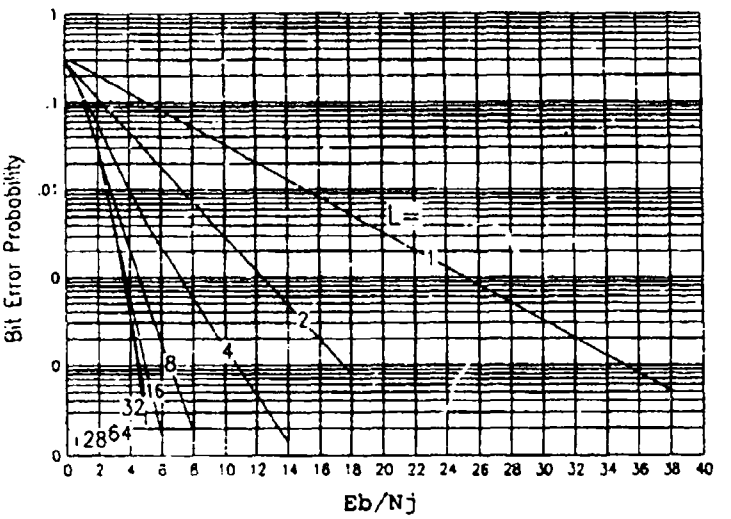

Figure 6. BPSK Rate 1/4, Soft Decision, M = 384

Discussion

B.Jackson, Thorn-EMI, UK

What parameters were assumed for the soft-decision coding modulation detection criteria?

Author's Reply

When I say 'soft decisions', that means we are actually quantizing the demodulator output into more than one bit. If I say 'hard decisions', that's one bit. When I say 'soft decisions' I usually mean 3-bit quantization. In order to maximize the advantage of soft decisions you can get by having 3-bit quantization you have to have a....reasonably good gain control mechanism, especially in a poor fading environment or in a jamming environment. Dr Olsen's assumption here when he goes through the analysis is that these things can be done (and that) all the quantization and dynamic range problems have been taken care of.

Dr B.Felstead, CRC, Canada

Would you explain in more detail how the diversity was accomplished, especially at the receiver?

Author's Reply

Diversity may not be the right word to use. It may have confused people here... We have assumed that there are 384 bits — I believe that's what Dr Olsen did — there are 384 bits per block. The message size is 348 bits. The message is blocked: the block is divided into smaller chunks, of hops. If all the message is transmitted in the one hop then we call that diversity of one. And if the message is divided into two hops — and sent on two different hops — we call that diversity of two.... You're not talking about having any kind of time diversity, having multiple links (or) having different kinds of interleavers....

Dr M.Safak, SHAPE Technical Centre, NL

Could you comment on the performance of BPSK and DPSK systems relative to FSK systems in a fast Rayleigh fading environment?

Author's Reply

In my second paper I'll show you a chart of fast-fading performance. What he meant by fast fading, I assume, is when the fading rate is faster than the bit period. I think that's what you mean by fast fading. On the FSK type of waveform, fast fading improvements can be gained if you have the tone spacing increased, in other words if you (make) the signal bandwidth... very large. On the DPSK and BPSK, as I'm going to show you later, I can get pretty close performance (between the two). If you compare (DPSK and BPSK) with FSK with a larger and larger (tone) spacing then their performance is inferior, but if you talk about FSK with minimum spacing, the performance is reasonably similar

Concatenated Coding with Two Levels of Interleaving (u)

Samuel Lim, Member of Technical Staff

Michael Newhouse, Member of Technical Staff

The Aerospace Corporation

P. O. Box 92957

M4/937

Los Angeles, CA 90009 USA

Abstract

(u) This paper documents a performance evaluation of an electronic counter counter measure (ECCM) communication system in a worst-case partial-band noise and partial-band tone jamming scenario. The ECCM communication system is composed of two levels of channel coding (concatenated coding) and two levels of interleaving. An analysis has been performed for a concatenated code consisting of either a Reed-Solomon or a convolutional outer code and a convolutional inner code, and the decoded bit error rates for typical binary modulation schemes (BPSK and DPSK) have been obtained. The performance of these coded waveforms has been compared with convolutionally encoded systems with respect to the required E_b/N_J to achieve an overall bit error rate of 10^{-5}. The results demonstrate a significant coding gain achievable from systems which adopt concatenated coding.

1 NOTATIONS (u)

(u) Below is a brief description of notations used:

n	:	R-S codeword size in symbols
m	:	Number of bits per R-S symbol
t	:	R-S codeword error correction capabilities in symbols
R_I	:	Inner Code Rate
R_O	:	Outer Code Rate
R	:	Code Rate (= $R_I R_O$ for concatenated code)
$p_b(e)$	:	Decoded bit error probability
$P(e)$	:	Decoded symbol error probability
$p_{vb}(e)$	:	Bit error probability at the output of the inner Viterbi decoder
$P_v(e)$	:	Symbol error probability at the output of the inner Viterbi decoder
$p_{cb}(e)$	:	Hard decision channel bit error probability
W_{ss}	:	Spread spectrum bandwidth
p	:	Fraction of the spread spectrum bandwidth jammed
N_J	:	Jammer noise density normalized to W_{ss}
E_{cb}/N_J	:	Channel bit energy to jammer noise density ratio
E_b/N_J	:	Information bit energy to jammer noise density ratio

2 INTRODUCTION (u)

(u) Concatenated coding uses two levels of coding to achieve its required system bit error rate (BER) performance objective. The inner code, defined as the code which interfaces with the channel, corrects most of the random channel errors. The outer code reduces errors further to a desired BER level. A benefit from selecting a concatenated code rather than a single coding operation is the possibility that for the identical required BER and available signal-to-noise ratio, an overall encoder/decoder implementation of less complexity can be achieved. Or concatenated coding can improve a performance of an existing communication system [1].

(u) A concatenated coding scheme commonly consists of a soft decision Viterbi decoded binary convolutional inner code combined with either a hard decision Viterbi decoded binary convolutional outer code or a Reed-Solomon (R-S) block outer code. The main reason that soft decision convolutional codes are usually used as inner codes is that they provide excellent error correction capabilities against random channel errors. Bit interleaving of channel bits is provided to randomize bursty errors that can occur in certain stressed environments. Since only hard quantized data is available at the output of the inner Viterbi decoder, hard decision convolutional codes are logical choices for the outer codes. But because the errors out of the Viterbi decoder tend to occur in bursts, a bit interleaver has to be placed in between the inner and the outer code to randomize the inner decoder output bit errors. An alternative is to use R-S block codes whose symbols are formed from m-bit ($m \geq 2$) segments of the binary data stream. R-S block codes are particularly useful for burst error correction. However, if the burst out of the Viterbi decoder is in the order of the R-S codeword length, the outer code performance will be severely degraded unless a m-bit symbol interleaver is placed in between the inner and the outer code to randomize symbol errors. The necessity for symbol interleaving can be explained by the general property of non-binary block codes of which R-S code is a member. R-S code performance solely depends on the number of symbol errors in a codeword. For a large number of symbol errors within a single codeword, the R-S code performance can be catastrophically degraded. Thus, a symbol interleaver is used to distribute bursts of symbol errors among several codewords to reduce the probability that symbol errors within a codeword exceed the error correction capability of the R-S decoder. The block diagram of a concatenated coding system is shown in fig. 1.

(u) In this paper, the decoded BER for BPSK and DPSK modulated waveforms using $R = 1/4$ concatenated codes will be studied. Both BPSK and DPSK modulations were selected in order to be representative of both coherent and non-coherent waveforms. The results will be compared against that of $R = 1/2$, $R = 1/3$, and $R = 1/4$, $K = 7$ Viterbi decoded convolutional code in both partial band noise and partial band tone jammed channels. The concatenated code consists of either a $R_I = 1/2$ inner code combined with a $R_O = 1/2$ outer code or a $R_I = 1/3$ inner code combined with a $R_O = 3/4$ outer code. The inner code is always a $K = 7$, 3-bit soft decision Viterbi decoded convolutional code. For convenience, the R-S outer code has 384 baseband bits per codeword. The hard decision Viterbi decoded outer code has either $K = 7$ for $R_O = 1/2$ or $K = 9$ for $R_O = 3/4$. The overall code rate of concatenated codes is always $R = 1/4$.

2.1 CHANNEL DESCRIPTION (u)

(u) Below is a brief description of the noise or tone jammed channels. For either case, the BPSK and the DPSK waveform carriers are assumed to be slowly frequency hopping.

2.1.1 PARTIAL BAND NOISE JAMMER (u)

(u) A partial band noise jammer can be described as a Gaussian noise jammer whose total power is restricted to a fraction $p(0 < p \leq 1)$ of the spread spectrum bandwidth W_{ss}. As seen in fig. 2, the jamming noise power is assumed to be spread uniformly over the restricted bandwidth $W_J = pW_{ss}$ resulting in an increased power density and a correspondingly degraded signal-to-jamnuer ratio in the jammed band. The jammer is assumed to occasionally move the jammed band within W_{ss} so as to prevent band avoidance countermeasures [2].

2.1.2 PARTIAL BAND TONE JAMMER (u)

(u) As seen in fig. 3, a partial band tone jammer spreads its available jamming power into multiple tones across a fraction $p(0 < p \leq 1)$ of the spread spectrum bandwidth W_{ss}. The jamming tones are spread with uniformly distributed tone spacing, ΔJ, over $W_J = pW_{ss}$ resulting in an increased power per tone relative to full band jamming and correspondingly a degraded signal-to-jammer ratio (SJR) in the jammed band. Again, the jammer is assumed to occasionally move the jammed band within W_{ss} so as to prevent band avoidance countermeasures [2]. In this paper, $\Delta J = 2$ Hz/bits/sec to guarantee that at most 1 jammer tone can reside within the signal's null-to-null bandwidth. Furthermore, non-coincidental jamming, where the jammer tone is uniformly distributed within the signal's null-to-null bandwidth, is assumed because the carrier hop granularity is much finer than the signal bandwidth.

3 ASSUMPTIONS (u)

(u) In order to reduce the complexity of the problem, several critical assumptions were made. First, the depth of interleaving for both the inner bit interleaver and the outer m-bit symbol interleaver was assumed to be sufficiently larger than the channel bit error burst length and the Viterbi decoded m-bit symbol error burst length respectively to insure independent channel bit errors and independent Viterbi decoded symbol errors. Note that m = 1 for binary convolutional outer code. Second, although symbol interleaving was performed, it was assumed that the bit errors out of the Viterbi decoder were uniformly distributed instead of in bursts regardless of the type of coding and demodulator decision schemes. This has no effect on the $p_b(e)$ performance if the outer code is a hard decision convolutional code since bit deinterleaving is performed prior to outer decoding. But for a R-S outer code where symbol interleaving is performed prior to R-S decoding, this amounts to an over-estimation of $P_v(e)$ out of the Viterbi decoder for a given $p_{vb}(e)$, since the bit error patterns actually do occur in bursts. However, this assumption will provide a sufficiently tight upper bound on the $p_b(e)$ performance. Furthermore, the relationship between $P(e)$ and $p_b(e)$ was assumed to follow a 2^m-ary symmetric memoryless channel model. Finally, perfect jammer side information (JSI) was assumed to exist. With this knowledge, a 3-bit quantization algorithm can be found for BPSK and DPSK which provides a $p_{cb}(e)$ vs. $p_{vb}(e)$ transfer function in optimized partial

The $p_{cb}(e)$ vs. E_{cb}/N_J for DPSK modulated waveform in optimum partial band noise jamming is given by [2]

$$P_{cb}(e) = \begin{cases} 0.184\left(\frac{E_{cb}}{N_J}\right)^{-1} & \frac{E_{cb}}{N_J} \geq 0.0\text{dB} \\ \frac{1}{2}\exp\left(-\frac{E_{cb}}{N_J}\right) & \frac{E_{cb}}{N_J} < 0.0\text{dB} \end{cases} \tag{5}$$

In case of optimum partial band tone jamming,

$$P_{cb}(e) = \begin{cases} 0.182\left(\frac{E_{cb}}{N_J}\right)^{-1} & \frac{E_{cb}}{N_J} \geq 1.98\text{dB} \\ \frac{1}{4\pi}\int_{-2\pi}^{2\pi}\frac{1}{2\pi}\int_{0}^{2\pi}\frac{1}{2}[u(-\cos|\theta_1(\phi,\varphi)|) + u(\cos|\theta_2(\phi,\varphi)|)]d\phi d\varphi & \frac{E_{cb}}{N_J} < 1.98\text{dB} \end{cases} \tag{6}$$

where $u(t)$ is the unit step function defined by

$$u(t) = \begin{cases} 1 & t \geq 0 \\ 0 & t < 0 \end{cases} \tag{7}$$

$$\cos(|\theta_1(\phi,\varphi)|) = \frac{\gamma^2(\varphi) + \cos(\varphi) + \gamma(\varphi)[\cos(\varphi+\phi) + \cos(\phi)]}{\sqrt{[\gamma^2(\varphi) + 1 + 2\gamma(\varphi)\cos(\varphi+\phi)][\gamma^2(\varphi) + 1 + 2\gamma(\varphi)cos(\phi)]}} \tag{8}$$

and

$$\cos(|\theta_2(\phi,\varphi)|) = \frac{\cos(\varphi) - \gamma^2(\varphi) + \gamma(\varphi)[\cos(\varphi+\phi) + \cos(\phi)]}{\sqrt{[\gamma^2(\varphi) + 1 - 2\gamma(\varphi)\cos(\varphi+\phi)][\gamma^2(\varphi) + 1 + 2\gamma(\varphi)cos(\phi)]}} \tag{9}$$

where

$$\gamma^2(\varphi) = \frac{E_b}{2N_J}\left(\frac{\varphi/2}{\sin(\varphi/2)}\right)^2 \tag{10}$$

The 3-bit soft decision Viterbi decoded convolutional code bit error probability in optimized partial band noise and tone jamming can be acquired by inserting $p_{cb}(e)$ of eqs. 1 - 10 into the $p_{vb}(e)$ vs. $p_{cb}(e)$ transfer function. The transfer function is empirically given by [1],

$$\log_{10}(p_{vb}(e)) = 8.48\log_{10}(p_{cb}(e)) + 6.26 \quad \text{BPSK}, \quad R_I = 1/2 \tag{11}$$

$$\log_{10}(p_{vb}(e)) = 6.73\log_{10}(p_{cb}(e)) + 4.00 \quad \text{DPSK}, \quad R_I = 1/2 \tag{12}$$

$$\log_{10}(p_{vb}(e)) = 12.2\log_{10}(p_{cb}(e)) + 7.45 \quad \text{BPSK}, \quad R_I = 1/3 \tag{13}$$

$$\log_{10}(p_{vb}(e)) = 9.45\log_{10}(p_{cb}(e)) + 5.34 \quad \text{DPSK}, \quad R_I = 1/3 \tag{14}$$

(u) Consider the case of C+RS concatenated code. Assuming independent bit errors,

$$P_v(e) = 1 - (1 - p_{vb}(e))^m \tag{15}$$

Now, $P(e)$ is also related to $P_v(e)$ by an upper bound expression as long as the symbol errors are independent. This is given by [1]

$$P(e) \leq \frac{1}{n}\sum_{j=t+1}^{n}\binom{n}{j}(j+t)P_v(e)^j[1 - P_v(e)]^{n-j} \tag{16}$$

This expression also applies to both extended and shortened R-S codes. The overall bit error probability is expressed as

$$p_b(e) = \frac{2^{m-1}}{2^m - 1}P(e) \tag{17}$$

(u) In case of C+C concatenated code, the hard decision Viterbi decoded convolutional code transfer function is empirically given by

$$\log_{10}(p_b(e)) = 5.43\log_{10}(p_{vb}(e)) + 4.43, R_O = 1/2 \tag{18}$$

and

$$\log_{10}(p_b(e)) = 3.26\log_{10}(p_{vb}(e)) + 3.55, R_O = 3/4 \tag{19}$$

band noise and optimized partial band tone jammed channels that is essentially equivalent to that of an AWGN channel.

4 ANALYSIS (u)

(u) From the assumptions above, a reasonable upperbound for the $p_b(e)$ vs. E_b/N_J performance can be acquired for the convolutional code concatenated with a R-S code (C+RS) and an exact $p_b(e)$ vs. E_b/N_J performance can be empirically derived for the convolutional code concatenated with a convolutional code (C+C).

(u) A shortened R-S code or an extended R-S code may have to be selected to meet the combined $R = 1/4$ criterion. A shortened R-S code is created by deleting a portion of the information symbols while maintaining all of the parity check symbols of a standard R-S code. An extended R-S code is created by adding as many as 2 additional information symbols to a standard R-S code while maintaining the same number of parity check symbols [3]. Denote a R-S code by RS$(n, n-2t, m)$. For an R-S code with 384 baseband bits per codeword, the two R-S codes for $R_O = 1/2$ and $R_O = 3/4$ R-S are given by RS(96,48,8) and RS(64,48,8) respectively.

4.1 THE BIT ERROR RATE EVALUATION (u)

(u) The decoded bit error rate performance, $p_b(e)$ vs. E_b/N_J, for concatenated codes will be evaluated in this section. The 3-bit soft decision Viterbi decoded convolutional inner code bit error probability in AWGN for $R_I = 1/2$ and $R_I = 1/3$ is available from simulation. By assuming perfect JSI, $p_{cb}(e)$ in optimized partial band noise and optimized partial band tone jamming can be derived by first evaluating the uncoded bit error probability for BPSK and DPSK in optimized partial band noise and optimized partial band tone jamming. The $p_{cb}(e)$ vs. E_{cb}/N_J performance of these uncoded waveforms in optimum noise and tone jamming is summarized below:

(u) The channel errors are assumed to occur strictly due to jamming. The $p_{cb}(e)$ vs. E_{cb}/N_J for BPSK modulated waveform in optimum partial band noise jamming is given by [2]

$$P_{cb}(e) = \begin{cases} 8.625 \times 10^{-2} \left(\frac{E_{cb}}{N_J}\right)^{-1} & \frac{E_{cb}}{N_J} \geq -1.5\text{dB} \\ Q\left(\sqrt{\frac{2E_{cb}}{N_J}}\right) & \frac{E_{cb}}{N_J} < -1.5\text{dB} \end{cases} \tag{1}$$

where

$$Q(x) = \int_x^\infty \frac{1}{2\pi} \exp\left(-\frac{y^2}{2}\right) dy \tag{2}$$

In case of optimum partial band tone jamming,

$$P_{cb}(e) = \begin{cases} 9.134 \times 10^{-2} \left(\frac{E_{cb}}{N_J}\right)^{-1} & \frac{E_{cb}}{N_J} \geq -0.8\text{dB} \\ \frac{1}{2}\int_{-1}^{1} g\left(\frac{E_{cb}}{2N_J}, x\right) dx & \frac{E_{cb}}{N_J} < -0.8\text{dB} \end{cases} \tag{3}$$

where

$$g(y,x) = \begin{cases} \frac{1}{\pi}\cos^{-1}\left(\sqrt{y}\frac{\pi x}{\sin(\pi x)}\right) & y < \left[\frac{\sin(\pi x)}{\pi x}\right]^2 \\ 0 & y \geq \left[\frac{\sin(\pi x)}{\pi x}\right]^2 \end{cases} \tag{4}$$

$p_b(e)$ is acquired by inserting $p_{ob}(e)$ of eqs. 11 - 12 into eq. 18 and $p_{ob}(e)$ of eqs. 13 - 14 into eq. 19.

(u) The the concatenated coding system information bit energy-to-noise density ratio is given by

$$E_b/N_J = R^{-1} E_{cb}/N_J \tag{20}$$

5 RESULTS (u)

(u) Bit error probability performance of the four $R = 1/4$ concatenated codes in optimized partial band noise and tone jamming have been obtained from the analysis of Section 4. The four concatenated codes are soft decision, $R_I = 1/2$, $K = 7$ Viterbi decoded convolutional code combined with either RS(96,48,8) block code or hard decision, $R_O = 1/2$, $K = 7$ Viterbi decoded convolutional code, and $R_I = 1/3$, $K = 7$ Viterbi decode convolutional code combined with either RS(64,48,8) block code or hard decision, $R_I = 3/4$, $K = 9$ Viterbi decoded convolutional code. Figs. 4 - 7 display the $p_b(e)$ vs. E_b/N_J curves for the 2 modulation and the 2 channel cases listed below:

	Jammer	Modulation
Case 1:	Partial Band Noise Jammer (PBNJ)	BPSK
Case 2:	Partial Band Tone Jammer (PBTJ)	BPSK
Case 3:	PBNJ	DPSK
Case 4:	PBTJ	DPSK

(u) Each graph depicts a BER comparison of the four $R = 1/4$ concatenated coding scheme. As seen from these graphs, using the lower rate inner code along with the higher rate outer code, as opposed to equal inner and outer code rates, provides superior performance in all options listed above. The performance improvement is very significant for BPSK modulation, 1.5 dB on the average for switching to unequal code rates, and barely noticeable for DPSK modulation, less than one-half dB. The difference between using a R-S inner code as opposed to a convolutional inner code is negligible. However, it must be noted that C+RS concatenated code performances are given in terms of an upperbound $p_b(e)$.

(u) The concatenated code decoded bit error performances at $p_b(e) = 10^{-5}$ are compared against $R = 1/2$, 1/3, and 1/4 convolutional codes [4]. This is shown in fig. 8 in terms of required E_b/N_J to achieve $p_b(e) = 10^{-5}$. As expected, all $R = 1/4$ concatenated codes of either inner/outer code rate combination outperform the $R = 1/2$ Viterbi decoded convolutional code in all cases at $p_b(e) = 10^{-5}$. For example, between 2 and 2.5 dB of coding gain is available by switching from a single $R = 1/2$ Viterbi decoded convolutional code to $R_I = 1/3$, $R_O = 3/4$ concatenated codes. Not as significant a coding gain, between 0.5 and 1 dB for $p_b(e) = 10^{-5}$, is achieved by switching to $R_I = 1/2$, $R_O = 1/2$ concatenated codes from $R = 1/2$ Viterbi decoded convolutional code. Compared with $R = 1/3$ and $R = 1/4$ Viterbi decoded convolutional code, the $R_I = 1/3$, $R_O = 3/4$ concatenated codes perform better at $p_b(e) = 10^{-5}$ for all cases but, the $R_I = 1/2$, $R_O = 1/2$ concatenated codes perform better at $p_b(e) = 10^{-5}$ only for DPSK modulation. About 1 dB of coding gain for BPSK and 1.5 dB of coding gain for DPSK is available for switching from a single $R = 1/3$ Viterbi decoded convolutional code to either $R_I = 1/3$, $R_O = 3/4$ concatenated codes. Conversely, about 1.5 dB of coding gain for BPSK and 1 dB of coding gain for DPSK is available from switching from a single $R = 1/4$ Viterbi decoded convolutional code to either $R_I = 1/3$, $R_O = 3/4$ concatenated codes. Therefore, the average coding gain achieved by switching to $R_I = 1/3$, $R_O = 3/4$ concatenated codes from the best single $R = 1/2$, 1/3, and 1/4 Viterbi decoded convolutional code for BPSK, which is $R = 1/3$, and for DPSK, which is $R = 1/4$, is 1 dB.

(u) As seen from fig. 8, a clear cut advantage for concatenated coding with $R_I = 1/3$ and $R_O = 3/4$ exists for all modulation schemes at $p_b(e) = 10^{-5}$. Furthermore, it is apparent that BPSK requires about 3 to 3.5 dB less E_b/N_J than DPSK to achieve $p_b(e) = 10^{-5}$ in either jamming environments.

6 CONCLUSION (u)

(u) In this paper, the performances of $R = 1/4$ concatenated codes were evaluated for different modulation schemes and optimum partial band jamming environments. Reasonable approximations were made to arrive at results displayed in fig. 8. If greater accuracy is desired, some of the simplifying assumptions cannot be used. Nevertheless, from this study, it is obvious that under the assumed constraints and in optimized partial band noise and tone jamming, concatenated coding provides significant coding gain in terms of required E_b/N_J for BPSK and DPSK. Furthermore the advantage of using a lower rate inner code and a higher rate outer code, as opposed to equal inner and outer code rates, is clear cut for the modulations studied. In conclusion, concatenated coding using $R_I = 1/3$ and $R_O = 3/4$ is very robust for either modulation scheme in optimum partial band noise or tone jammed environments.

References

[1] Odenwalder, J. P., *Error Control Coding Handbook*, Linkabit Corporation, San Diego, Calif., July 15, 1976.

[2] Simon, M. K., Omura, J. K., Scholtz, R. A., and Levitt, B. K., Spread Spectrum Communications (V. II), Rockville, Maryland, Computer Science Press, Inc., 1981.

[3] Sklar, B., Digital Communications, Englewood Cliffs, New Jersey, Prentice Hall, 1988.

[4] Bogusch, R. L., *Digital Communications in Fading Channels: Modulation and Coding*, Mission Research Corporation, Santa Barbara, Calif., March 11, 1987.

ACKNOWLEDGEMENTS

Special thanks go to Mr. A. Yamada and Mr. T. Eng of the Aerospace Corporation for their invaluable assistance.

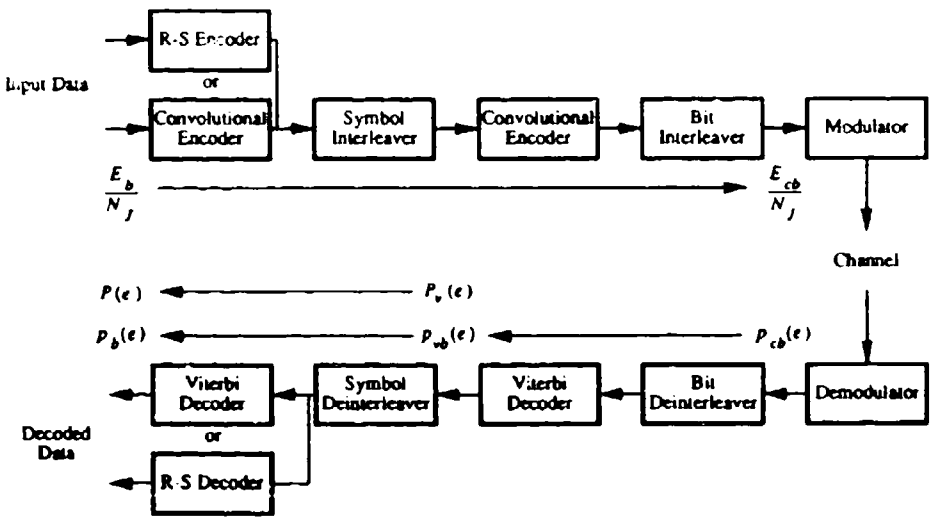

Fig. 1. (u) A concatenated coding system with a Reed-Solomon or convolutional outer code and convolutional inner code.

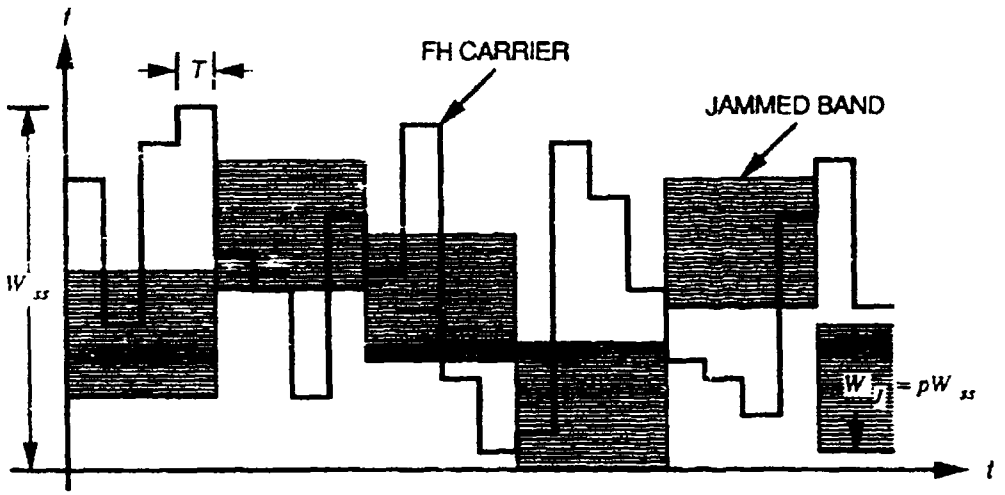

Fig. 2. (u) Partial band noise jamming of FH system: Jammer concentrates power in a fraction of the spread spectrum bandwidth. Carrier frequency changes every symbol period.

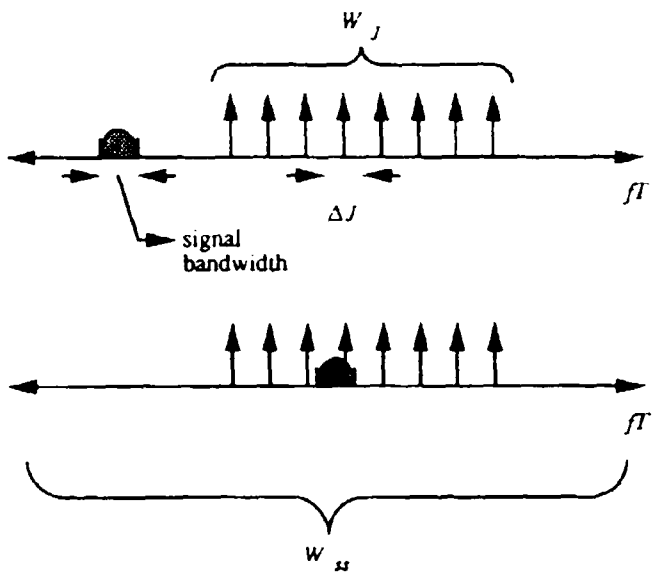

Fig. 3. (u) Partial band tone jamming of FH system: Jammer concentrates power into multiple tones within a fraction of the spread spectrum bandwidth. Carrier frequency changes every symbol period.

(u) BER for Coded BPSK in Optimum Partial Band Noise Jamming

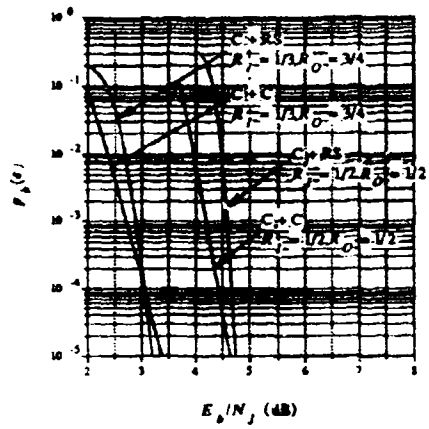

Fig. 4. (u) Probability of bit error for slow frequency hopped BPSK in a optimum partial band noise jamming channel.

(u) BER for Coded BPSK in Optimum Partial Band Tone Jamming

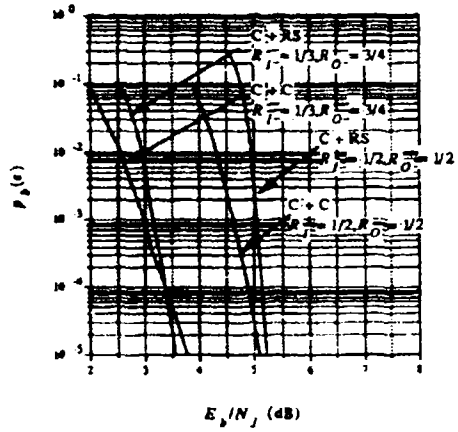

Fig. 5. (u) Probability of bit error for slow frequency hopped BPSK in a optimum partial band tone jamming channel.

(u) BER for Coded DPSK in Optimum Partial Band Noise Jamming

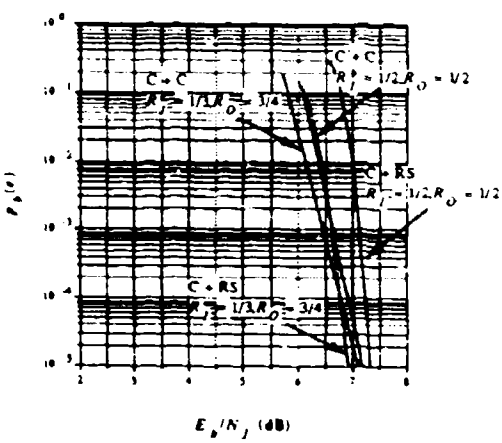

Fig. 6. (u) Probability of bit error for slow frequency hopped DPSK in a optimum partial band noise jamming channel.

(u) BER for Coded DPSK in Optimum Partial Band Tone Jamming

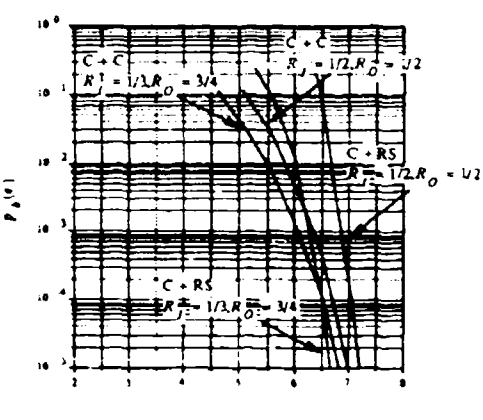

Fig. 7. (u) Probability of bit error for slow frequency hopped DPSK in a optimum partial band tone jamming channel.

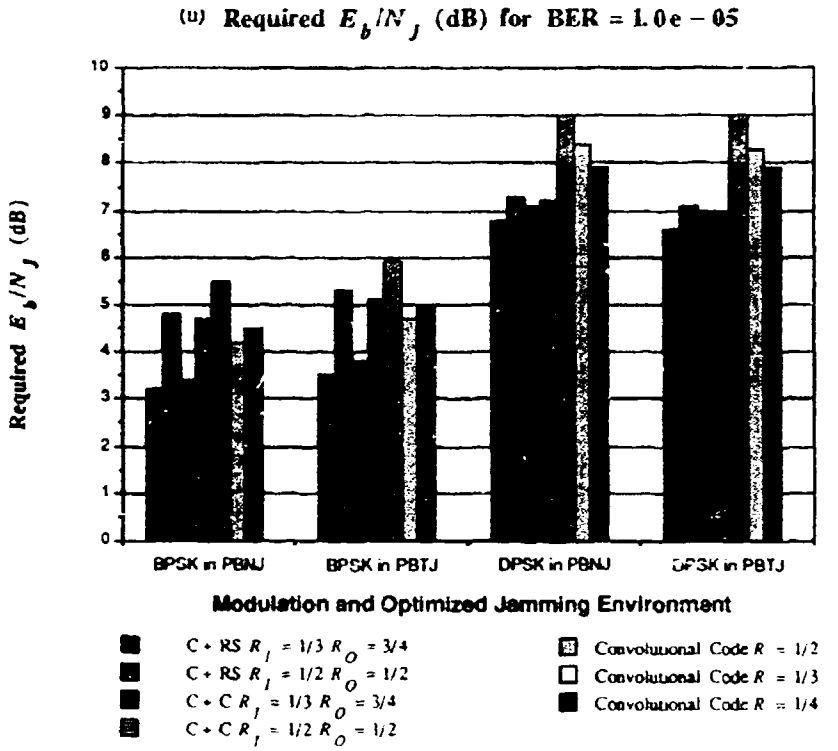

Fig. 8. (u) Required SNR for coded BPSK and DPSK in optimal partial band noise and tone jamming to achieve BER = 10e-05.

ADVANCED ECCM TECHNIQUES FOR GPS PROCESSING

Edmund Balboni, John Dowdle
Joseph Przyjemski
Charles Stark Draper Laboratory
Cambridge, Massachusetts 02139
United States of America

Ellen Mallery
Wright Research and Development Center
Wright-Patterson Air Force Base, Ohio 45433
United States of America

Introduction

Two advanced Electronic Counter Countermeasures (ECCM) enhancement techniques have been shown to significantly improve the antijam performance of Global Positioning System (GPS) receivers. The first method, Amplitude Domain Processing (ADP), is a nonlinear precorrelation processing technique which adapts to a changing ECM environment and exploits the statistical properties of strong nonGaussian jammers to significantly reduce their effectiveness. ADP has been demonstrated in hardware against a heavily jammed GPS signal; measured performance shows a reduction in continuous wave (CW), pulsed CW and swept CW jammer power of 36 dB, 25 dB, and 26 dB, respectively.

The second technique, Extended Range Adaptive Tracking, is a correlation process which optimally adjusts tracking loop bandwidths and multiple correlator weights in response to changing levels of GPS signal dynamics and ECM power levels. The extended range feature tolerates the growth of tracking error beyond the ±1 chip conventional limit to ±5 chips to guard against loss-of-lock under exceptionally severe combinations of jamming and dynamics. Analysis and simulation have shown that this technique can extend the receiver tracking threshold by an additional 26 dB. A hardware demonstration of this technique is currently under development. Both Extended Range Adaptive Tracking and ADP are suitable for efficient, low power Very Large Scale Integrated Circuit (VLSI) implementation.

Amplitude Domain Processing (ADP)

ADP is an ECCM technique which acts to improve precorrelation signal-to-noise ratio to enhance the antijam performance of a GPS receiver. ADP exploits the statistics of the jammer's amplitude probability distribution function by deriving a functional which is used to reassign a new value to each of the ADP's input samples. Reassignment is performed in a way that deemphasizes those samples in which signal detection is unlikely, thereby effecting a signal-to-noise improvement. ADP has been shown to provide significant rejection of all current jamming threats.
ADP is a signal processing technique that is based on statistical decision theory (Ref. 1) in which a derived optimal nonlinearity operates on the amplitude, r, of a combined strong interference, n, and a weak signal, s, to effect signal-to-noise (SNR) improvement. The nonlinearity is based on the amplitude probability distribution function (PDF) of the received input, $f_x(r)$, which, under the above conditions, can be approximated by

$$f_x(r) = f_{s+n}(r) \approx f_n(r) \qquad (1)$$

That is, the PDF of the composite input is essentially that of the interfering waveform. By processing this input by the nonlinear operator, g(r),

$$g(r) = \frac{-\,d[f_n(r)/r]/dr}{f_n(r)/r} \qquad (2)$$

it can be shown that SNR enhancement will occur in all cases in which the interference in non-Gaussian.

Amplitude Domain Processing is depicted in Figure 1. (See Figures 1 through 18 on pages 5 through 12.) The incoming waveform is resolved into inphase (I) and quadrature (Q) components in an RF-to-baseband converter, and are transformed to a polar representation in magnitude (R) and phase (ϕ). The phase component is delayed to compensate for an equivalent delay associated with the processing of the signal's magnitude. This processing consists of PDF estimation and the subsequent derivation of the nonlinear function used to reassign enhanced value to each input sample. These samples are then retransformed to quadrature form prior to final correlation and data detection.

ADP Simulation

A simulation of ADP was conducted for the case of CW, pulsed CW and swept CW jammer (Ref. 2). Figure 2a illustrates the probability density function of a CW jammer generated in histogram fashion and Figure 2b is the derived nonlinear mapping function. These plots are based on 2048 8-bit samples of the signal's magnitude. When applied to the input signal, this function produces the results shown in Figure 3, which illustrates a comparison between the ADP's input and output power spectral densities. ADP has reduced the CW jammer to the level of the background noise resulting in a theoretical 3 dB total noise increase. This increase is a favorable tradeoff when viewed in the context of significant jammer reduction.

Figures 4 and 5, respectively, show simulated ADP performance in the cases of pulsed CW and swept CW jamming, both of which show virtually complete jammer rejection.

ADP Proof-of-Concept Demonstration

Figure 6(a) illustrates an ADP architecture designed to minimize size and power requirements in a future VLSI implementation as well as provide design guidelines in a near-term discrete component proof-of-concept hardware demonstration. Figure 6(b) is an associated sequencing diagram to illustrate its operation. The operations of Random Access Memorys (RAM) A, B, and C are identical but offset by 120 degrees in a processing cycle consisting of three modes. This provides for the continuous generation of f(r) from

samples of r while allowing time for the processor to compute g(r), thereby providing real-time processing of the input. During Mode 1, histogram formation, the input data addresses a RAM, increments its contents by one, and stores the results in the same location. After 2048 data points have been similarly processed; Mode 1 is complete and an estimate of f(x) is contained in the memory in histogram fashion.

In Mode 2, a counter sequentially addresses the RAM, thus serially reading out f(r). A Finite Impulse Response (FIR) filter is used to smooth the function to reduce errors in its derivative. The nonlinearity, g(r), is then computed and stored in the same block of memory. A signal normalization scale factor (SF) is also computed from g(r) and df(r)/d(r).

During Mode 3, the original delayed input data addresses the memory containing g(r), thereby mapping itself to the ADP output. The memory is then cleared to again begin the cycle.

An evaluation of the ADP hardware was conducted with inputs consisting of a GPS C/A code signal at the L1 (1575 MHz) frequency, thermal noise and a single jammer. Power spectral densities were measured for the CW, pulsed CW and swept CW waveform cases before and after Amplitude Domain Processing. The measurements are in excellent agreement with simulation results.

Figures 7, 8 and 9 show the measured spectrum at the ADP input and output and are counterparts to the simulated results of Figures 3, 4 and 5, respectively. As shown, jammer rejection is nearly complete in all cases. Other frequency components are present in the upper (input) spectrum of Figures 7 and 8. These spurious components appear to be the result of RF receiver implementation anomalies such as analog-to-digital (A/D) converter nonlinearities or intermodulation products. It is important to note that ADP tends to suppress these components as well as the intended jammer. The decreasing power level of the input swept CW jammer shown in Figure 9 is the result of low pass filtering operation applied at the A/D input prior to Amplitude Domain Processing. As predicted, and as shown in Figures 7 and 8, background noise increases slightly at the ADP output when a jammer is present. In Figure 9 the noise floor at the ADP input is obscured by the in-band aliased second harmonic component of the swept CW jammer.

In addition to substantiating jammer suppression, tests were performed to ensure that ADP processing does not have a deleterious effect on the GPS signal itself. The results of post-correlation data measurements are shown in Figures 10 through 13 and illustrate data recovery performance at the ADP output. Figure 10 shows a baseline measurement without jamming, resulting in ADP processing of the GPS signal buried in additive white Gaussian noise. The measurements consist of spectral analyses of a square wave which was substituted for GPS data to facilitate evaluation.

The upper half of Figure 10 shows the fundamental and odd order components of the waveform with ADP disabled. In this test, data undergoes forward and inverse coordinate transformation without intermediate processing by ADP. A comparison with the lower half of the figure in which ADP resumes operation shows minimal degradation of the data. There is also no detectable increase in the noise floor, a result predicted by theory. The net result is that, in the absence of a jammer, ADP produces no significant degradation of SNR.

Figures 11, 12 and 13 show the results of data measurements with and without ADP processing for the cases of CW, pulsed CW and swept CW jamming, respectively. In Figures 11 and 12, ADP is seen to suppress the jammer component at 20 Hz whereas the spectrum of the square wave data is essentially left intact. What appears to be an increase in the power levels of the square wave line spectrum is attributed to D/A decompression resulting from the ADP removal of the high level jammer. That is, in the absence of ADP suppression, the jamming waveform tends to saturate the D/A resulting in decreased gain to the GPS signal and an increase in spurious generation.

Figure 13 shows data recovery with ADP operating on a swept CW jammer. Again, the spectral components of the square wave are essentially left intact during jammer suppression.

Extended Range Correlation (XRC)

Extended Range Correlation provides a means of maintaining code lock when tracking loop errors exceed those that can be tolerated by a standard correlator. A simulation and analysis of extended range adaptive tracking has shown that correlation over ±5 code chips is sufficient to bound code tracking errors under combinations of jamming and dynamics that significantly exceed those specified for GPS. An XRC design based on this analysis is shown in Figure 14. Samples of the wideband signal are distributed to 21 complex correlation channels, each spaced in 0.5 code chip increments to subtend the required range. Spacing is controlled by correct phasing of the local reference code applied to each channel. The indicated initial integration interval following code removal is limited by the decorrelating effects of full carrier Doppler which is removed by complex multiplication prior to final accumulation. Total XRC integration time can be varied from 1.0 to 20 ms.

The XRC's initial accumulators also decrease throughput, thereby, permitting the implementation of a shared multiplier/final accumulator to efficiently process their outputs. A Doppler wipeoff signal is provided to the multiplier by a numerically controlled oscillator/look-up table which derives optimal Doppler frequency estimates from an adaptive carrier tracking loop. The XRC's final outputs are sequentially forwarded to an adaptive loop processor which utilizes measurements of dynamics and jamming levels to optimally weight each correlation value before final summation and tracking. All functions illustrated in Figure 14 are currently being integrated in a single VLSI design with a complexity of approximately 20,000 gates.

Code Loop Processing

The design of the code tracking loop for the XRC requires that a sophisticated approach be employed to extract maximal information from the available 21 correlator outputs. Intuitively, the algorithm should perform two functions: (1) process the XRC outputs to form an error signal that drives the loop; and (2) filter the error signal to generate an estimate of the code phase delay. Moreover, both functions should optimally adapt to GPS signal dynamics and jamming conditions.

An adaptive tracking loop with the above properties was developed for the XRC using methods from nonlinear filtering theory (Ref. 3). The loop has the structure shown in Figure 15, which indicates the major functions of the XRC and its output weighting, the filtering functions of state estimation and covariance propagation, and rate-aiding by an Inertial Navigation System.

The operation of the adaptive code loop is most easily understood by first considering its estimation covariance algorithms. The estimation algorithm, which is a second-order loop that estimates residual code phase and its rate, performs the usual filtering function of traditional code tracking loops. However, as is typical with state estimation algorithms, and in contrast to typical GPS receivers, the adaptive loop also continuously adjusts its bandwidth to the environment by modifying the loop gains as a function of the estimated jamming level and the covariance of the estimation error. It is through this process, which depends upon the covariance algorithm reliably predicting the statistics of the tracking error, that the tracking loops can respond to high dynamics while minimizing the effects of high jamming. This covariance algorithm is similar to that found in standard Kalman filters, except that its development was based upon a nonlinear measurement model of the XRC operating as a square-law detector. The algorithm responds to the residual acceleration, which is a function of the modeled INS error parameters and the instantaneous vehicle dynamics, and to the jamming environment, which can be estimated from outputs of the XRC. Since the algorithm is based upon nonlinear filtering methods with covariance responding directly to the outputs of the XRC, the adaptive tracking loops, in contrast to those of a typical Kalman filter, promises improved robustness because its estimation error directly affects the covariance via feedback through the correlator.

Following an estimation of residual code phase rate, INS rate-aiding is introduced to develop an estimate of line-of-sight (LOS) velocity. This is subsequently integrated by the NCO to produce an estimate of code phase delay, which closes the loop through the XRC. INS rate-aiding lowers tracking loop bandwidth requirements by reducing the bandwidth of the signal processed by the code loop. That is, the loop only needs to track the residual between the true LOS and that estimated by the INS. Consequently, the tracking loop can maintain lock under high jamming with significantly lower bandwidth to improve accuracy by providing a lower-noise code phase estimate.

The XRC estimator and covariance weights, which are computed optimally based upon the solution to the nonlinear filtering problem, are driven primarily by the variance of the code phase estimation error. In severe environmental situations in which the computed variance of the tracking error is large, range extension occurs with an automatic increase of the estimator weights for correlators that are far-removed from the on-time or prompt channel. As environmental conditions improve and the error variance decreases, these weights adjust so that only those correlators near the on-time estimate are weighted. This ensures that the code phase tracking error is always within the detection envelope, and facilitates automatic reacquisition of the code phase when conditions improve. The covariance weights are adjusted by the algorithm to ensure that the statistics of the estimation error are consistent with measurements observed at the output of the XRC. If the measurements indicate that the actual error is larger than the predicted 1-sigma value, then the weighted XRC measurements tend to cause the covariance to increase. Conversely, if the observed tracking accuracy is better than predicted, then a corrective term in the algorithm causes the covariance to decrease. As an overall consequence, the entire tracking loop is less sensitive to modeling and measurement errors associated with residual dynamics and the jamming environment.

The adaptive code tracking loop was evaluated via Monte-Carlo simulation of a variety of stressing scenarios which included initial acquisition as well as tracking of both CW and broadband jamming. Figures 16(a) and 16(b), respectively, depict the LOS acceleration between the receiver and a GPS satellite and the simulated jamming-to-signal (J/S) ratio at the receiver input for a broadband jammer. Note that the LOS acceleration varies between ±6 g with jerk levels in excess of 10 g/s, and J/S ranges from 32 dB to 80 dB at the receiver input. Under these conditions, the adaptive loop performance is shown in Figure 16(c), with the solid graph representing the code phase estimation error and the dashed graph is the standard deviation of the error predicted by the covariance algorithm. It is observed that the tracking error generally remains well within a code chip (approximately 30 m) throughout the entire scenario, even during periods where J/S is 80 dB, and that the computed standard deviation of the code tracking error typically agrees quite well with the actual error.

Carrier Loop Processing

The conventional approach to carrier tracking loop design employs a Costas tracking loop to process the on-time correlator's inphase channel to produce an estimate of the encoded data, utilizes that estimate to data-demodulate the quadrature measurement, and filters the resulting error signal to track carrier phase and Doppler. Typically, the Costas loop is nonadaptive and therefore, suffers performance degradation and loss-of-lock when jamming and dynamics vary significantly from the baseline design point.

Two features which provide significant benefit over conventional Costas loop are INS aiding and adaptive tracking. As in the case of the code tracking loop, INS aiding permits lower bandwidths to reject jammer power by reducing the dynamics that must be processed. This also improves accuracy by reducing the effects of jammer-induced noise on the carrier phase and Doppler estimates, but primarily serves to extend the receiver's loss-of-lock threshold. As in the code loop, gain adaptation improves the carrier loop performance by optimally adjusting loop bandwidth in response to measurements of the environment. However, since the Doppler-induced dynamics processed by the carrier loop are significantly higher than those of the code loop, a sufficiently accurate implementation of the aiding measurement requires a more detailed accounting of error sources including lever arm effects and the latency and update rate of the INS data.

The adaptive carrier tracking loop operates on the XRC's prompt output in a manner analogous to the Costas loop discussed previously by processing the inphase channel to estimate the data while utilizing the quadrature channel to drive the tracking loop (see Figure 17). However, in contrast to the Costas loop, which implements a hard limiter to estimate the data bit, the adaptive carrier loop employs an adaptive soft limiter (or a hyperbolic tangent) for this function. The advantage of this approach, which is based upon maximum likelihood estimation, is that, whereas in high-jamming situations the hard limiter behaves erratically by responding primarily to noise, the soft limiter adapts to the predicted tracking error variance and the computed inphase noise variance to initiate a gain reduction when conditions are severe, thus resulting in more stable operation. Under benign conditions of tight carrier loop tracking and negligible jamming the soft limiter revert to a hard limiter.

After data estimation, the quadrature signal is data demodulated to provide a signal proportional to the carrier phase tracking error for the loop filter. The loop filter is derived using nonlinear estimation (Ref. 3) and consists of a third-order estimation algorithm to compute carrier phase, Doppler, and residual acceleration. An additional covariance algorithm is used for gain adaptation and to adjust the parameters of the soft limiter.

The adaptive carrier loop was analyzed via Monte-Carlo simulation for a variety of scenarios, including the LOS acceleration profile shown previously in Figure 16(a). Of primary interest was the J/S loss-of-lock thresholds for broadband and CW jamming environments. Under the ±6 g acceleration profile it was found that loss-of-lock occurs at approximately 52 dB for the broadband case and at 49 dB under CW jamming. This represents as much as 10 dB improvement over traditional approaches. Moreover, the resulting velocity error is approximately 0.02 m/s at 50 dB of broadband jamming and 48 dB of CW jamming. The carrier loop tracking error response to 45 dB of CW jamming is shown as the solid curve in Figure 18. Note that the spikes occur at times of large LOS jerk (≈ 10 g/s), but rapidly decay. The 1-sigma standard deviation computed by the covariance algorithm (dashed curve) is shown to track the actual error closely.

Conclusions

Amplitude Domain Processing and Extended Range Adaptive Tracking are advanced signal processing techniques that have been shown to substantially increase the ECCM capability of GPS receivers. ADP has been demonstrated in hardware to significantly suppress CW, pulsed CW and swept CW jammers. An additional significant level of jammer rejection is provided by Extended Range Adaptive Tracking which is currently being implemented in a proof-of-concept demonstration. Adaptive tracking loops provide an advantage over conventional tracking loops in that measurements of jamming and dynamics are used to optimize tracking performance. Extended range correlation maintains code lock for errors greater than 1 chip and lowers the need for reacquisition. Overall, the benefits to be realized by these advanced signal processing techniques are improved positioning, velocity estimation, free inertial performance, and faster reacquisition. Both techniques can provide enhanced baseline ECCM processing for future GPS systems and, as a VHSIC/VLSI insertion, can provide an efficient, near-term performance upgrade in current GPS receivers.

REFERENCES

1. Capon, J., Optimum Coincident Procedures for Detecting Weak Signals in Noise, IEEE Transactions on Information Theory, 1960.

2. Advanced GPS Receiver Technology Program, Critical Design Review, CSDL-P-2904, The Charles Stark Draper Laboratory, Inc., Cambridge, MA, Nov. 1989.

3. Jazwinski, A.H., Stochastic Processes and Filter Theroy, Academic Press, New York, 1970.

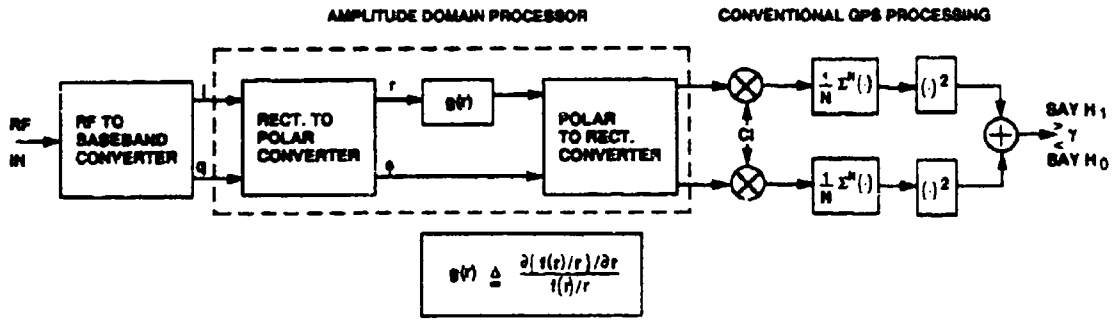

Figure 1. Amplitude Domain Processor.

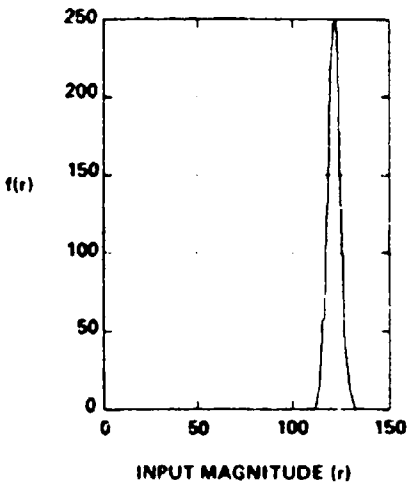

Figure 2a. ADP PDF estimate.

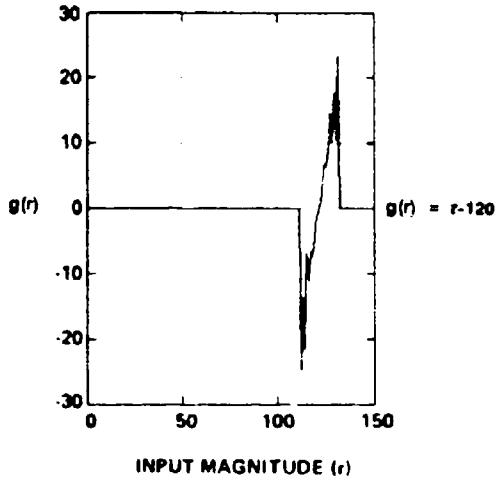

Figure 2b. ADP nonlinearity.

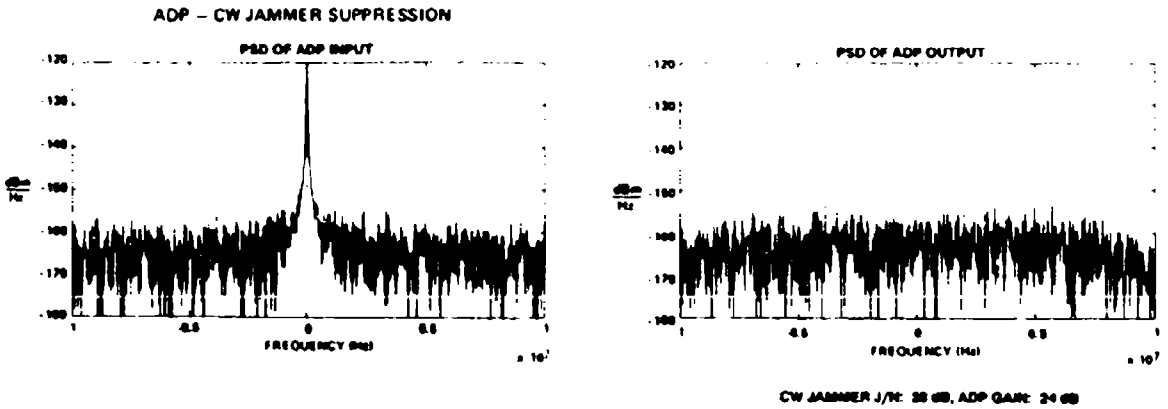

Figure 3. ADP simulation - CW jammer suppression.

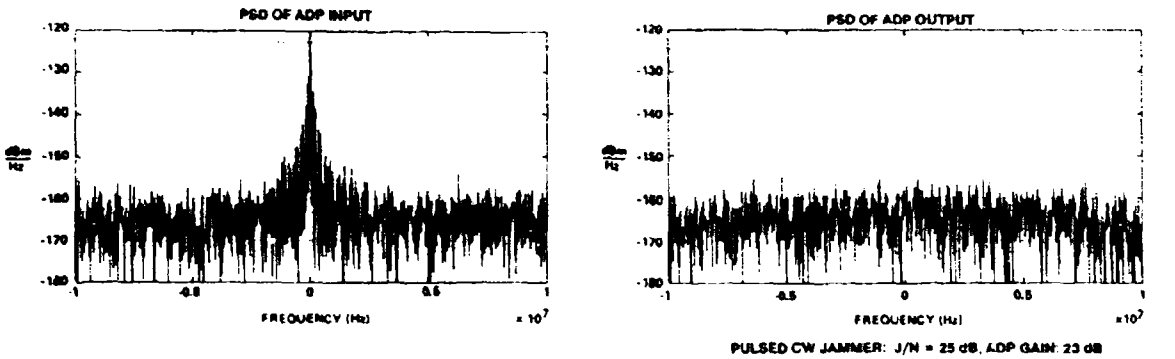

Figure 4. ADP simulation - pulsed jammer suppression.

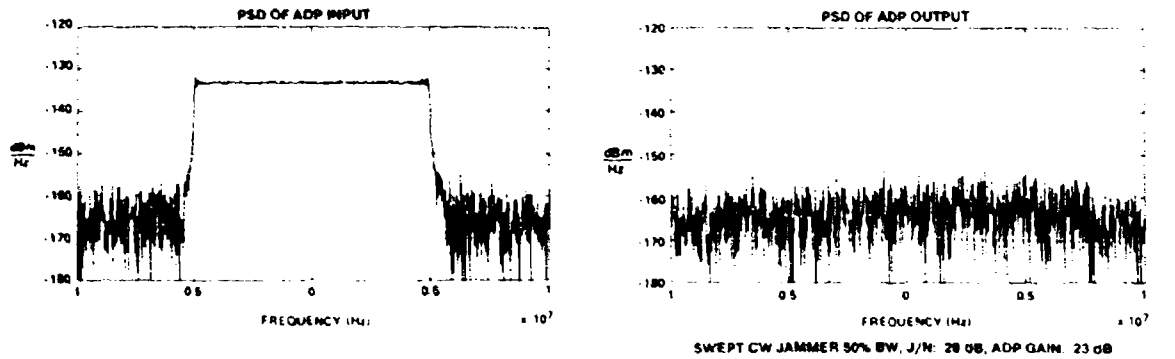

Figure 5. ADP simulation - swept CW jammer suppression

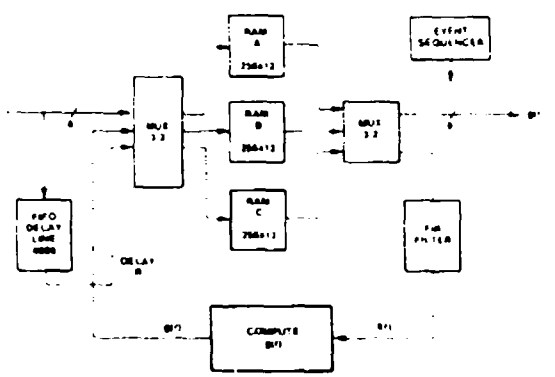

Figure 6(a) Amplitude processor - block PDF processing

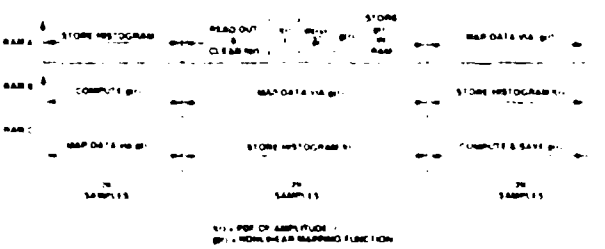

Figure 6(b). Amplitude processor algorithm

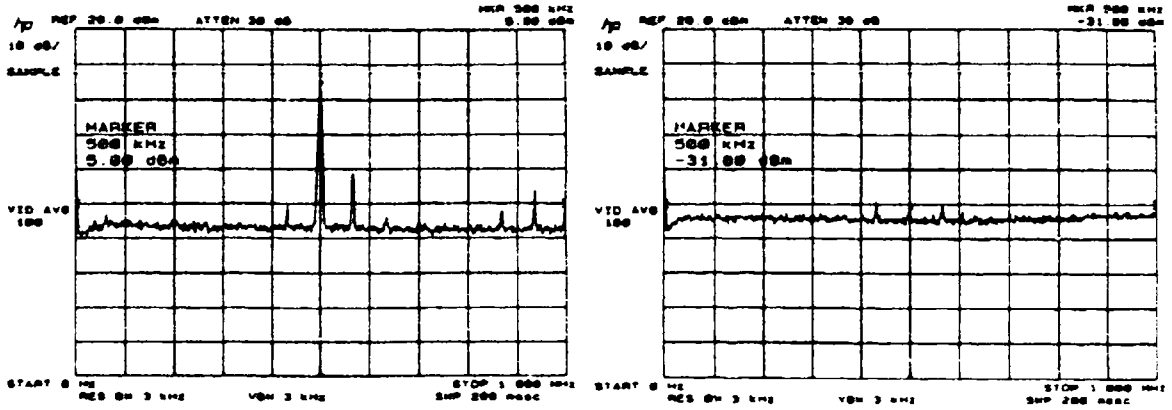

Figure 7. ADP measured performance: CW jammer.

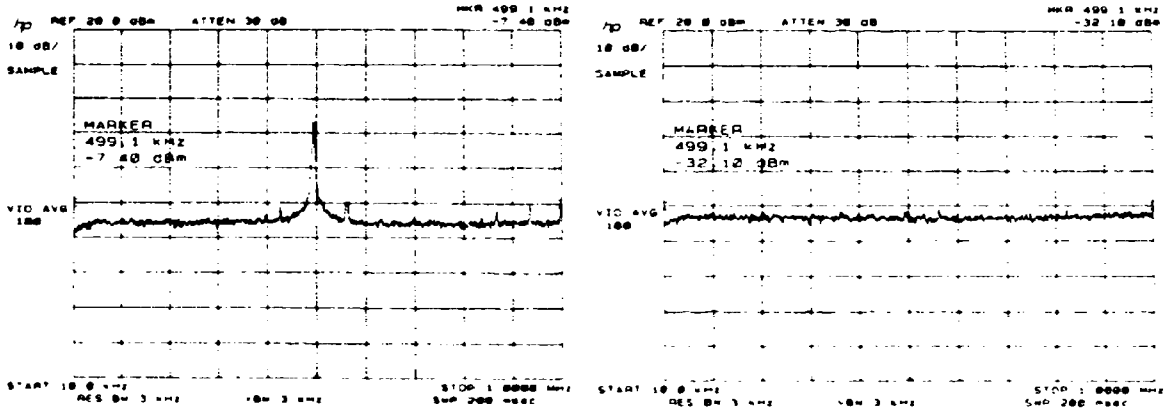

Figure 8. ADP measured performance: pulsed CW jammer

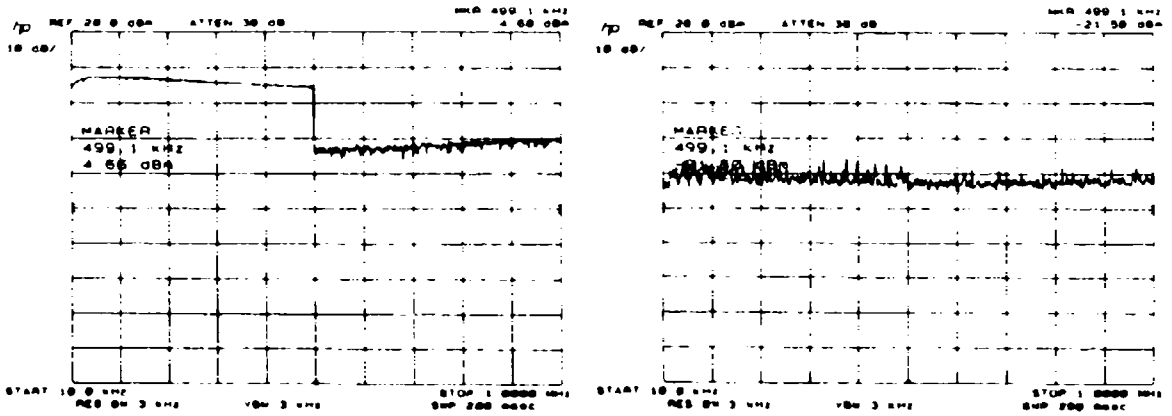

Figure 9. ADP measured performance: swept CW jammer

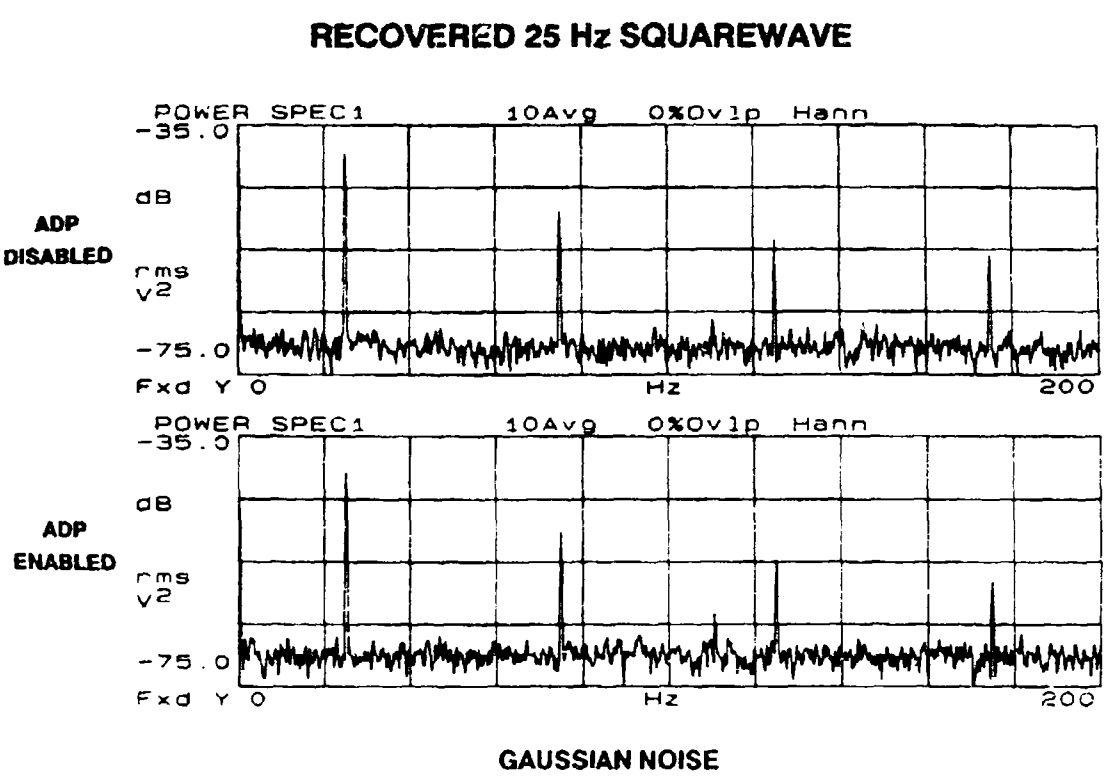

Figure 10. ADP insertion loss: no jamming.

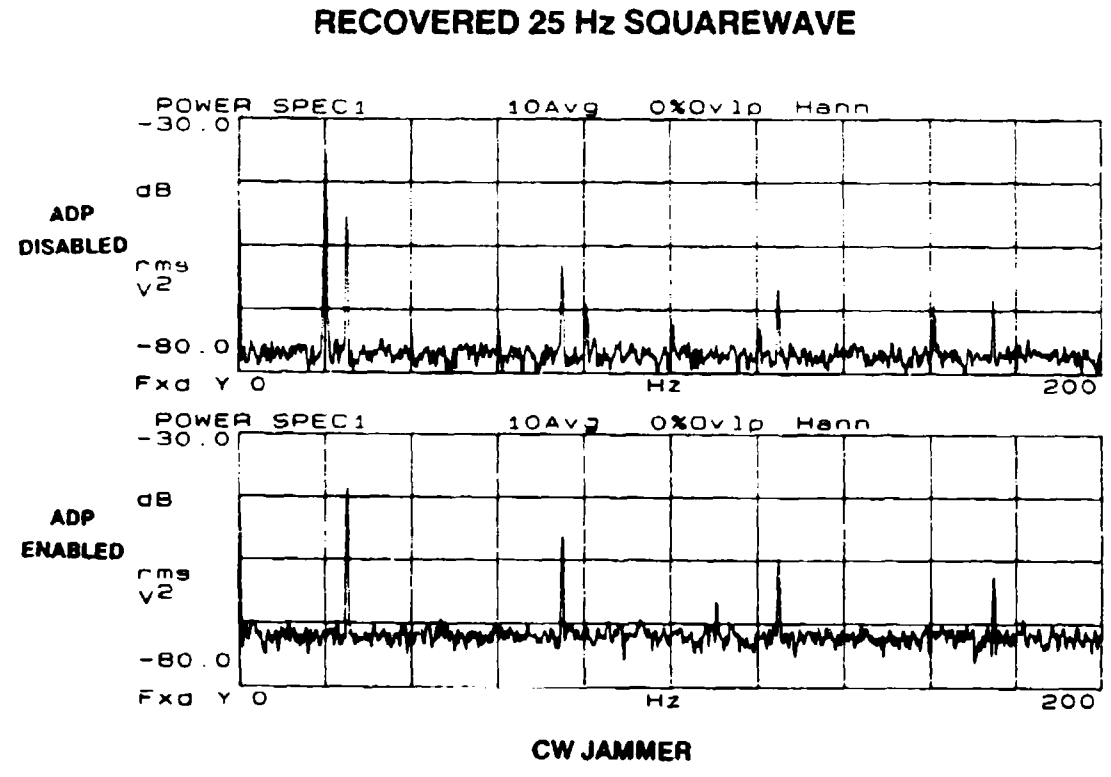

Figure 11. ADP data recovery: pulsed CW jammer

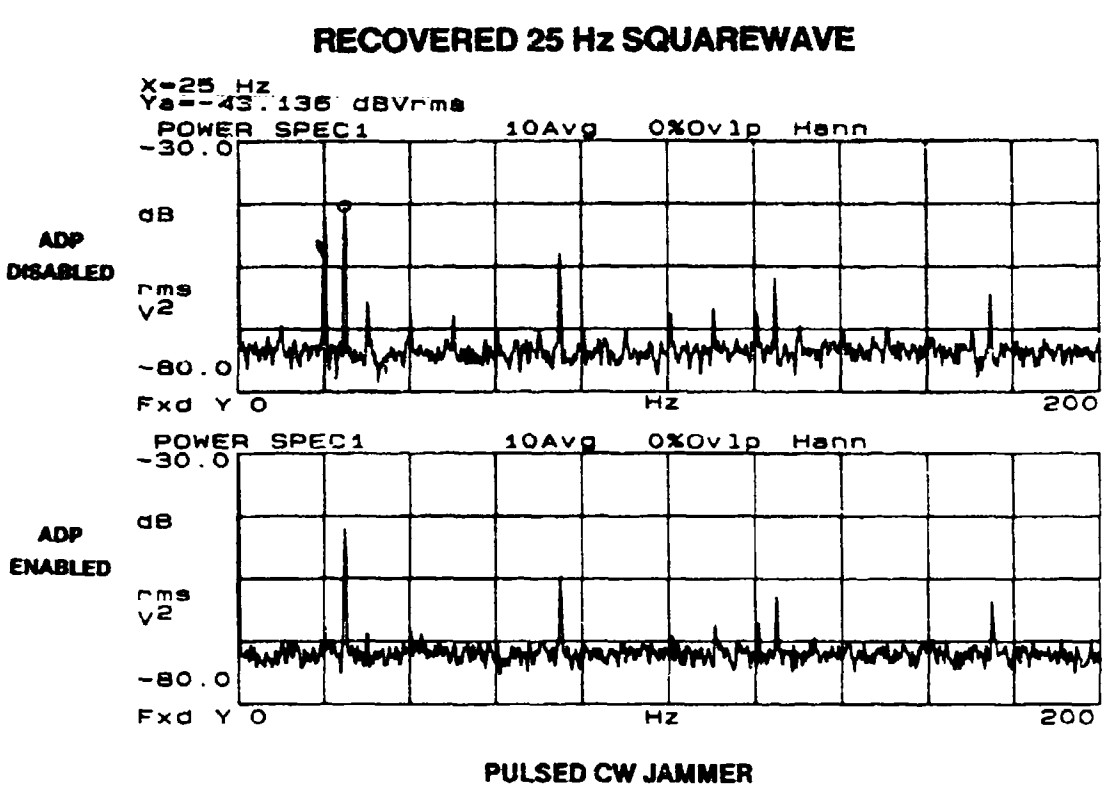

Figure 12. ADP data recovery: pulsed CW jammer.

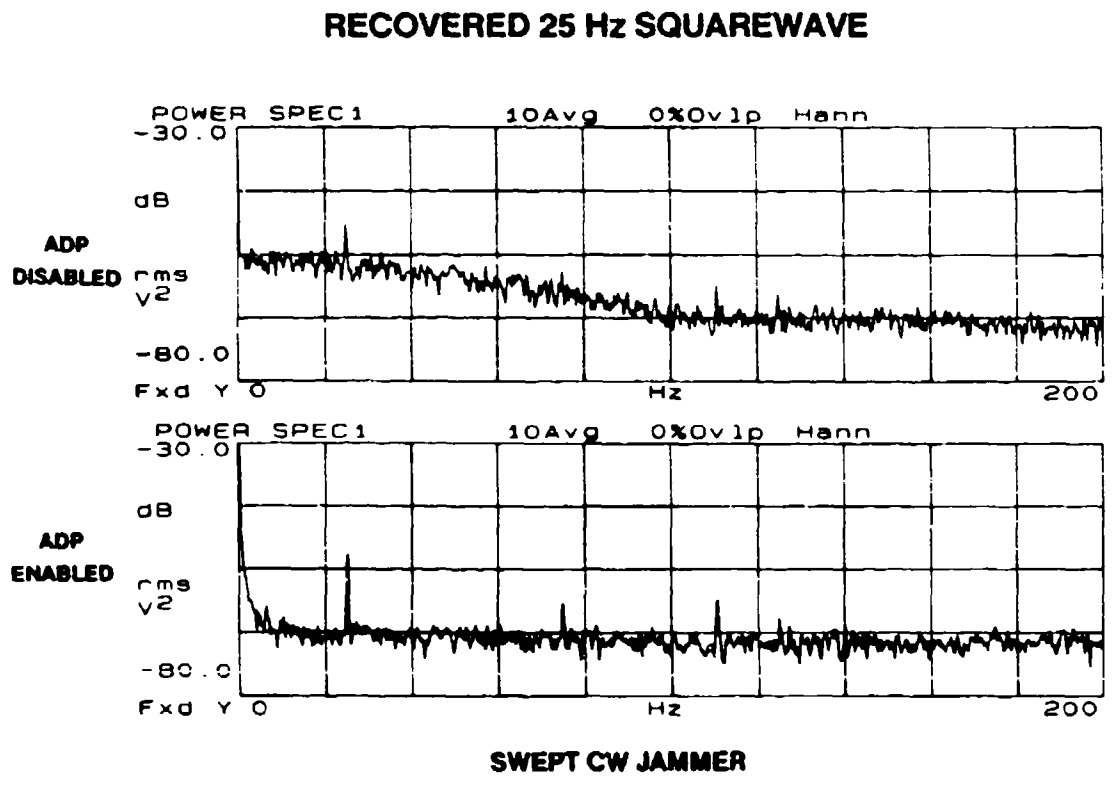

Figure 13. ADP data recovery: swept CW jammer

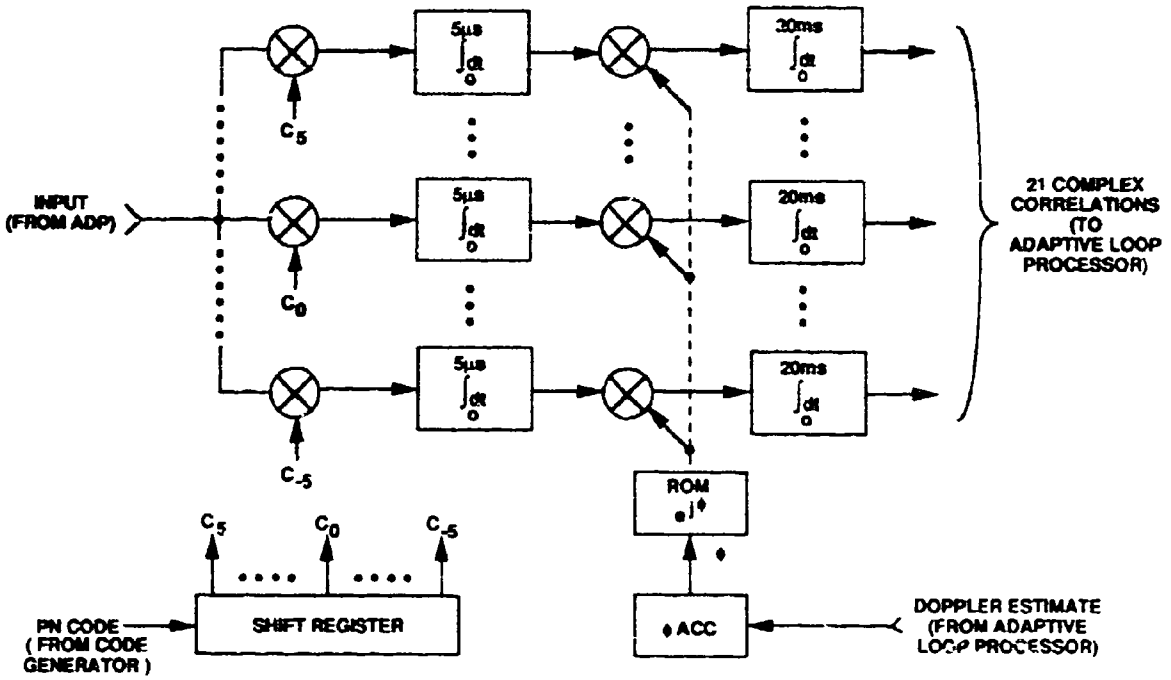

Figure 14. Extended Range Correlator (XRC).

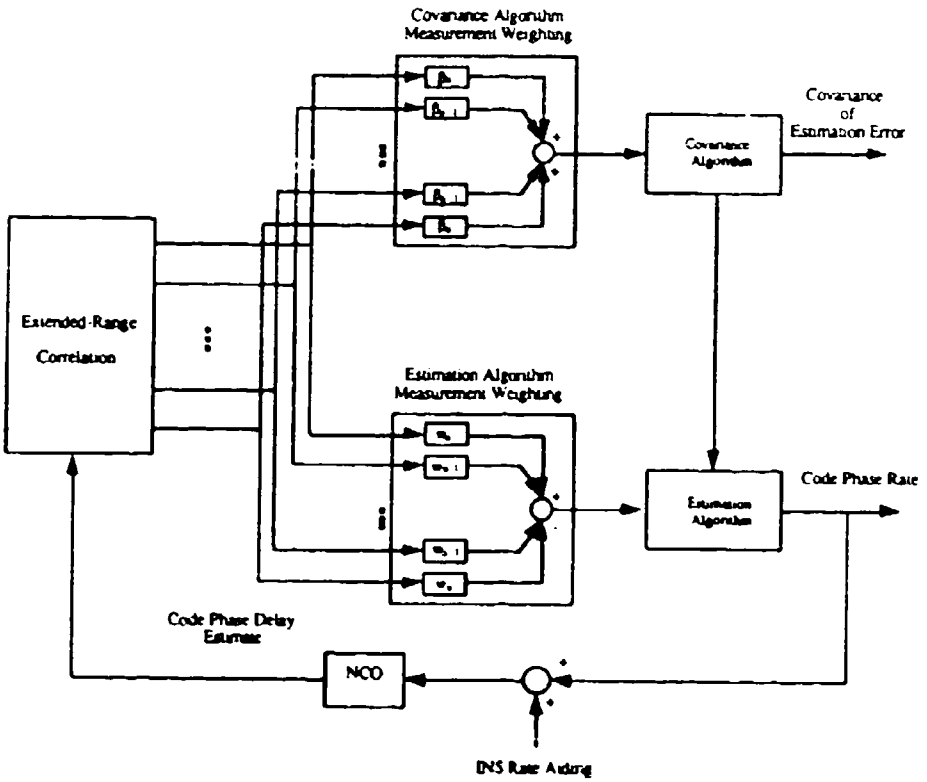

Figure 15. Adaptive Code Tracking Loop.

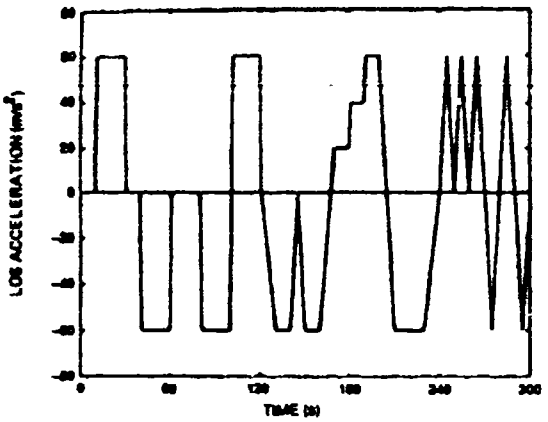

Figure 16(a). LOS acceleration.

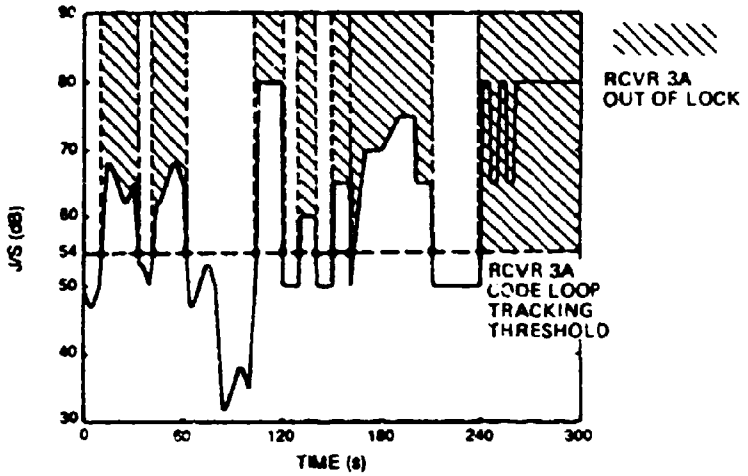

Figure 16(b). J/S levels.

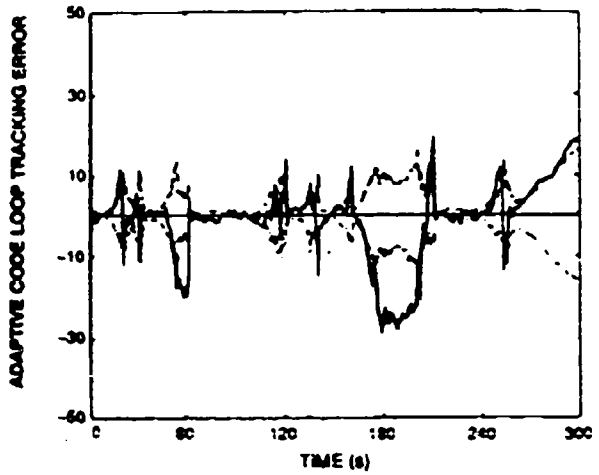

Figure 16(c). Code tracking error.

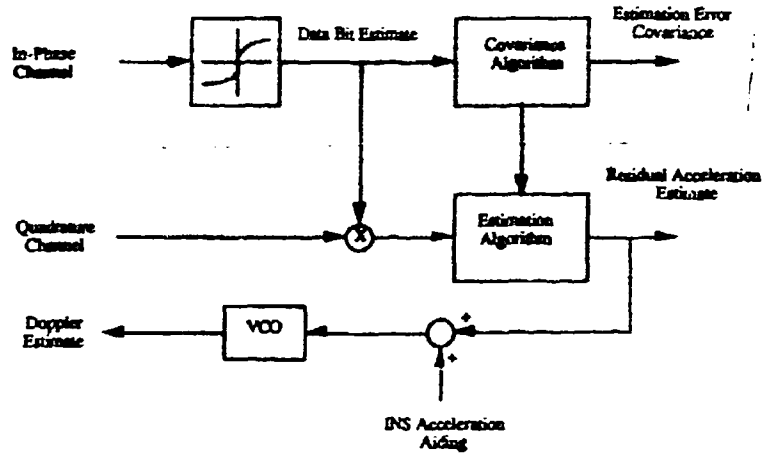

Figure 17. Adaptive Carrier Tracking Loop.

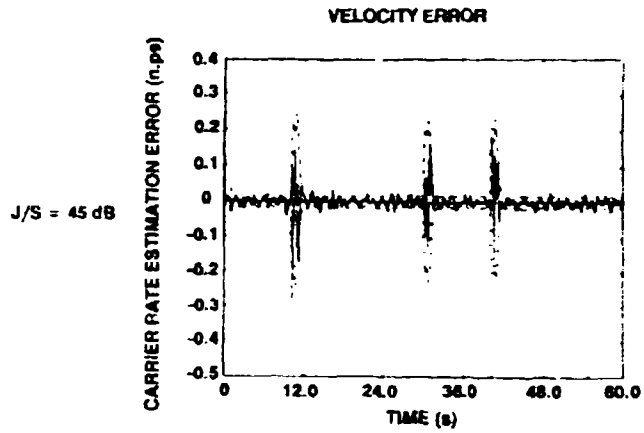

Figure 18. Adaptive Carrier Loop Performance.

Discussion

Dr Voles, UK

If the adversary knew that you were using ADP, what would be the optimum signal he should use to achieve maximum effectiveness — and what then is the overall effect on the GPS system?

Author's Reply

ADP provides no process gain against Gaussian jamming and multiple jammers that tend to appear Gaussian at the ADP input. Generating a purely Gaussian jammer is impossible due to the infinite dynamic range necessary. A clipped Gaussian appears optimal at this time. ADP will provide some process gain against this jamming format with additional ECCM due to the reduced ERP. At this time the optimal clipping level is not known.

Question

My question is also related to ADP. If for instance the jammer is a constant-envelope type the I and Q components are correlated, or they aren't statistically independent. Did you take into account this effect in your simulation?

Author's Reply

The simulation was a Monte-Carlo simulation, and hence it included a software replica of an IF to baseband converter. So it did very well simulate the correlation between I and Q channels for a CW or constant-envelope jammer.

Improving the ECCM Performance of Fast Frequency Hopping by Diversity Combining

by

Dr. E. Barry Felstead
Communications Research Centre
P.O. Box 11490, Station H
Ottawa, Ontario, Canada, K2H 8S2

and

Dr. T. Aaron Gulliver
Defence Research Establishment Ottawa
Ottawa, Ontario, Canada, K1A 0Z4

Summary

The anti-jam performance of fast frequency hopping spread spectrum communications is proportional to the ratio of the spread bandwidth to the hop rate. In fast hopping, there are $L \geq 1$ hops per data symbol transmitted. In the presence of very strong jammers, improvement of the anti-jam performance may be required. Extra ECCM performance can be obtained by using the redundancy, L in a process called diversity combining. To date, the predominant type of diversity combining uses some nonlinearity to reduce the effect of a very powerful jamming signal on a few of the L hops. Normalized envelope detection (NED) is the best example of this type. A new type, called the "moment subtraction" method, is introduced here. Examples of both types are described and then error performance results are presented for very large noise and multitone jamming (SJR = 0 dB). It is found that bit error rates as high as 0.4 can be reduced to <0.1 for $L < 10$ by both types of diversity combining and that one of the moment methods does even better than the baseline NED method.

1 Introduction

Frequency hopping (FH) spread spectrum (SS) is a very powerful ECCM technique for combatting the effects of jamming on digital radio links. A number of current military radio systems, both terrestrial and satellite, use FH for anti-jam protection. FH has become the SS technique of choice in applications where very strong jammers are a threat. This popularity over other SS techniques arises from the combination of two facts: the anti-jam protection afforded by any SS system is proportional to the spread bandwidth and, for a number of practical implementation reasons, it is easier to implement the largest spreading with FH.

In strong jamming, fast FH becomes necessary and is the form considered in this paper. Here, fast hopping is in the relative sense, and means that the hop rate is greater than or equal to the data symbol rate. It is assumed here that the absolute hop rate is sufficiently high so as to eliminate follower jammers as a threat.

The usual assumption, that the jammer has a limited average power but can arrange this power so as to cause the worst (highest) error performance in the communications link, is used here. It is further assumed that the jammer knows all the parameters of the FH link except the pseudo-random hopping pattern. An intelligent jammer of intermediate power level has available some simple jammer EC^{3}M strategies that can make much more effective use of the available jamming power and degrade communications performance well below that expected for a given jammer level [1]. These strategies include partial-band noise (PBN) jamming and multiple-tone (MT) jamming [1]. Fortunately, such EC^{3}M jammer strategies can easily be countered by forward-error-correction (FEC) techniques.[2].

If the jammer has sufficient power, then the worst case EC^{3}M jamming strategy becomes the simple one of spreading the jamming uniformly across the hopping band. Under such conditions, the error rate becomes unacceptably high, even with a combination of fast FH and normal FEC coding. The reason for this breakdown is that FEC coding is normally used to reduce a moderate bit-error rate (BER) ($<10^{-2}$) to less than a target BER, say $<10^{-5}$. Since in strong jamming the BER at the input to the decoder may be $>10^{-1}$, an intermediate step is required. Fortunately, an EC^{4}M technique called "time diversity" is available to provide this step. It involves the use of redundancy by repeating the transmitted symbol on L hops at the expense of bit rate. This simple diversity can be viewed as repetition encoding. At the receiver, the received L hops must be combined in some manner so as to

determine the actual symbol transmitted. A variety of such diversity combining techniques have been devised.

A good diversity combining technique should not only give good performance enhancement against large levels of PBN or MT jamming, but also be robust to changes in jamming strategy. Although numerous techniques have been proposed, only a relatively small number satisfy both of these criteria. In this paper, the best of these diversity combining techniques are discussed. A new class of diversity combining that uses moment subtraction techniques is introduced.

First, in this paper, the basic fast FH system, and the signal and interference are described. Next the concept of processing gain, when FH and diversity combining are combined, is discussed. Then diversity combining in general is described followed by a discussion of the two principle forms, namely, across-bin, and across-hop diversity combining. Finally, simulation performance results are presented.

2 FH System Description

The system model considered in this paper is shown in Fig. 1. Transmitted signals are noncoherent M-ary frequency shift keyed (MFSK) orthogonal signals that frequency hop over a total spread-spectrum bandwidth of W_{ss}. The M-ary symbol rate, R_s, is related to the bit rate, R_b, by $R_s = R_b / \log_2 M$. The hop rate is R_h so that the diversity level is

$$L = R_h / R_s . \tag{1}$$

It is assumed here that the hop period, T_h, is $T_h = 1 / R_h$. The frequency hopping pattern is generated from a pseudo-random (PN) sequence which can be encrypted (transec) to prevent an enemy from determining the sequence. The smallest step size between two adjacent hop frequencies should be no more than R_h and generally is less in order to defeat certain jammer strategies. Multiple users can easily be accommodated by use of frequency division multiple access (FDMA).

At the receiver, the signal is dehopped by mixing with a replica of the original hopping pattern. The MFSK signal is demodulated by a bank of M matched filters. A good method of performing this demodulation and simultaneously separating multiple users is to use a Fourier transform processor which is mathematically equivalent to the bank of matched filters. The output of the transformer is envelope detected and then sampled to give, for the ith hop and the mth frequency bin, the sample z_{mi}, where $m = 1,2,...M$, and $i = 1,2,....L$. For L hops, there are LM envelope sample values available for determining which of the M possible symbols was actually transmitted.

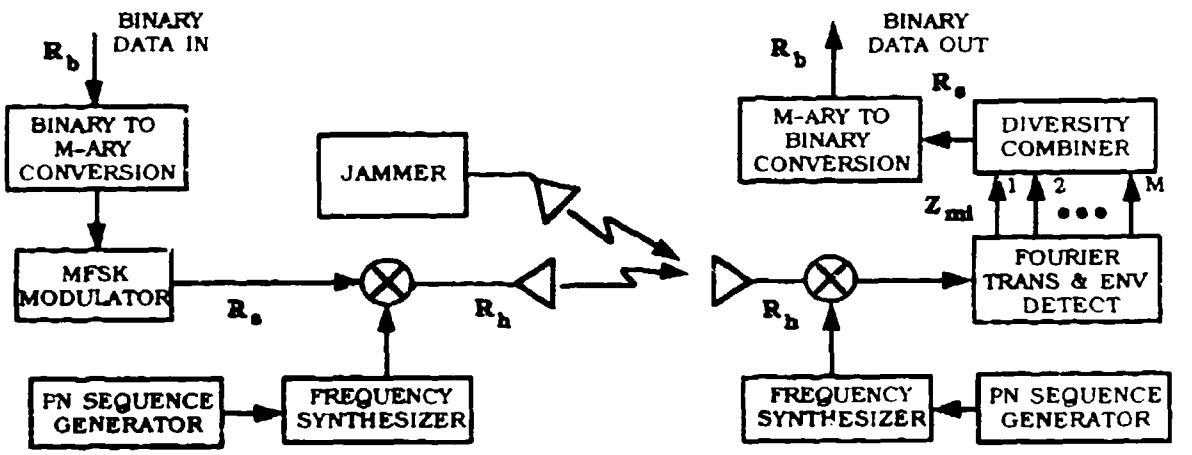

FIG. 1. A block diagram of the fast frequency hopping M-ary NCFSK system.

3 Signal and Interference Description

The power in a received M-ary signal tone is P_s, so that the energy per symbol is $E_h = P_s T_h$. The receiver system noise is assumed to be additive white Gaussian noise (AWGN) with single sided power spectral density N_o. The signal to noise ratio used here is then SNR = E_h / N_o.

The total average jamming power is assumed to be limited to some value J_t. The jamming can be in the form of AWGN or in the form of tones.

For noise jamming, a jamming noise power spectral density is often defined as $J_o = J_t / W_{ss}$ which is the power density that would occur if the jamming power were uniformly spread across the entire hop bandwidth. The *effective* partial-band noise (PBN) SJR is then $SJR_{PBN} = E_h / J_o$. For PBN jamming, a fraction γ of the band W_{ss} is jammed at a power density of J_o / γ, and the remaining fraction 1- γ of the band is not jammed.

For tone jamming, a spectral density is not meaningful. The starting point for defining an equivalent multi-tone SJR, is to calculate the power P_j in a single tone if the total jamming power, J_t, were spread in N tones at a spacing of R_h across the band, γW_{ss}, so that $N = \gamma W_{ss} / R_h$. Here it is assumed that the jammer is the worst case in Houston's sense [1] so that in the bands jammed, there is only one jamming tone per M-ary channel. Thus the effective SJR is $SJR_{MT} = (M/\gamma)(P_s / P_j)$.

For this paper, it will always be assumed that the effective SJR is low, say ≤ 5 dB. For such levels, it can be shown [5] that for worst case jamming with either PBN or MT jamming, $\gamma = 1$, i.e., the jamming is spread uniformly across the entire hop band, W_{ss}. Therefore, we always use $\gamma = 1$ here, so that

$$SJR_{PBN} = E_h / J_o \tag{2a}$$

and

$$SJR_{MT} = MP_s / P_j . \tag{2b}$$

The above parameters were defined at the input to the receiver in Fig. 1. For the subsequent analysis, the parameters at the output of the Fourier transformer are of more interest and are now given.

The envelopes, z_{mi} at the output of the FT device can be expressed in terms of two components

$$z_{mi} = (x_{mi}^2 + y_{mi}^2)^{1/2} . \tag{3}$$

If the input interference consists of system noise plus full band noise jamming then the two components are

$$x_{mi} = A_{sm} \cos\theta_i + n_{cmi} \tag{4a}$$

and

$$y_{mi} = A_{sm} \sin\theta_i + n_{smi} \tag{4b}$$

where the signal amplitude is

$$\begin{aligned} A_{sm} = 2\sqrt{E_h T_h} = 2T_h\sqrt{P_s} \equiv A_s \quad & \text{in the signal bin} \\ = 0 \quad & \text{in the other } M-1 \text{ bins.} \end{aligned} \tag{5}$$

The noise interference components, n_c and n_s, are Gaussian random variables with zero mean and variance

$$\sigma^2 = (N_o + J_o)T_h \tag{6}$$

where $N_o + J_o$ is the sum of the system- and jamming-noise power spectral density *before* the Fourier transform. The signal to interference ratio is then SIR = $E_h/(N_o + J_o)$. The parameter θ_i is a random phase uniformly distributed between 0 and 2π.

If the input interference consists of system noise plus MT jamming, then the two components of z_{mi} are

$$x_{mi} = A_{sm} \cos\theta_i + n_{cmi} + A_j(i,m) \cos\phi_i \tag{7a}$$

and

$$y_{mi} = A_{sm} \sin\theta_i + n_{smi} + A_j(i,m) \sin\phi_i \tag{7b}$$

where ϕ_i is a uniformly distributed random phase between 0 and 2π. For worst case (Houston's sense) jamming there is a single jamming tone located randomly, hop-to-hop, in one of the M bins at a power level of MP_j. The amplitude of the jamming tone *alone* is

$$\begin{aligned} A_j(i,m) = 2T_h\sqrt{MP_j} = A_{ji} \quad & \text{in the jammed bin on the ith hop} \\ = 0 \quad & \text{in the } M-1 \text{ non jammed bins on the ith hop.} \end{aligned} \tag{8}$$

The "1" in the subscript of A_{j1} indicates that there is only a single jamming tone per M-ary channel. The value of P_J is found from the given SJR_{MT} by (2b) for $\gamma = 1$ and worst case jamming in Houston's sense. For more than one jamming tone, the relation (2b) can be modified appropriately.

For noise interference only, i.e. no tones, the probability density function (pdf) of the envelopes z_{mi} is Rician [3]. The moments of interest here are the first, second and fourth, given by [3]

$$E[z] = \sigma\sqrt{\pi/2}\ \exp(-A_{sm}^2/4\sigma^2)\left[(1 + A_{sm}^2/2\sigma^2)\, I_0(A_{sm}^2/4\sigma^2) + (A_{sm}^2/2\sigma^2)\, I_1(A_{sm}^2/4\sigma^2)\right] \tag{9}$$

$$E[z^2] = 2\sigma^2 + A_{sm}^2 \tag{10}$$

and

$$E[z^4] = 8\sigma^4 + 8A_{sm}^2\sigma^2 + A_{sm}^4 \tag{11}$$

For system noise plus tone jamming, the pdf becomes more complicated than Rician because of the interaction of the signal and jamming tones according to (7a) and (7b). However, if the SNR is sufficiently high, then the slight effect of the system noise can be ignored and the probability distribution of each bin on each hop can be found. Regardless of the form of interference, the one-half, first, second and fourth moments are calculated from the envelope measurements z_{mi} by

$$\eta_{pm} = \frac{1}{L}\sum_{i=1}^{L} z_{mi}^p \qquad p = 1/2,\ 1,\ 2,\ \text{and}\ 4 \tag{12}$$

respectively. In the moment methods of diversity combining, these estimates of the moments are used in various combinations.

4 Processing Gain

A measure of the performance improvement of a spread spectrum system is the *processing gain*. The concept of processing gain is valid only for noise interference that is spread uniformly across the spread band, W_{ss}. For other types of jamming, such as PBN and MT jamming, PG has less significance. Nonetheless, it can be used as an ideal objective at which to aim. It is particularly applicable when diversity combining is used because then, the worst-case jamming distribution is uniform noise or multitone jamming across the entire band. Therefore, the jammer is forced to broad band jamming which, fortuitously, is the condition under which FH performs the best!

It is common to define the processing gain of an SS system as

$$PG_{ss} = W_{ss} / R_b \tag{13}$$

where R_b is the information bit rate. For fast FH this definition is incorrect and gives an optimistic value compared to the correct definition

$$PG_{fh} = W_{ss}/R_h \tag{14}$$

This definition is justified by a simple argument. The effective jamming power spectral density for wideband noise was seen to be $J_o = J_t / W_{ss}$. For the signal, recall that $E_h = P_s / R_h$. Thus the effective SJR defined by (2a) can be rearranged to give, for full band noise jamming

$$SJR_{FBN} = \frac{E_h}{J_o} = \frac{P_s}{J_t} \times \frac{W_{ss}}{R_h} \tag{15}$$

which shows that the effective SJR is the actual input SJR increased by a factor which is PG_{fh} defined by (14). Therefore, (14) represents the improvement in performance of an FH system in the presence of wideband noise jamming.

If the jammer uses PBN or MT jamming strategies, definition (14) for PG_{fh} becomes meaningless and the PG actually achieved can be tens of dB below that predicted by (14). For larger values of effective SJR, say, about ≥10 dB, this very large degradation in performance can be mostly recovered with standard error-correction (EC) coding techniques [2].

If the jamming is large, say SJR << 10 dB, then the processing gain defined by (14) will not be sufficient to provide a large enough effective SJR to result in an acceptable bit error rate (BER). If $R_s < R_h$, there is a redundancy arising from the diversity, L, given by (1), that can be exploited to obtain additional processing gain which is denoted the diversity processing gain

$$PG_L = R_h/R_s \tag{16}$$

It is not yet known if PG_L given by (16) can be obtained, or if it is even a limiting factor. From some results to date it appears that it can not only be achieved, but exceeded.

In order to exploit the potential PG arising from the diversity redundancy, a means of diversity combining at the receiver is required and is the subject of this paper. This diversity can be viewed as $(L,1)$ repetition coding.

5 Diversity Combining in General

The LM envelope samples, z_{mi} collected on L hops in the M bins, are available to make a decision as to which one of the M symbols was actually transmitted. An example of a set of LM such samples is shown in Fig. 2 for tone jamming plus system noise. In this example, M=8, and L=7. The system noise is seen to cause the signal, located here in bin number 1, to vary in amplitude. The system noise in the non-signal bins is omitted for clarity. The following heuristic discussion on diversity combining is for the tone jamming example of Fig. 2 but is equally valid for noise jamming.

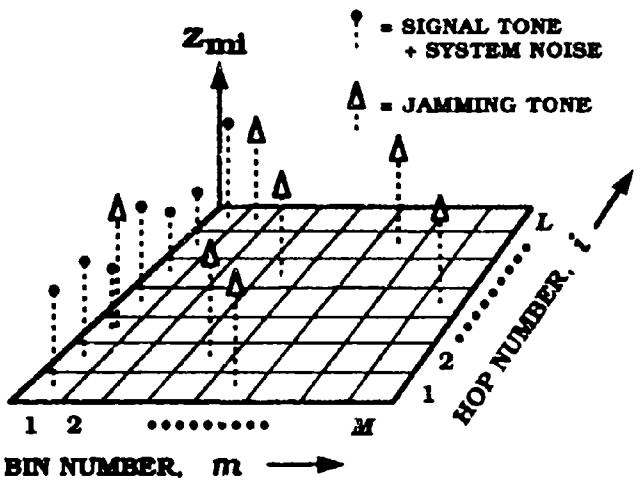

Fig. 2. Example of the $L \times M$ matrix of samples, z_{mi}, for tone jamming. System noise causes the signal level to vary. The system noise in the non-signal bins is omitted for clarity.

Linear diversity combining can be considered the basic or baseline diversity combining method in that the LM values, z_{mi} are not preprocessed in any manner. In linear combining, the L values in each frequency bin (see Fig. 2) are added to form the M sums

$$y_m = \sum_{i=1}^{L} z_{mi} \tag{17}$$

The bin with the largest sum, y_m, is declared to correspond to the received symbol. Linear combining can be viewed as soft decision decoding of the $(L,1)$ repetition code. This method works well in wide band noise but is very susceptible to jammer strategy attacks. For example, a single large tone in one of the non-signal bins on just one hop could cause a symbol error.

In an attempt to overcome the considerable vulnerability of linear combining to jammer strategy changes, a wide variety of other diversity combining techniques have been devised. These techniques can be divided into two types that depend upon whether the initial processing of the samples z_{mi} is done across bins on each hop, or across hops on each frequency bin. They will be called here, across-bin, and across-hop diversity combining, respectively.

In the across-bin approach, on each hop (see Fig. 2) the M values of z_{mi} are processed in a manner that reduces the effect of non-signal bins containing very large jammers. Numerous nonlinear operations have been suggested to implement this reduction. This operation results in M modified values, z'_{mi}, for the ith hop. Then the L modified values are added to form the M sums

$$y_m = \sum_{i=1}^{L} z'_{mi} \tag{18}$$

Again, the bin with the largest sum, y_m, is declared to correspond to the received symbol.

In across–hop diversity combining, the L values of z_{ml} are processed in each bin to produce a single value, y_m . Once again, the largest value of y_m is declared to correspond to the received symbol. The processing across the hops is designed to reduce the effects of jamming.

Since the across–bin and across–hop combining methods can be considered orthogonal methods, there is some thought that it might be possible to apply both techniques simultaneously. No significant work has yet been done on this possibility. The major difficulty is determining two good complementary methods.

Many methods have been proposed that use "side information." By some means, one attempts to determine if a particular hop has been jammed or not and to use this information to either discard jammed hops entirely, or to assign a quality value to the hop. There are considerable disadvantages to the use of side information. First, the side information tends to be unreliable and can complicate the overall system quite considerably. Secondly, diversity combining approaches we have looked at are prone to simple jammer strategy attacks that make performance worse than if side information were not used. The worst disadvantage is that in the presence of very large jamming, which is of interest here, all hops could be jammed, rendering side information useless. Thus, we do not consider side information here.

If at the transmitter, the diversity repetition L is replaced by a low-rate, $r = 1/L$, EC encoding [4], then at the receiver, the diversity combining becomes decoding. In effect, a more complex code replaces the simple $(L,1)$ repetition code. Generally, hard decisions are required before the decoding because, otherwise, the jammer could devise some simple counter strategies to nullify the benefits of the coding. Low rate encoding has the major disadvantage of being somewhat more complex to implement than the diversity methods considered here. Also, there is little flexibility to change the code rate as compared to simple diversity. There is concern that low-rate coding may exhibit the same failure mechanism found in high-rate codes where the output error rate of the decoder becomes higher than the input error rate once a certain input error rate is exceeded. Since the application here is to very low SJR.s, the input error rate is expected to be very high so such a failure would be likely, and is therefore, unacceptable. Finally, it appears from early results that some of the diversity combining techniques considered here perform as well or better than low-rate EC coding even if the other problems can be overlooked. Therefore, low-rate EC coding, beyond an $(L,1)$ repetition code, is not considered in any depth in this paper

6 Across–bin Diversity Combining

Although a large variety of across–bin diversity combining techniques have been discussed in the literature, we will highlight just a few.

Hard decision majority vote (HDMV) [5], [1] is probably the earliest and simplest of the nonlinear diversity combining methods. It consists simply of choosing the bin with the largest value on each of the L hops. The bin with the most "votes" is declared to correspond to the received symbol. It works moderately well against tone jammers and is not degraded by changes in jammer strategy. Some analysis is found in [5] and [1], and results for $L = 3$ to 9, and for M from 2 to 16 are given in [1]. The HDMV combining method also can be viewed as hard decision decoding of the $(L,1)$ repetition code. Since it discards useful information in forming the hard decisions, it tends to be a poor performer. From another viewpoint, it can be seen as being at the extreme end of the across-bin methods with linear combining being at the other extreme. All other across-bin methods fall between these two extremes.

There are numerous methods of diversity combining that attempt to reduce the effect of very strong jammers occurring on the occasional hop without going to the extreme of the HDMV method. A few of these are discussed below.

Ratio–threshold combining [6] provides some protection against worst case jamming, but a means of determining the proper threshold is required. Similarly, the clipping–combining technique [7] clips large signal levels to a value determined by measuring the output voltage level. In practice, this measurement can be difficult to obtain, and can vary greatly from hop to hop. Both of these methods require external information and involve the setting of levels or thresholds which makes them

vulnerable to intelligent or powerful jammers. In this paper, we consider only those combining techniques that use the *LM* samples alone to provide the most robust performance possible.

The normalized-envelope detection (NED) method [8] has stood the test of time. It performs as well or better than all the other across-bin diversity combining techniques, is robust to changes in jammer strategy, and is relatively easy to implement in real time [9]. NED combining will be used here as the premier example of across-bin combining. In the NED combining method, the envelope samples in all M bins for the ith hop are normalized by dividing by their sum to give a normalized set of values

$$g_{mi} = z_{mi} / \sum_{m=1}^{M} z_{mi} . \tag{19}$$

At the end of L hops, the L values, g_{mi}, in each bin are summed according to

$$y_m = \sum_{i=1}^{L} g_{mi} , \tag{20}$$

and the y_m with the largest value is declared to correspond to the symbol received. The normalization process (19) reduces the effect of very large jamming signals.

There are a number of combining techniques that operate in a manner similar to NED. In the list-metric method [10], each of the M bins on each hop is given a weight according to its rank in an ordered list. The weighting scheme is clearly important and is chosen to reduce the effects of very large jamming tones. At the end of L hops, the L weights for each frequency bin are combined in some manner and the largest chosen. It is probably slightly more difficult to implement than NED and should perform about as well. In ratio-statistic combining [6], the M sample values, z_{mi}, on each hop are divided by the maximum of the M samples. Thus, the largest bin will have a modified value of unity, regardless of the amplitude of any jamming, and all other bins will have a smaller value. It is slightly more difficult to implement than NED and should perform about as well. Another method closely related to NED is self-normalizing combining [11].

7 Across-hop Diversity Combining

There seems to be far fewer across-hop methods of diversity combining than the large number of across-bin methods. The only across-hop method known to the authors until now is the order-statistic method [12]. In this method, the largest value in each of the M bins is discarded. Then the linear sum, as in (17), is made of the remaining $L-1$ values and the bin with the largest sum is chosen. Although this method throws out information, it seems to perform reasonably well.

A new form, a far as we know, of across-hop diversity combining was introduced in [13]. It is called, for lack of a better name, "moment subtraction" diversity combining. In this approach, the L samples in each bin are considered together. Because this topic is new, it will be described in more detail than were other combining methods.

To explain the method, consider the signal bin, bin number 1, in Fig. 2. The sample values z_{1i} fluctuate because of the system noise and because a jammer tone hits one of the hops. However, the sample values should, in the absence of any interference, be constant and equal the amplitude of the signal. Similarly, the value of the samples in the non-signal bins fluctuates because of system noise and interference, but, in the absence of any interference, the samples would be constant with amplitude zero. Therefore, the approach taken is to consider any fluctuations over L hops in any of the M bins to be caused by interference. Various moments of the L samples are calculated and are used in a subtraction process in an attempt to reduce the fluctuations and make a better estimate of the base amplitude (A_s in the signal bin and zero in the $M-1$ non-signal bins). The bin with the largest amplitude after the moment-subtraction process has been completed is selected as the one corresponding to the received symbol.

At this writing, three forms of moment subtraction have been considered and are named the fourth-and-second moment (4-2M) method, the second-and-first moment (2-1M) method, and the first-and-one-half moment (1-1/2M) method, after the moments used in the particular method. Note that the "one-half moment" is not a formally known moment but is found useful here.

The basis of the moment subtraction method came from the observation in [14] that in the presence of AWGN only, the moments in (10) and (11) can be combined to give

$$2\{E[z^2]\}^2 - E[z^4] = A_m^4 . \tag{21}$$

Note that in this operation, the resultant is the desired signal to the fourth power with no interference whatsoever! This equation was used directly to generate the (4–2M) method. The estimates, η_{4m} and η_{2m}, of the fourth and second moment from (12) are calculated for each of the M bins, and then these two are combined according to

$$v_m = 2\eta_{2m}^2 - \eta_{4m} . \tag{22}$$

The bin with the largest value of v_m is selected as corresponding to the received symbol. In simulation results it was found that this method indeed did well against AWGN. However, it did poorly against multitone jamming. At this point, other moment subtraction methods were sought that did well in both noise and tone jamming.

In an ad hoc search the (2–1M) algorithm given by

$$q_m = 2\eta_{1m}^2 - \eta_{2m} , \tag{23}$$

gave very impressive performance against tones combined with respectable performance against noise. Then, it was reasoned that if going from the fourth and second moments to the smaller second and first moments improved tone performance, then going to even smaller moments might be better. The (1–1/2M) algorithm given by

$$b_m = 2\eta_{1/2m}^2 - \eta_{1m} , \tag{24}$$

was found to give even better performance against tones at the expense of reduced performance against noise.

8 Example Performance Results

The performance of linear, HDMV, NED, 4–2M, 2–1M, 1–1/2M, and order statistic (OS) diversity combining methods was evaluated by simulation analysis. The performance was evaluated in both full band noise and multitone jamming. In order to provide realistic results, in all the simulations, system noise was added at a level of E_b/N_o = 13.35 dB. In all the results presented here, an SJR, as defined in (2), of 0.0 dB was used. This level of jamming implies a very large jammer that exceeds the processing gain capability of the FH alone. The performance is presented in Figs. 3 and 4 as the resulting bit error rate as a function of the diversity L from 1 to 32.

For noise jamming, it is seen in Fig. 3 that all the methods correct the very high BER of about 0.4 down to <0.1 for diversity levels $L \geq 16$, and that all methods function within a relatively small range of each other. Within this range, the HDMV is clearly the worst performer whereas the linear combining has a very slight advantage over the closest rivals, the NED, OS, and 4–2M methods.

For tone jamming, as shown in Fig. 4, there is a considerable difference in performance of the 7 methods. The HDMV method gives no performance improvement at all and the 4–2M method gives very little improvement. The linear, OS and NED methods, all give very good performance enhancement and are within a very small range of each other. Although the linear method did well against the tones, it is cautioned that a simple change in the level of the tones could be used to greatly degrade its performance. Finally, it is seen that the 2–1M, and especially the 1–1/2M method perform extremely well. For example, a diversity of L = 6 is sufficient to bring the BER from about 0.4 to $\leq 10^{-2}$.

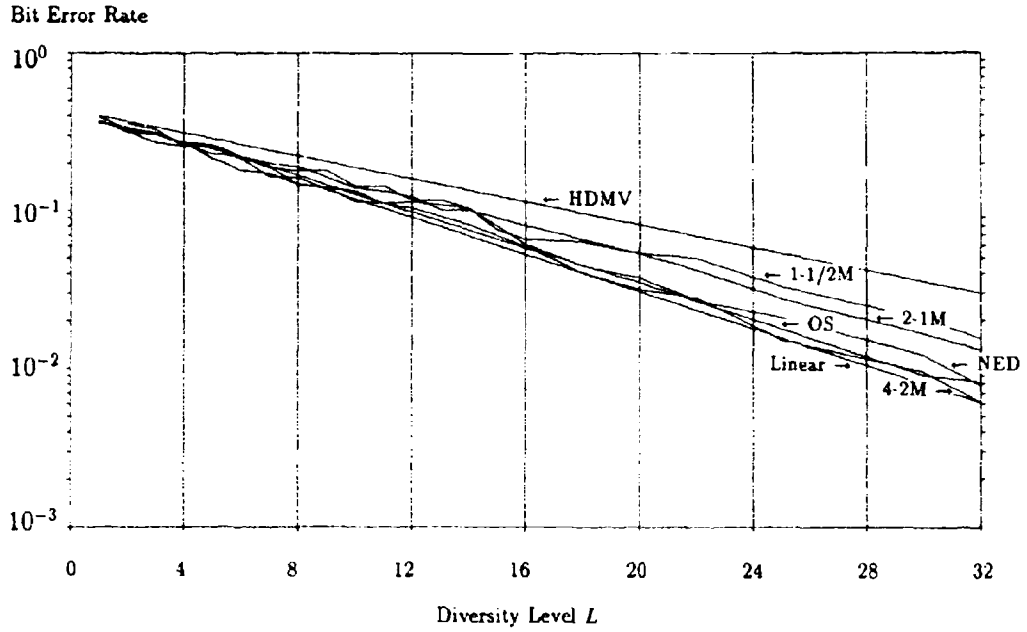

Fig. 3. The bit error rate calculated via simulation of 7 diversity combining methods in the presence of system noise at SNR=13.35 dB plus wideband noise jamming at SJR= 0.0 dB.

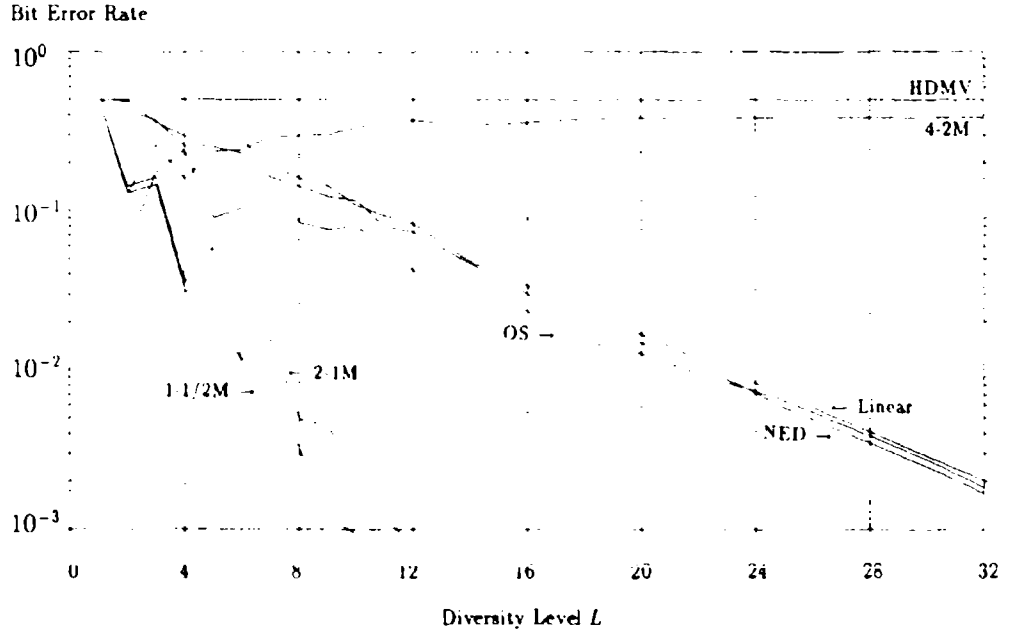

Fig. 4. The bit error rate calculated via simulation of 7 diversity combining methods in the presence of system noise at SNR=13.35 dB plus wideband tone jamming at SJR= 0.0 dB

9 Conclusion

It has been shown that diversity combining techniques can indeed extend the performance of fast FH SS. For all of the 7 methods simulated, it was found that there was substantial performance enhancement against noise jamming. Furthermore, all these methods performed similarly with linear being slightly the best and HDMV being the worst. In tone jamming, there was a wide variation in the performance of the 7 methods. The HDMV and the 4-2M methods failed to provide any significant enhancement. The OS, NED, and linear methods provided very substantial improvement. Finally, two of the moment subtraction methods, the 2-1M, and 1-1/2M methods, provided exceptionally good performance enhancement.

The above results seem to indicate that the linear, OS, NED, 2-1M, and 1-1/2M methods should be considered further. It is particularly important to consider various tone jamming strategies. For example, the linear method performed well in the tone jamming assumed for the simulations whereas there are likely simple tone jamming strategies that would eliminate its capability. Similarly, it is important to search for strategy vulnerabilities for all the methods.

10 References

[1] J.S. Bird, and E.B. Felstead, "Antijam performance of fast frequency–hopped M–ary NCFSK—An overview," IEEE J. on Selected Areas on Commun., vol. SAC–4, pp. 216–233, March 1986.

[2] Q. Wang, T.A. Gulliver, V.K. Bhargava, and E.B. Felstead, "Error correcting codes for fast frequency hopped MFSK spread spectrum satellite communications under worst case jamming," Int. J. of Satellite Commun., vol. 7, pp. 115–128, Jul.–Sept. 1989.

[3] H. Urkowitz, *Signal Theory and Random Processes*, Artech House, Dedham MA, 1983.

[4] P.D. Shaft, "Low–rate convolutional code applications in spread–spectrum communication," IEEE Trans. Comm., vol. COM–25, pp. 815–821, August, 1977.

[5] W.E. Stark, "Coding for frequency–hopped spread–spectrum communication with partial–band interference—Part II: Coded performance," IEEE Trans. Comm., vol. Com–33, Appendix A, pp. 1055–1056, October, 1985.

[6] C.M. Keller, and M.B. Pursley, "Clipped diversity combining for channels with partial–band interference—Part II: Ratio–statistic combining," IEEE Trans. Commun., vol. COM–33, pp. 145–151, February, 1989.

[7] C.M. Keller, and M.B. Pursley, "Clipped diversity combining for channels with partial–band interference—Part I: Clipped–linear combining," IEEE Trans. Commun., vol. COM–35, pp. 1320–1328, December, 1987.

[8] K.S. Gong, "Performance of diversity combining techniques for FH/MFSK in worst case partial band noise and multi–tone jamming," Proc. IEEE Milcom '83, pp. 17–21, October, 1983.

[9] P. Tardiff, and E.B. Felstead, "Measurement of diversity–combining performance enhancement for fast–FH," Proc. IEEE Milcom 89, pp. 16–19, October, 1989.

[10] P.J. Crepeau, M.A. Creighton, and J.K. Omura, "Performance of FH/MFSK with list metric detection against partial band noise and random tone jamming," Proc. IEEE Milcom '83, pp. 225–228, October, 1983.

[11] L.E. Miller, J.S. Lee, and A.P. Kadrichu, "Probability of error analyses of a BFSK frequency–hopping system with diversity under partial–band jamming interference — Part III: Performance of square law self–normalizing soft decision receiver," IEEE Trans. Commun., vol. Com–34, pp. 669–675, July 1986.

[12] S.L. March, and J.A. Ritcey, "Performance of an order statistic based diversity combining M–ary frequency–hopping system in a partial–band jamming environment," Proc. IEEE Milcom 89, pp. 11–15, October, 1989.

[13] T.A. Gulliver, and E.B. Felstead, "Moment methods for diversity combining of fast frequency hopped noncoherent MFSK," Proc. of the 1990 Queen's Sym on Commun., pp. 13–16, June 1990.

[14] T.R. Benedict, and T.T. Soong, "The joint estimation of signal and noise from the sum envelope," IEEE Trans. Inf. Theory, vol. IT–13, pp. 447–454, July 1967

Discussion

A.Yamada, Aerospace Corp., US

What is the sensitivity of your approach to the MFSK symbol size? Can the approach be used to counter fading, simultaneous with jamming?

Author's Reply

Our simulations haven't gone beyond M = 8 so we really don't know, in answer to your question. There's usually always a debate (as to) what values of M should be chosen and I'm sure it will make a difference. But the kind of system we've been looking at tends to be working at M = 8 so that's why we concentrated on it. There may be better values, it's quite true. Now the second question... He wants to know, if you had simultaneous fading *and* jamming would these methods work? I think, obviously, if the diversity L was large enough it certainly would, and I think intuitively that even smaller values of L would help as long as the L hops span the decorrelation time of the fading — just like any interleaving would do.

E.Balboni, Charles Stark Draper Laboratory, US

A trend is evident by using progressively lower moments as a metric in diversity combining. Have you considered using M 1/2 — M 1/4 as a metric?

Author's Reply

Week by week we come up with a new method and, yes, that is the trend, but I don't know if we'll continue that trend to one-quarter and one-half moment combining. If you look at the paper or at the graphs you'll see that although it's getting better against tone jamming it's starting to get worse against noise jamming. So I think we've come to the limit of how low we can go with these moments. But that is a good question and we certainly thought about it.

AN OVERVIEW OF ECCM FACTORS IN MILSATCOM SYSTEMS

M. Safak

SHAPE Technical Centre
Communications Division
P.O. Box 174
2501 CD The Hague
The Netherlands

SUMMARY

This paper aims to identify and discuss the relative significance of the factors affecting the ECCM performance of MILSATCOM systems. These factors are identified through the performance predictions for MILSATCOM systems, operating with geostationary satellites, under up- and downlink jamming. The factors influencing the system performance against signal exploitation and repeat-back jamming are also discussed. The paper also provides a discussion of the effects of the frequency of operation (SHF and EHF bands) on the ECCM factors.

1. INTRODUCTION

Balanced protection of communication resources against postulated threats is one of the key requirements of military communications systems. To this end, one first needs a threat description which consists of identifying plausible threat scenarios against which the system must be protected. Then comes the assessment of the threat, which provides a detailed projection or estimation of the enemy's capabilities for designated threat scenarios. The performance of the user system can then be predicted vis-à-vis the postulated threats and as a function of equipment and waveform designs of both the user and the enemy. The provision of electronic counter-countermeasures (ECCM) for improving the system performance may require a re-evaluation of the designated threat scenarios and re-assessment of the threat.

Implementation of cost-effective ECCM for the realization of robust military satellite communications (MILSATCOM) systems clearly depends on the identification of the relative effectiveness of all the relevant factors. The ECCM to be provided should be carefully planned between often conflicting requirements. The system vulnerability should be balanced between the ground segment, space segment and the propagation path as well as with other protective measures such as those countering nuclear and physical threats. The relative importance of a MILSATCOM system in the whole military communication framework should also be borne in mind. The survivability of the system cannot and should not be at any cost and there should be a trade-off between the system survivability and the minimization of attendant costs.

This paper is based on Ref. 1 and is a logical follow-up to Ref. 2, which provides a brief description and assessment of postulated threats to MILSATCOM systems. The factors influencing the ECCM performance of MILSATCOM systems are identified and discussed. The paper presents predictions for the performance of MILSATCOM systems, operating with geostationary satellites, under up- and downlink jamming as a function of jammer and user system parameters and investigates the vulnerability of the user system against signal exploitation and repeat-back jamming (RBJ). The implications of anti-jamming (AJ) and low probability of exploitation (LPE) modes of operation in super-high frequencies (SHF) and extremely high frequencies (EHF) bands are also studied. The relative advantages of the two main spread spectrum systems (frequency hopping and direct sequence) and discussed vis-à-vis the ECCM they provide to MILSATCOM systems. The relevant ECCM to improve the system performance are identified and discussed.

2. JAMMING

SATCOM systems can be jammed on the downlinks and the uplinks. A jamming technique can be chosen on the basis of the information available on the characteristics of the satellite and the ground segment. Brute-force jamming operates on the premise that if enough jamming power is radiated into a receiver, the user signal will be indistinguishable from the jamming signal and the system will collapse. If the complete degradation of the system would be impractical, a jammer may aim to create sufficient disruption in the system to delay the correct appreciation of the threat situation until it is too late to take counter-action. A jammer may also opt for low-level (nuisance) jamming to create confusion as to the source of malfunctioning in the system. Specific weaknesses of a system can also be exploited by an intelligent jammer.

A jammer may exploit the frequency scale by distributing its power over the whole or part of the spreading bandwidth, which corresponds respectively to full-band and partial-band jamming. Another strategy may consist of distributing the jamming power into a series of tones (generally of equal frequency spacing and power) which occupy part or all of the spreading bandwidth. As a special case of this, jamming power may be contained in a single tone, operating in pulsed or continuous

---

All views and opinions expressed are those of the author and do not necessarily represent those of SHAPE or NATO.

wave (CW) mode. Partial-band jamming is effective when the jammer power is not sufficient to cause high enough bit error rate (BER) in the channel by jamming the whole bandwidth. Under these conditions, the jammer trades the jamming bandwidth with jamming power density (noise or tone) so as to be more effective. Percentage of the frequency bandwidth that can be jammed increases with increasing jamming power and full-band jamming becomes feasible when it is sufficiently high. THe use of forward error correction (FEC) coding and increasing the spread spectrum processing gain constitute the principal countermeasures to such attacks.

Similarly, a pulsed jammer can exploit the time scale by jamming at duty cycle values less than or equal to unity. Pulsed jamming can also be used to jam several targets by time-sharing. Coding and interleaving can alleviate the degradation caused by pulsed jamming.

Apart from these, a jammer may have recourse to deception, spoofing and hit-and-run attacks to put the user system in a better defended, but less capable posture- or even to reveal wartime or otherwise inconspicuous capabilities.

2.1 UPLINK JAMMING

Uplink jamming is a net-wide threat and affects all the users. The position of a geostationary satellite to be jammed can easily be located, for example by monitoring the beacon. Different transponders of a satellite can be jammed by time-sharing if the jammer bandwidth is narrower than the satellite bandwidth. A jammer may jam a single satellite or could jam multiple satellites, for example, by beam-switching.

Satellite transponders saturated by an uplink jammer operate at a maximum downlink power level which is apportioned to downlink carriers in proportion to their received uplink power levels. Consequently the effect of a jamming signal is to steal power from the wanted signals. When the jamming power dominates the total uplink power received by the jammed transponder, the power of the wanted signal becomes too low to be detected by the user satellite ground terminal (SGT). A "constant envelope" uplink jammer can cause up to 6 dB suppression of the user signals by driving a hard-limiting satellite transponder into saturation. Consequently, the small signal (which is the jammed user signal in this case) can be suppressed up to 6 dB so that jammer-to-signal power (J/S) ratio at the output of a hard-limiting transponder becomes 6 dB higher compared to the J/S ratio at the transponder input. Spread spectrum signals are as vulnerable to this attack as other signals. This is a specific weakness of hard-limiting transponders and can be countered by the use of on-board processing.

A jammer can also exploit the non-linear characteristics of a satellite transponder by sweeping its signal frequency through regions of worst AM/PM conversion of the transponder (Ref. 3). A jammer can thus fool, for example, the carrier tracking loop and communication demodulator. At high jammer effective isotropically radiated power (EIRP) levels, the satellite transponder becomes saturated and the downlink signals undergo AM modulation; the modulation coefficient and its rate may be chosen to maximize the degradation in gain control/tracking loop responses.

Similarly, a pulsed jammer saturates the satellite transponder during the pulse interval; all communications signals are then deeply suppressed. By choosing a "worst-case" duty cycle and pulse repetition frequency, the damage caused to the system can be maximized. Most affected system components from such a jamming strategy would be decoders and phase-locked loops performing acquisition and tracking duties.

Under normal operating conditions, the total capacity available from a satellite is apportioned among various SGTs and each SGT has a satellite resource budget (power and bandwidth) according to its traffic requirements; various SGTs may be competing with each other for a share of the satellite capacity.

Under jamming, on the other hand, the capacity available for a SGT is set mainly by the jamming level and, to some extent, by the presence or absence of other SGTs accessing the same transponder. In particular, if the "constant envelope" jamming signal is the dominant signal in the transponder, then the traffic capacity that may be supported by a particular SGT will not be reduced, but can even be increased, by the presence of other signals in the same saturated transponder (Ref. 4).

The symbol rate, R_s (symbols/s), that can be supported by a hard-limiting transponder against uplink jamming, may be expressed as (Ref. 5):

$$R_s = \frac{f \times EIRP_s \times G_{SGT}}{L_d \times M_L \times \frac{E_s}{N_o} \times \left[\frac{(1-f) \times EIRP_s \times G_{SGT}}{L_d \times W_s} + k \times T_{SGT} \right]} \quad (1)$$

where:

$EIRP_s$ – satellite EIRP;

G_{SGT} – gain of the SGT receiving antenna;

L_d – downlink free-space loss;

W_s – spreading bandwidth;

T_{SGT} – the noise temperature of the SGT receiving antenna;

k – Boltzmann's constant (1.38×10^{-23} J/K);

E_s/N_o – required energy per symbol to noise power density ratio to achieve a specified BER;

f – $S'/(L_s \times P_t)$ – percentage of transponder EIRP used by the desired signal;

S' - desired signal power received by the satellite. For frequency-hopping (FH) systems, it designates the sum of all FH tones accessing the jammed transponder.

L_s - limiter suppression loss;

P_t - total power received by the jammed transponder, which consists of the uplink jammer power, noise power and the sum of all signal powers;

M_L - link margin (typically 9 dB for ships and 6 dB for other SGTs in the SHF band).

When the internal noise of the receiving SGT is negligible compared to the noise caused by downlink signals, i.e. for small values of f (this is a reasonable assumption for SGTs with antenna sizes larger than approximately 20 ft at high jammer EIRP levels), the second term in the bracket in the denominator of (1) becomes negligible compared to the first one. Then, (1) can be approximated by:

$$R_s = \frac{f \times W_s}{(1 - f) \times (\bar{E}_s/N_o) \times M_L} \qquad (2)$$

Under these circumstances the percentage of transponder EIRP used by the desired signal, spreading bandwidth and the energy per bit to noise power density ratio become obviously the major parameters determining the supportable data rate. Also note that R_s is inversely proportional to uplink jammer power because f is defined as the ratio of desired signal power to total power (dominated by jammer) received by the jammed transponder.

The data rate R_b (bits/s) is related to the symbol rate R_s by:

$$R_b = R_s \times r \times M \qquad (3)$$

where r - code rate;

M - bits/symbol (e.g. $M = \log_2 m$ for m-ary FSK).

Figure 1 shows the traffic capacity of a SGT with an EIRP of 95 dBW and operating in a spreading bandwidth of 40 MHz. E_b/N_o required to achieve an operationally acceptable BER is assumed to be 10 dB and the EIRP of the considered satellite transponder is taken as 35.5 dBW (Ref. 6).

Note that the number of additional SGTs present in the network becomes insignificant for very high jammer EIRPs. However, other user uplink signals accessing the jammed transponder do cause a slight increase in the traffic capacity when their total power becomes high enough so as to prevent the jammer from stealing signal power (Refs. 4 and 6).

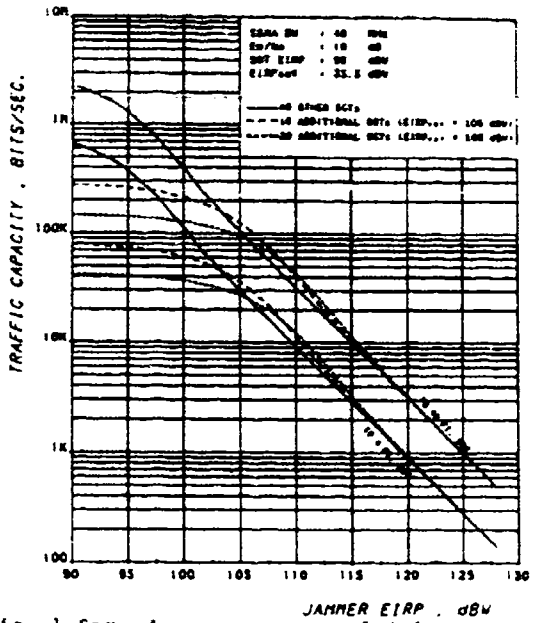

Fig. 1 Spread spectrum multiple access (SSMA) traffic capacity of a single SGT as a function of the uplink jammer EIRP (from Ref. 6)

Figure 2 shows a set of curves depicting the traffic capacity at 7.5 GHz that can be supported by a SGT under uplink jamming for three different SGT antenna sizes (40 ft with an EIRP of 95 dBW, 20 ft with an EIRP of 83 dBW and 8 ft with an EIRP of 70 dBW). These curves assume the utilization of two separate 40 MHz spread sub-bands in the same transponder and an equivalent EIRP of ten large static SGTs (with a total EIRP of 105 dBW) accessing the same transponder in addition to the considered user SGT. The jammer is assumed to be dividing its power equally between the two spread sub-bands. The effect of deploying a nulling antenna has not been included in these curves (Ref. 6).

As a countermeasure to uplink jamming, the user can:

(i) increase its EIRP and the EIRP of some other spread spectrum channels in order to minimize the power stolen by the jammer,

(ii) reduce the number of individual channels within the wanted signal,

(iii) increase the figure-of-merit, G/T, of the receiving SGT antenna,

(iv) reduce the data rate,

(v) increase the spreading bandwidth; the maximum operating bandwidth in SHF MILSATCOM systems do not exceed 500 MHz while the EHF frequencies permit the use o a bandwidth as wide as 2 GHz including the guard-bands;

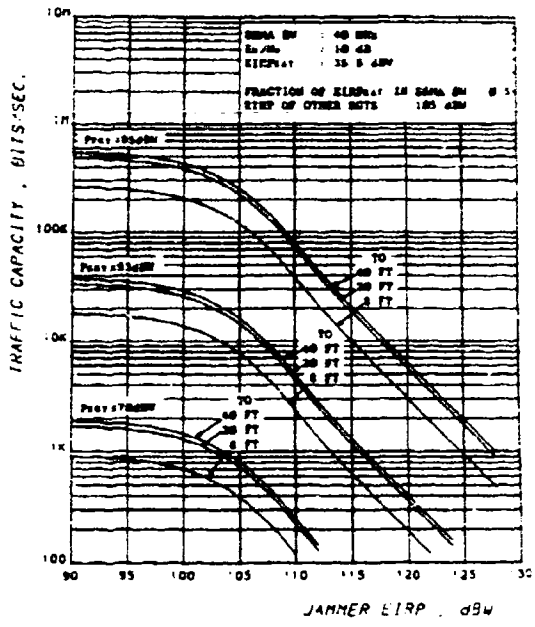

Fig. 2 SSMA traffic capacity of a single SGT in the presence of uplink jamming for various values of SGT EIRP and for various receiving antenna sizes (from Ref. 6)

(vi) use on-board processing; the efficient use of unequal up- and downlink bandwidths makes the deployment of on-board processing an attractive choice for EHF systems (Refs. 7 and 8),

(vii) use reconfigurable antenna on board the spacecraft (Ref. 9), and

(viii) use appropriate modulation and coding techniques (Refs. 10 and 11).

2.2 DOWNLINK JAMMING

Downlink jamming differs from uplink jamming in several ways. With the exception of space-borne jamming, the downlink jamming typically devotes an operationally significant platform (air-borne, ship-borne or land-based) to defeat a single SGT. By contrast, uplink jamming aims against the entire SATCOM network.

Downlink jamming is closely connected to detection and localisation of victim SGTs. Thus, the primary threat is to identified users or operating areas. From a user's perspective, the main consideration in downlink jamming is that the operational personnel recognize the situation and clearly differentiate it from equipment malfunctions so that the SGT can immediately take necessary actions and restore communication as soon as the local jammer goes away. The worse case would be that the problem is guessed to be an equipment malfunction (e.g. low noise amplifier) and that a maintenance activity is initiated that could further reduce the availability of the SGT.

If a mobile SGT, say a ship, whose downlink is to be jammed, is transmitting at least intermittently, its uplinks can be intercepted to aid in directing the jammer. The role of the air-borne jammer becomes especially prominent here because of its potential dual role in interception and jamming. Similar arguments apply to jamming the downlink signals to a submarine.

A downlink jammer can jam the satellite beacon and telemetry signals as well as the communication channels. The jammer may attack to distort the timing information provided by the satellite beacon in order to increase the acquisition time for new links, to disturb the satellite tracking or to cause the loss of telemetry data. The beacon signal received at a user SGT may be downlink-jammed either by a stronger pseudo-beacon signal, simulating the actual beacon, or by another jamming signal not necessarily resembling the actual beacon. A jammer may also resort to downlink-jamming a control terminal. As a countermeasure to this attack, one can envisage a survivable control concept and a robust method of transfer of control to the alternate control terminal.

To identify the fundamental factors in downlink jamming, assume a basic jamming scenario as shown by Fig. 3. The received jamming power, J, at the front-end of the user terminal, can be written as:

$$J = \frac{EIRP_J \cdot G_R(\theta)}{L_J \times L_{aJ}} \qquad (4)$$

where: $EIRP_J$ - EIRP of the jammer transmitter;

$G_R(\theta)$ - user receiver antenna gain in the direction of the jammer;

L_{aJ} - atmospheric loss in the path between the user receiver and the jamming transmitter;

$L_J = (4\pi R_J/\lambda)^2$ - free-space loss in the path between the user receiver and the jamming transmitter;

R_J - distance between the jammer and the user receiver.

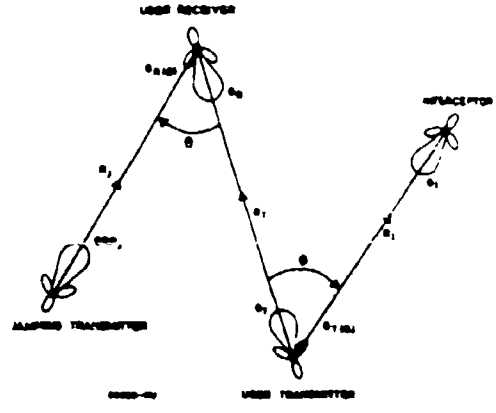

Fig. 3 Basic scenario for jamming and interception

Similarly, the received signal power at the front-end of the user terminal can be written as:

$$S = \frac{EIRP_T \times G_R}{L_T \times L_{aT}} \qquad (5)$$

where: $EIRP_T$ - EIRP of the user transmitter;

G_R - user receiver antenna gain in boresight direction;

L_{aT} - atmospheric loss in the path between the user transmitter and the user receiver;

L_T - $(4\pi R_T/\lambda)^2$ - free-space loss in the path between the user transmitter and the user receiver.

The jammer EIRP required to cause a J/S power ratio, at the front-end of the user terminal, is found from (4) and (5):

$$EIRP_J = \frac{J}{S} \times EIRP_T \times \frac{G_R}{G_R(\theta)} \times \frac{L_{aT}}{L_{aJ}} \times \left(\frac{R_J}{R_T}\right)^2 \qquad (6)$$

A close look at (6) shows that the capability of a jammer to degrade the performance of a user terminal is determined by many factors such as the J/S ratio required to sustain communication at a specified data rate with an acceptable BER, the user EIRP, the gain and the sidelobe level of the user receiver antenna, atmospheric losses in the two paths and the square of the ratio of jammer and user path lengths.

The jammer and user EIRPs are mainly determined by the nature of the jamming platform and the design of the user system respectively. Space-borne and air-borne antenna gains are limited mainly by size, while the platform dynamics (pointing errors) determine the ship-borne antenna gain. This is in contrast with the case for large ground-based antennas, where reflector surface errors, pointing errors and the angle-of-arrival jitter constitute the major limitations on the gain (Ref. 12). The transmitter power is platform-dependent and may be limited by efficiency, operating frequency, prime power, cooling requirements, bandwidth, cost, mobility, reliability, tunability etc. (Ref 1).

The ratio $G_R/G_R(\theta)$ is determined by the peak gain and the sidelobe characteristics of the user receiver antenna. For example, a fixed NATO SGT antenna is a 42-ft dish with a peak gain of G_R = 58 dBi at 7.5 GHz. Antenna sidelobes' envelope is assumed to be bounded by the CCIR reference pattern for $D/\lambda > 100$ (D denotes the antenna size) (Ref. 13):

$$G(\theta) = \begin{cases} 32-25\log\theta & 1^\circ \le \theta < 48^\circ \\ -10 & \theta > 48^\circ \end{cases} \quad dBi \qquad (7)$$

In military communication systems, ECCM requirements and frequency coordination problems impose stringent requirements on antenna sidelobe levels. It is possible to realize sidelobe levels much lower (as low as -40 dBi) compared to the CCIR reference pattern at the expense of increased cost, weight, size and decreased aperture efficiency (hence gain). The main contribution to far out sidelobes comes from electromagnetic fields diffracted from edges and struts. Therefore, the sidelobe reduction techniques such as shaping the rim with a large curvature (so as to reduce diffraction), the use of serrated edges, loading the antenna rim with absorptive material, using tunnels around the reflector edge, oversizing the reflector (to reduce edge illumination) and tapering the aperture illumination, all aim to reduce the level of edge-diffracted fields (Refs. 14-16).

Antenna sidelobe levels can also be suppressed in certain angular regions by using adaptive sidelobe cancellation techniques which basically consist of subtraction of the undesired signals from the wanted signals (Refs. 17-21).

One can as well reduce the effective power radiated in or received from the direction of far-out sidelobes by using site-shielding effects. Hills, vegetation, embankments and pits, buildings and fences can be used for shielding purposes. It is reported that carefully selected site-shielding techniques can provide considerable improvement (up to 40 dB) in effective sidelobe performance (Ref. 22).

In the SHF band, the atmospheric attenuation is negligibly small. In the EHF band, the atmospheric attenuation suffered by a space-borne platform would be similar to that observed in a SATCOM link. However, air-borne and ground-based platforms can experience much higher losses, in proportion to the path length remaining under the maximum rain height. The atmospheric attenuation experienced by an earth-based platform operating at EHF frequencies can be much higher compared to that observed by a SATCOM link. However, provided that an air-borne platform is kept well away from a SGT, increased height results in more effective downlink jamming and interception, because of the reduction in atmospheric attenuation. Note that the atmospheric attenuation at EHF downlink frequencies (20 GHz) is much less compared to that in the uplink frequencies (44 GHz). At heights more than about 10 km, the gaseous attenuation is reported to be close to that for a SATCOM link with the same elevation angle (Ref. 23).

Propagation effects have different impacts on the communication and interception/jamming paths. For example, rain attenuation that is likely to occur for a small percentage of time is of considerable importance to the user who is concerned with the information transmission with high reliability. Therefore, the margin for the user path is often a permanent feature of the communication system unless the uplink power or FEC are adaptively controlled (Refs. 24-26), and this aids an interceptor. However, the importance of rain attenuation is significantly less for an interceptor or jammer who does not neces-

A typical area coverage quiescent pattern for each of the antennas is shown in Figure 2. The beams were weighted equally and the beam spacings were chosen to produce a uniform gain over the coverage area. As shown in Figure 2, the gain is fairly uniform out to 0.75 degrees for each of the four cases. The first sidelobe is approximately 25 dB down from peak gain for the 7-beam antenna, 20 dB down for the 9-beam antenna, 35 dB down for the 16-beam antenna and 33 dB down for the 19-beam antenna.

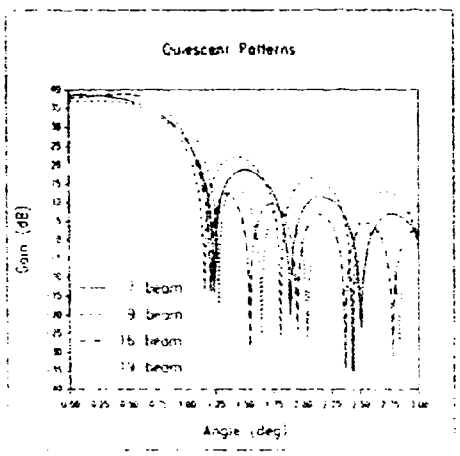

Figure 2. Area coverage quiescent antenna patterns

III Area Coverage

Area coverage performance assumes that the satellite is servicing a user at an unknown location within a specified area. The quiescent pattern consists of all the beams being "on" and equally weighted to produce a uniform coverage over the fixed area.

Three jammer scenarios are considered for the area coverage statistics. The first scenario consists of one mobile jammer within the coverage area. The second scenario consists of one mobile jammer within the coverage area and one fixed jammer outside of the area coverage. The third scenario consists of two mobile jammers within the coverage area and one fixed jammer outside of the coverage area. The mobile jammer signal is assumed to be 15 dB greater than that of the user signal at the receiver; the fixed jammer signal is assumed to be an additional 10 dB stronger. The statistics were generated by randomly selecting ten positions of the mobile jammer(s) within the area coverage. Two additional cases are included in the statistics in which the mobile jammer(s) is located at one of the double and one of the triple/quadruple crossovers to ensure that worst case jammers are properly considered. The addition of these cases may lead to somewhat more conservative results.

The antenna system "cancels" an interfering signal by measuring the incoming signals and adapting the weights applied to each of the elements to place a pattern null in the direction of the undesired source [4]. For an N-beam antenna, the steady state weights W are determined by the N x N correlation matrix C at the antenna elements and the initial pointing (weighting) vector P:

$$W = C^{-1}P$$

where

$$P = [1,1,\ldots,1]$$

Phasing has not been applied to the initial weights. Phasing would reduce the percent area coverage loss due to the narrowing of the null in the desired direction. This effect becomes less pronounced for multiple nulls [3]. System performance was measured by calculating the signal to interference plus noise ratio (SIR) and from that computing the energy per chip divided by the noise ($EChip/N_0$). This value was then compared to a threshold of 12.4 dB which was assumed for link closure.

The percent area coverage available for communication as a function of data rate is shown in Figure 3 for each of the four antenna configurations and three jammer scenarios. As shown in this figure, the percent area coverage is a decreasing function of data rate. In the one jammer scenario, for example, the percent area coverage decreases from approximately 97% to 82% as the data rate increases from 1 MChips to 64 MChips for the smaller aperture antenna, and drops from 99% to 91% for the larger aperture antenna. The larger aperture antennas outperform the smaller aperture antennas for each of the three jammer scenarios, and performance for each of the antennas decreases as additional jammers are present. In general, the hexagonal configuration (7-beam, 19-beam) outperforms the comparable square configuration (9-beam, 16-beam), an effect which is more evident as the number of jammers increase.

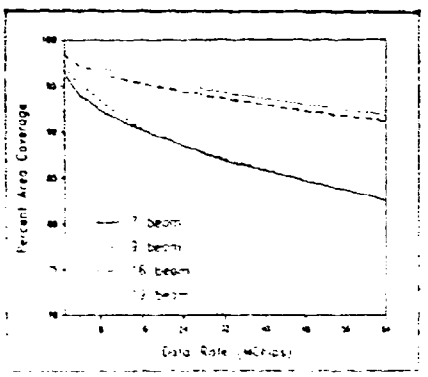

(a)

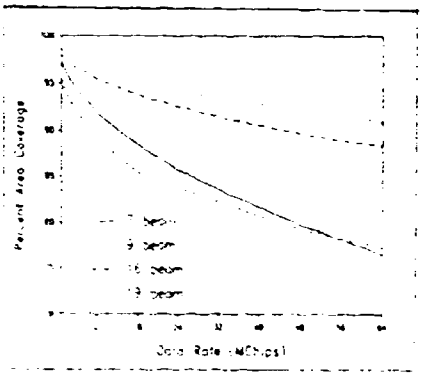

(b)

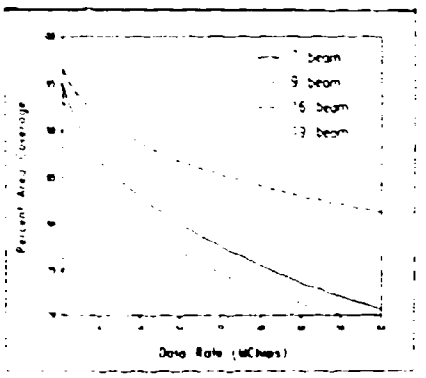

(c)

Figure 3 Coverage area availability for each of the four antennas
(a) One jammer scenario
(b) Two jammer scenario
(c) Three jammer scenario

$$\left(\frac{C}{N_o + J/W}\right)_R \approx \left(\frac{C}{N_o}\right)_R \times \left(\frac{N_o}{J/W}\right)_R \qquad J/W >> N_o \quad (9)$$

where $(C/3_o)_R$ is given by (8). J denotes the jammer power in a receiver bandwidth of W.

Similarly, carrier-to-noise power density ratio at the interceptor may be written as:

$$\left(\frac{C}{N_o}\right)_I = \frac{P_T \times G_T(\theta)}{k \times L_I \times L_{aI}} \times \left(\frac{G}{T}\right)_I \qquad (10)$$

where: $G_T(\theta)$ - transmitter antenna gain in the direction of the interceptor;

L_I - $(4\pi R_I/\lambda)^2$ - free-space loss in the path between the transmitter and the interceptor;

L_{aI} - atmospheric loss between the transmitter and the interceptor;

$(G/T)_I$ - figure-of-merit of the interceptor antenna in the direction of the transmitter.

The parameter d^2, which is a measure of the post-detection (output) signal-to-noise power ratio of a radiometer (energy detector), can be shown to be related to $(C/N_o)_I$, the carrier-to-noise power density ratio required at the input of the intercept receiver for a specified P_D (probability of detection) and P_{FA} (probability of false alarm) (Refs. 32 and 33):

$$d = \frac{1}{\eta} \times \left(\frac{C}{N_o}\right)_I \times \sqrt{\frac{T}{W_I}} \qquad (11)$$

where: η - correction factor in using Gaussian statistics at the output of the energy (square law) detector when it should be chi-square statistics. It is a function of P_D, P_{FA} and the TW_I product. For a spread spectrum signal, the time-bandwidth product is large enough (even for relatively small values of T) to allow the use of Gaussian statistics, then $\eta = 1$;

T - total integration time,

W_I - bandwidth of interception receiver.

The post-detection signal-to-noise power ratio required to achieve a certain P_D and P_{FA} depends on the interception receiver. A signal is assumed to be detectable with a P_D and P_{FA}, if d exceeds some threshold value SNR. In a non-jamming environment, this leads to an interception range R_I, which is found from (10) and (11):

$$R_I < \frac{\lambda}{4\pi} \times \left[P_T \times G_T(\theta) \times \frac{1}{L_{aI}} \times \frac{(G/T)_I}{k \times \eta \times SNR} \times \sqrt{\frac{T}{W_I}}\right]^{1/2} \qquad (12)$$

A close look at (12) shows that the interception range changes with some factors which are determined by the user transmitter, the atmospheric losses and the characteristics of the interception receiver (Ref. 31). Since some of these factors are already discussed in connection with jamming factors, we will be concerned with those associated only with interception:

(i) The figure-of-merit of the interceptor antenna is a primary trade-off parameter for detection, since the search area within the field-of-view of the interceptor decreases with increasing antenna gain. Note that the interception range is directly proportional to the interception receiver antenna size. The desire to maximize P_D favours antennas with large beamwidths so that large spatial sectors can be rapidly searched; however, detection and sensitivity considerations will likely be the primary drivers for the antenna design. To increase the detection capability for a fixed coverage area, interceptor can opt to use larger antennas and a greater number of them. Another alternative is to use scanning antennas, which implies a reduced integration time. Assuming that the period of the scanning cycle is less than or equal to the transmission duration, then only a fraction of the transmission time could be observed by an interceptor. Recent advances in phased arrays and multi-beam antennas will evidently offer many advantages to an interceptor (Refs. 9, 34 and 35).

(ii) $EIRP_T$ (thus P_T) is determined by the system design. Obviously, the EIRP in the direction of the interceptor, $P_T G_T(\theta)$, should be kept at minimum for decreasing the interception range. This can be achieved by minimizing the transmitter power and the sidelobe levels of the user transmitter antenna.

(iii) SNR denotes the effective post-detection signal-to-noise ratio at the interceptor to achieve certain detection and false alarm probabilities. This depends on the interceptor design, the integration time and the interception bandwidth.

(iv) Forcing an interceptor to use a wider bandwidth and a shorter integration time is a clever strategy to reduce the

interception range (see (12)). However, because of the $(T/W_I)^{\frac{1}{4}}$ type dependence, the likely effect of this strategy may not be very significant. For example, an increase in the interception bandwidth from, say, 40 MHz (typical for SHF band) to 2 GHz (at 44 GHz) would decrease R_I by a factor of 2.7. In case where the whole SHF satellite bandwidth (= 340 MHz) is used, R_I would be reduced by only a factor of 1.55.

As far as the LPE performance is concerned, superiority of one or the other of the two main spread spectrum techniques, namely direct sequence (DS) and FH, is a controversial issue (Refs. 36-38). The frequency hopping waveform provides the interceptor with options in receiver design that can improve interceptor performance such as dividing the spreading bandwidth (which may be much wider compared to that offered by DS systems) into channels and dedicating a narrowband receiver to each channel. While this approach does require a greater investment on the part of the interceptor, it increases the probability of interception (Ref. 38). On the other hand, DS signals can easily be detected by carrier and chip-rate detectors which are relatively simple and inexpensive. In practice, most of the interception techniques offer similar performance to that of a wideband radiometer.

In slow FH systems, an interceptor may be able to detect and recover information from each hop. Fast hopping may be generally better since it reduces the integration time and consequently leads to reduced interception range. However, when the hopping rate exceeds the data rate, non-coherent combining losses at the user receiver would require a matching increase in the EIRP of the user transmitter, thus potentially reducing the ECCM capability of the system. For an improved ECCM performance, the system designer has to determine the optimum hopping rate as a trade-off between non-coherent combining losses, dehopping implementation, synchronization and vulnerability to RBJ (Ref. 36). However, practical considerations may probably dominate in the choice of hopping rate, particularly as arguments about the enemy's ability to detect and possibly follow a FH signal are highly speculative.

3.1 AN EXAMPLE: UPLINK INTERCEPTION

To compare the effectiveness of the interception threat at SHF and EHF frequencies, let us consider an interception receiver with a ½-ft diameter antenna and 400°K noise temperature. Assume that the interception receiver operates with a P_D = 0.9 and $P_{FA} = 10^{-6}$; this requires a post-detection SNR of at least 7.6 dB. The assumed integration time of τ = 62.5 ms corresponds to one hop duration of a 16 hops/s FH system. The interception bandwidth is taken as 2 GHz for EHF uplinks while, in the SHF band, spread bandwidths of 40 MHz (typical for DS systems) and 340 MHz (typically maximum available FH bandwidth) are considered. Atmospheric losses are ignored in the SHF band but, in the EHF band, they are assumed to be 12 dB (range: 240 km, interceptor height: 9.1 km) for an air-borne uplink interception platform and 4 dB (CCIR region H, 5% outage and 20° elevation angle) for a space-borne uplink interception platform (Refs. 1 and 36).

Based on the above assumptions, the variation of the interception range with the EIRP of the user transmitter in the direction of an interceptor, $P_T G_T(\theta)$, is shown in Fig. 5, from which the following conclusions can be drawn:

(i) EHF offers an improved LPI performance compared to SHF.

(ii) The user signals, with EIRPs higher than approximately 20 dBm in the direction of an interceptor in the SHF band and 35 dBm in the EHF band, can be detected at ranges closer than 300 km or so. Note that an EIRP of 20 dBm, in the direction of an interceptor, can be achieved with far-out sidelobe levels as low as -30 dBi and 100W transmitter power. With a 6-ft antenna size, such a transmitter can realize a peak EIRP of 89 dBm (in the direction of the user satellite) at 7.5 GHz (Ref. 39). This terminal can hardly support a 75 bits/s link even under nuisance-jamming conditions. This may provide a clear example for showing the vulnerability of user systems against interception under jamming.

(iii) Since the interception range is directly proportional to the interceptor antenna size (see (12)), doubling the interceptor antenna size (1 ft instead of ½ ft in Fig. 5) doubles the interception range.

In view of the above considerations one can conclude that the LPE performance of MILSATCOM systems can be improved and the interception range can be minimized by the following:

(i) Operation in the EHF band. Although it is highly scenario-dependent, it is obvious that the EHF band is more suited for LPE purposes compared to the SHF band.

(ii) Maximizing the effective spread spectrum processing gain, i.e. reducing the data rate and/or increasing the spreading bandwidth.

(iii) Reducing the sidelobe level of the user transmitter antenna, to decrease the power radiated in the direction of potential interceptors and to increase the antenna discrimination against jamming signals.

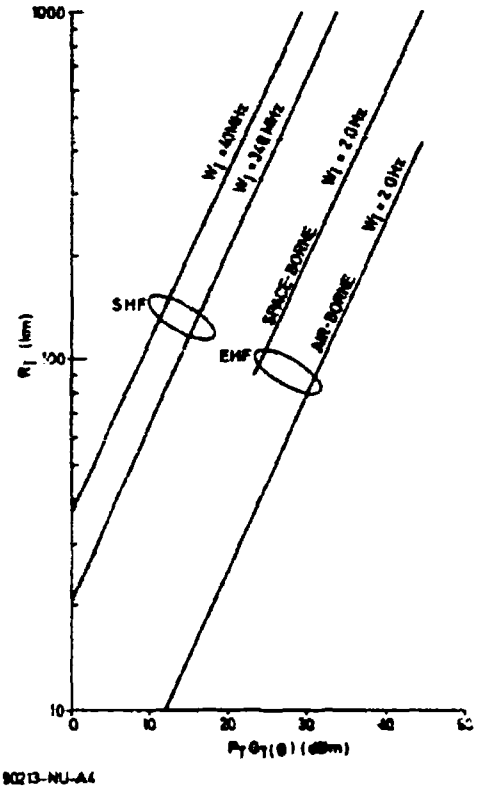

Fig. 5 Variation of the interception range versus the EIRP of the user transmitter in the direction of an interceptor. P_D = 0.9, P_{FA} = 10^{-6}, SNR = 7.6 dB. Integration time T_I = 62.5 ms. $(G/T)_I$ = -6 dB at 7.5 GHz and 7 dB at 44 GHz. L_{AI} = 0 dB for SHF, and 12 dB and 4 dB for respectively air-borne and space-borne EHF interception platforms.

(iv) Minimize the user EIRP and the duration of transmitted signals subject to communications requirements. To satisfy higher EIRP requirements, one should increase the antenna size instead of the transmitter power while keeping the sidelobe levels as low as possible. Thus, sidelobe radiation is kept at a minimum for AJ and LPE purposes.

(v) Take full advantage of site shielding and propagation effects.

(vi) The LPE waveform of choice is FH over as wide a spreading bandwidth as possible. Where LPE rather than AJ is the overriding consideration, time spreading in addition to frequency spreading may also be considered (Ref. 30). Note that AJ and LPE represent often conflicting modes of operation.

(vii) Ensure adequate operator training in LPE procedures.

4. REPEAT-BACK JAMMING

RBJ, which is a threat mainly against slow FH and hybrid systems, consists of intercepting, processing and re-transmitting the signals, received from the user transmitter, to the user receiver before the user system hops to a new set of frequency channels.

To be effective in RBJ, the differential path delay between the repeat-back jammer and the user receiver (the difference in time delay between the propagation path and the path via the repeat-back jammer) should be less than the difference between the FH signal dwell time and the time required to process the intercepted signals (Refs. 30 and 40). Thus, higher the hopping rate, more protected the FH system is against RBJ and closer the RBJ platform must be to the propagation path.

Apart from the above restrictions, there are other problems associated with RBJ. A large portion of the hopping bandwidth must usually be monitored by the interception receiver of a RBJ platform. In presence of many communicators in different channels, the interception receiver may be faced with a formidable signal-sorting problem (e.g. time of arrival, direction of arrival, etc.) in attempting to isolate a small number of the intercepted signals to be targeted (Ref. 40).

RBJ applies to both up- and down-links. In contrast to an uplink repeat-back jammer, a downlink repeat-back jammer can intercept all downlink channels within the coverage area of the satellite.

RBJ can therefore be a potential threat only against slow FH systems. This threat can be countered by increasing the hopping rate. This, in turn, increases the cost and decreases the reliability of the RBJ platform, makes the synchronization more difficult and puts limitations on the switching time of FH synthesizers (Ref. 40).

Recently, there has been considerable interest in the vulnerability of FH systems to RBJ and the required countermeasures (Refs. 41-44). Among the techniques suggested to partially alleviate this threat is a random FH/FSK system which differs from the traditional methods based on fast FH techniques (with attendant synchronization problems) and consists of a slow FH system which is yet not susceptible to RBJ. This technique involves the selection of the FSK signalling tones (during each hop) pseudo-randomly from all signalling tones available in the FH bandwidth. The effectiveness of a repeat-back jammer can thus be reduced drastically since such a jammer can follow and jam only the signalling tone frequency over which the data is sent (Ref. 41).

5. CONCLUSION

This paper aims to identify the relative significance of the factors determining the performance of MILSATCOM systems against electronic attacks. This is evidently very important for the realization of robust MILSATCOM systems since it leads to the provision of balanced and cost-effective ECCM.

The relative significance of the ECCM factors are identified from the performance predictions for MILSATCOM systems, operating with geostationary satellites, under up- and downlink jamming. The system vulnerability against signal exploitation and RBJ is considered. The implications of AJ and LPE modes of operation in SHF and EHF bands are also discussed.

There are many aspects of MILSATCOM systems that can be exploited by an enemy and most of these aspects can be improved by various ways. Therefore, the provision of necessary ECCM is often a costly and complex process. It is crucial, at the first stage, to develop an awareness of the relative importance of the ECCM factors. The specific ECCM required by a system can be implemented in a balanced, integrated and cost-effective way only at the design stage, not in isolation but when balanced with countermeasures against nuclear and physical threats as well.

This paper is concerned with MILSATCOM systems operating with geostationary satellites. Use of alternative orbits and the proliferation of SGTs and spacecraft as countermeasures to electronic, nuclear and physical attacks are not considered.

REFERENCES

1. M. Safak, An assessment of the jamming and interception threats to the NATO SATCOM system, SHAPE Technical Centre Technical Memorandum STC TM-872 (draft), December 1988 (NATO Secret).

2. M. Safak, An overview of threat assessment for the NATO SATCOM system, AGARD Symposium on ECCM measures for avionics sensors and communication systems, 1-4 October 1990, Munich, paper No. 4.

3. V.K. Bhargava and Q. Wang, Jamming and electronic countermeasures, AGARD Conf. Proc. No. 420 (AGARD-CP-420), Effects of electromagnetic noise and interference on performance of military radio communication systems, Lisbon, 26-30 October 1987, pp. 20-1/11.

4. A.E. Feyrin, NATO IV satellite loading plans, SHAPE Technical Centre Technical Note STC TN-174, February 1988 (NATO Restricted).

5. Analysis of MILSATCOM systems in a stressed environment, 19 May 1986, Defense Communications Agency, Military Satellite Communications Systems Office, Washington, D.C. (NATO Unclassified).

6. Revised report of the NATO SATCOM Enhancement Working Party, DS/C/EL(88)465 (AC/302(SG/8) Serial 136), 6 September 1988 (NATO Secret).

7. L.P. Riddle, On-board processing of faded satellite communication signals, MILCOM '88, Vol. 1, pp. 13.5.1-5.

8. S.I. Sayegh et al., On-board processing architectures and technology, IEEE EASCON 1988, 21st Annual Electronics and Aerospace Conference, Arlington VA, 9-11 November 1988.

9. I. Ohtomo and H. Kumazawa, On-board multibeam antenna technologies for future communication satellite, 18th European Microwave Conference, 12-15 September 1988, Stockholm, pp. 61-69.

10. W.W. Wu et al., Coding for satellite communication, IEEE Journal Selected Areas in Communications, Vol. SAC-5, No. 4, May 1987, pp. 724-748.

11. Q. Wang et al., Error correcting codes for fast frequency-hopped MFSK spread-spectrum satellite communications under worst case jamming, Intern. Journal Satellite Communications, Vol. 7, pp. 115-128, 1989.

12. M. Safak, Limitations on reflector antenna gain by random surface errors, pointing errors and the angle-of-arrival jitter, IEEE Trans. on Antennas and Propagation, Vol. 38, No. 1, January 1990, pp. 117-121.

13. Handbook satellite communications: fixed-satellite service, ITU, Geneva, 1988.

14. C.M. Knop and Y.B. Cheng, A note on the mitigation of EMI caused by wide-angle radiation from parabolic dish antennas, IEEE Trans. Electromagnetic Compatibility, Vol. 30, No. 4, pp. 583-586, November 1988.

15. P.A. Beeckman, Control of far-field radiation patterns of microwave reflector antennas by using serrated edges, IEEE Proc., Vol. 134, Pt. A, No. 3, pp. 270-274, June 1987.

16. O.M. Bucci et al., Control of reflector antenna performance by [illegible] loading, IEEE Trans. Vo AP-[illegible], No. 5, pp. 773-779, 1981

17. J.T. Mayhan and L.J. Ricardi, Physical limitations on interference reduction by antenna pattern shaping, IEEE Trans. Antennas Propagation, Vol. AP-23 No. 5, pp. 639-646, September 1975

18. J.T. Mayhan, Nulling limitations for a multiple-beam antenna, IEEE Trans. Antennas Propagation, Vol. AP-24, No. 6, pp. 767-779, November 1976.

19. A.J. Fenn, Maximizing jammer effectiveness for evaluating the performance of adaptive nulling array antennas, IEEE Trans. Antennas Propagation, Vol. AP-33, No. 10, pp. 1131-1142, October 1985.

20. J.T. Mayhan, Area coverage adaptive nulling from geosynchronous satellites: phased arrays versus multiple-beam antennas, IEEE Trans. Antennas Propagation, Vol. AP-34, No. 3, pp. 410-419, March 1986.

21. M.L. Burrows, Closer spacing of geostationary satellites through adaptive nulling at the ground terminal, IEEE Trans. Antennas Propagation, Vol. AP-35, No. 7, pp. 870-873, July 1987.

22. R.G. Gould and C. Schmitt, Interference reduction techniques for satellite earth stations, Proc. IEEE Electromagnetic Compatibility Conference, Montreux, 1977, pp. 285-292.

23. D.P Haworth, Outage calculation for atmospheric propagation effects, Annex I to AC/302(SG/8)R/17, 3 April 1985 (NATO Unclassified).

24. J Horle, Uplink power control of satellite earth-stations as a fade countermeasure at 20/30 GHz communications systems, Intern. Journal Satellite Communications, Vol. 6, pp. 323-330, 1988

25. M.F Khan et al., Further studies on efficient AFEC schemes for Ka-band satellite systems, IEEE Trans Aerospace and electronic systems Vol. AES 25 No 1, pp 9-19 January 1989

26 M J Willis and B G. Evans Fade countermeasures at Ka band for Olympus, Intern. Journal Satellite Communications, Vol 6, pp. 301-311, 1988

F Carassa et al., Frequency diversity and its applications, Inter. Journa. Satellite Communications Vol 6, pp 313-3.. 1988

L. Ippolito Jr. Radiowave propagation in satellite communications Van Nostrand Reinhold Company New York, 1986

.. Nicholson Spread spectrum signal design, LPE & AJ systems, Computer Sciences Press, Rockville, MD 1988

30 D J Torrieri, Principles of secure communication systems Artech House Norwood, MA 1985.

31 L L Gutman and G E Prescott, System quality factors for LPI communications, IEEE AES Magazine, pp. 28-28, December 198

32. J.D. Edell, Wideband, noncoherent, frequency-hopped waveforms and their hybrids in low-probability of intercept communications, Naval Research Laboratory, NRL Report 8025, 8 November 1976

33. D.G. Woodring, Performance of optimum and suboptimum detectors for spread spectrum waveforms, Naval Research Laboratory, NRL Report 8432, 30 December 1980.

34. H.E. Schrank, Low sidelobe phased array antennas, IEEE Antennas and Propagation Society Newsletter, April 1983, pp. 5-9.

35. G. Cochier and F. Gautier, Overview of phased arrays for future airborne radars, Military Microwaves '88, Conf. Proc., Wembley Conference Centre, London, UK, 5-7 July 1988, pp. 123-127.

36. D.P. Haworth and R.L. Harris, Exploitation of mm waves for MILSATCOM, Proc. NATO/CNAD Conference on mm waves, 28 January 1988 (NATO Restricted.

37. E.W. Chandler and G.R. Cooper, Development and evaluation of LPI figure-of-merit for direct sequence and frequency-hop systems, MILCOM '85, pp. 603-608, paper No. 333.

38. M. Spellman, A comparison between frequency hopping and direct spread PN as antijam techniques, IEEE Communication Magazine, Vol. 21, No. 2, March 1983, pp. 37-51.

39 L Koolen, Satellite communications in NATO maritime communications aspects, SHAPE Technical Centre, Briefing Notes, 1988.

40 D.J Torrieri, Fundamental limitations on repeater jamming of frequency-hopping communications, IEEE Journal Selected Areas in Communications, Vol 7, No 4, pp. 569-575, May 1989.

41 J.E. Blanchard A slow frequency hopping technique that is robust to repeat jamming, MILCOM '82, pp. 14.1-1/9

42 R S. Orr, Performance of MFSK in simultaneous partial-band and repeat-back jamming, MILCOM '82, pp. 28 1/4.

43 F Amoroso, Hidden preamble for frequency hopped anti-jam synchronization, MILCOM '8' Vol. 1 pp 33 1 ..5.

44 L.E Miller et al., Performance of frequency-hopped random MFSK in follow-on and partial band noise jamming, GLOBECOM 86 (IEEE Global Telecom Conference), Houston, USA, 1-4 December 1986, Vol. 2, pp. 743-749

Discussion

Prof. Ince

In your chart, where you showed throughput verus jammer EIRP, you were assuming that the receiver was not linear: Am I right or wrong?

Author's Reply

I think we assumed that the receiver, to show an acceptable performance, should have an E_b/N_0 which is equal to 10 dB. 10 dB is sufficient for an acceptable performance. That is a generic number — it doesn't necessarily correspond to a particular specific equipment. But it doesn't have to saturate the receiver.

Dr B.Felstead, CRC, Canada

(i) What form of intercept device did you assume? Was it a wideband radiometer?

(ii) Have you done any example calculations of detection range? I am concerned that, even with spread spectrum, detection ranges can be hundreds of kilometres.

Author's Reply

(i) To keep the results more general, we modelled the interception receiver in terms of the post-detection signal-to-noise ratio required to achieve a certain probability of detection and probability of false alarm. So, the results apply to any interception receiver.

(ii) The results of the sample calculation are presented in Figure 5 of the paper. Figure 5 confirms your opinion that detection is possible at very long ranges even when spread spectrum systems are used.

PERFORMANCE OF MILSATCOM ADAPTIVE ANTENNA SYSTEMS IN PULSE JAMMER ENVIRONMENTS

W. B. Gail and I. M. Weiss
The Aerospace Corporation
P.O. Box 92957, Los Angeles, Ca. 90009
U.S.A.

ABSTRACT

MILSATCOM antennas which use a linear gradient adaptive nulling algorithm to cancel interference respond differently to pulse jammers than to continuous wave (CW) jammers with the same peak output power. For a pulse jammer, the antenna adapts to cancel the interference when the jammer is on and recovers toward the unadapted state when the jammer is off. The adaptation time constants are approximately proportional to the received jammer signal power and the system noise respectively; the "attack" time constant is generally much smaller than the "release" time constant. An effective pulse jammer exploits this time dependence to prevent the antenna from fully cancelling the interference.

For a particular antenna system, the worst case pulse jammer for a given waveform can be expected to occupy a well-defined region of the operating space defined by the aspect angles, signal power, jammer power, duty cycle, and pulse repetition frequency (PRF). In this paper, the effect of each of these parameters on antenna performance is investigated for a multiple pulse jammer environment. The worst case operating space is identified for typical MILSATCOM antennas and the characteristics of the operating spaces are compared. Under certain well-defined conditions, antenna performance in a pulsed interference environment is worse than in a CW interference environment.

I. INTRODUCTION

Adaptive antenna processors which use a linear gradient least-mean-squares (LMS) nulling algorithm to cancel interference are potentially vulnerable to pulse jammers. Such algorithms can be characterized by "attack" and "release" time constants which describe adaptation to the jammer on and off states respectively. An effective pulse jammer exploits these time constants to prevent the antenna from fully cancelling the interference. Previous work in this area [1-4] suggested that the vulnerability of a particular antenna system can be highly dependent on parameters such as jammer aspect angle, jammer duty cycle, and cooperative effects of multiple pulse jammers.

In this paper, the performance of multiple beam (MBA) antennas in the presence of pulse jammers is investigated. The four antennas which were considered, 7-element and 9-element arrays using an aperture diameter of 71 cm and 16-element and 19-element arrays using an aperture diameter of 111 cm, were designed to provide an area coverage diameter of approximately 1.5°. A similar comparison between a 7-element linear array and a 7-element MBA was described in a previous paper [5].

The basic theory of how a linear gradient nulling system responds to pulsed interference has been given in [1]. The complex weights which are used to control the output of an adaptive antenna satisfy the equation

$$\frac{dW}{dt} + k\Phi W = kS \qquad (1)$$

where W is the complex weight vector, Φ is the covariance matrix, k is the LMS loop gain, and S is the steering vector. A pulsed interference source is characterized by discontinuous amplitude changes which occur at discrete times $t = t_i$. If it is assumed that the interference amplitude is constant within the interval between $t = t_i$ and $t = t_{i+1}$, the transient response of the weight vector during the interval is given by

$$W(t) = e^{-k\Phi(t-t_i)}\left[W(t_i) - \Phi^{-1}S\right] + \Phi^{-1}S \qquad (2)$$

where $W(t_i)$ is the weight vector at the start of the interval. It is generally convenient to define a normalized time variable

$$\tau = k\sigma^2 t\,, \qquad (3)$$

where σ^2 is the variance of the assumed white Gaussian noise, and a normalized covariance matrix

$$\Phi = \frac{\dot{\Phi}}{\sigma^2} \qquad (4)$$

so that the results are independent of the particular choices for k and σ^2. The unit of time in this formalism, $\tau = 1$, corresponds to the "release" time constant $t = 1/(k\sigma^2)$ which characterizes the time required for the weights to reach their equilibrium values in the absence of jamming.

II. THEORY

Consider a single jammer with fixed amplitude, position, pulse-repetition frequency (PRF), and duty cycle. If the jammer turns on at time $\tau = 0$, the weights will exhibit a transient response as they settle toward equilibrium (Figure 1). The equilibrium response of the weights is characterized by a time-variation that is the same from one jammer period to the next; the weight vector at the beginning of the jammer period is thus equal to the weight vector at the end of the jammer period (Figure 2a). By equating these weight vectors, an expression for the equilibrium weight vector W_0 at the beginning of the jammer period can be obtained:

$$W_0 = (1 - E_2E_1)^{-1} \left[E_2(1 - E_1)\Phi_1^{-1}S + (1 - E_2)\Phi_2^{-1}S\right] \qquad (5)$$

where

$$E_i = e^{-\Phi_i(\tau - \tau_i)} \qquad (6)$$

is the exponential matrix for the i^{th} interval between jammer state changes, τ_i is the time at the start of the interval, and Φ_i is the covariance matrix for the interval. The time-dependence of the weight vector for the entire jammer period can be obtained easily from Equation 2 once this initial weight vector is known.

Figure 2b shows the generic response of the weights to an interference environment which includes several such jammers. If the state of one or more of the jammers changes at time $\tau = \tau_n$, the weight vector responds according to Equation 2. Assume that there is a master jammer period T_J such that T_J/T_i is an integer for all of the individual jammer periods T_i. Since the weights at the end of the master interval must equal the weights at the beginning of the master interval, an expression for W_0 can again be obtained:

$$W_0 = \left(1 - \prod_{i=1}^{n} E_i\right)^{-1} \left[\sum_{i=1}^{n-1}\left(\prod_{j=i+1}^{n} E_j(1 - E_i)\Phi_i^{-1}S\right) + (1 - E_n)\Phi_n^{-1}S\right] \qquad (7)$$

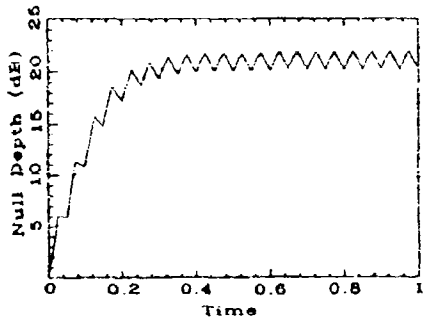

Figure 1: Typical transient response of null depth to a pulse jammer

where n is the number of intervals in the master interval (equal to the master interval divided by the shortest jammer period).

III. ANALYSIS TECHNIQUE

In order to investigate the adaptive antenna response to pulsed interference, a computer code was written to solve for the equilibrium time-history of the weights, using Equations 7 and 2, and calculate the signal-to-interference plus noise ratio (SINR) as a function of time over the master jammer period. The antenna performance was then evaluated in terms of the mean bit error rate, given by

$$\overline{P_e} = \frac{1}{2T_J}\int_0^{T_J} e^{-SINR(t)}dt \,, \qquad (8)$$

by assuming a differential phase-shift keyed (DPSK) waveform. This relation is valid as long as the bit rate is much larger than the jammer PRF. In order to approximate the effect of hardware errors, null depth was artificially limited in the computer code to a maximum value of 30 dB.

The analysis was performed for two feed packing geometries for each of two MBA aperture diameters. The patterns for these antennas are shown in Figure 3. For the 71 cm aperture, 7-element hexagonal and 9-element square pack feeds were considered. For the 111 cm aperture, 16-element hexagonal and 18-element square pack feeds were considered. For all four antennas, the peak gain of the individual beams and the beam spacing were chosen to produce an area coverage with comparable gain and a diameter of approximately 1.5°. The 71 cm antennas used a uniform feed illumination with a 5 dB edge taper while the 111 cm antennas used a Bessel on a 10 dB pedestal feed illumination with a 10 dB edge taper. The elevation angle is defined as the angle between the ray direction and boresite. The specifications for these antennas are listed in Table 1.

The variables which describe the jammers (power, bandwidth, elevation and azimuth, period, and PRF), the receiver (bandwidth), and the user (power, elevation and azimuth) define the parameter space for a particular antenna system. The goal of this work was to identify those portions of the parameter space for which $\overline{P_e}$ is worse for pulse jammers than for CW jammers and to compare the results for different MBA configurations. Unfortunately, the large number of dimensions in this space made an exhaustive search of all parameter combinations unfeasible. Instead, the code was set up to loop over two parameters at a time so that an extensive directed search could be performed. In this manner, it was possible to develop a qualitative understanding of how $\overline{P_e}$ varies with each of the parameters. Based on this understanding, those portions of the parameter space for which the pulse jammer $\overline{P_e}$ was worse than that for a CW jammer were identified and further analysis was performed on these subspaces. The parameter space which was searched is shown in Table 2.

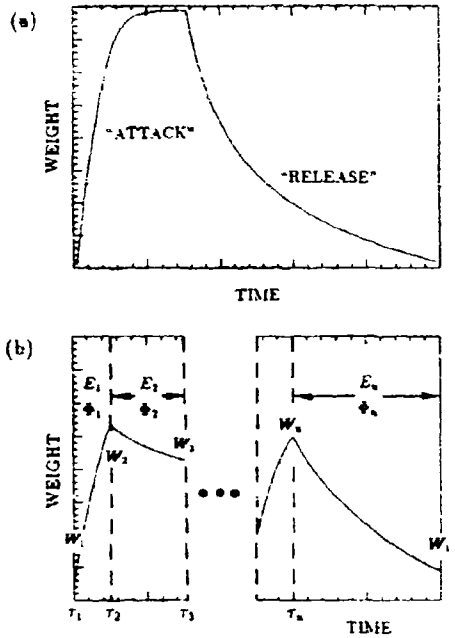

Figure 2: Typical time-variation of equilibrium weights for: a) one jammer, b) multiple jammers

IV. SINGLE PULSE JAMMER

The results of the analysis for a single pulse jammer are shown in Figures 4 and 5 for the 7-element and 9-element MBA's. Each plot in these figures shows $\overline{P_e}$ as a function of one of the operating parameters (jammer elevation, jammer PRF, jammer power, and user power) with curves parametric in duty cycle. Because only two parameters vary in each plot, the others were chosen so that interesting portions of the parameter space are represented.

7-element MBA. Figure 4a shows $\overline{P_e}$ as a function of elevation for duty cycles from CW to 10^{-5} in powers of 10 for the 7-element hexagonal pack MBA. The solid lines represent $\overline{P_e}$ when the antenna has fully adapted to cancel the interference and the dashed lines indicate the corresponding $\overline{P_e}$ for an unadapted antenna. The jammer period in this example is 0.01, the jammer power is 20 dBN (dB above noise), the jammer azimuth is 0°, and the jammer is assumed to be monochromatic. The user is on boresite with a power of 0 dBN. Near the 0° elevation of the user, the antenna is not very good at cancelling jammers and CW jammers maintain an advantage simply on the basis of larger average power. In the flanks of the coverage area, however, pulse jammers can be considerably more effective than CW jammers. In this region, nulling becomes less effective with decreasing duty cycle so that $\overline{P_e}$ approaches the unadapted value. The effect is particularly evident for the 10^{-5} duty cycle jammer. Outside of the coverage area, the sidelobes are sufficiently low that no jammers produce bit error rates above the clipping level of $\overline{P_e} = 10^{-9}$. The results for other azimuths are qualitatively similar due to the approximate circular symmetry of the elements.

The variation of $\overline{P_e}$ with the other parameters can be demonstrated by fixing the jammer elevation at 0.8°, corresponding to a jammer in the flanks of the coverage area. Figure 4b shows how $\overline{P_e}$ varies with PRF for such a jammer. For slow pulse jammers (i.e., the PRF is less than 1, equivalent to a jammer period less than the system time constant), $\overline{P_e}$ increases with increasing PRF until a maximum is reached near PRF=1. At higher PRF's, $\overline{P_e}$ decreases again to the CW value for higher duty cycles, but for lower duty cycles $\overline{P_e}$ becomes independent of PRF. At the lower duty cycles,

Table 1: Antenna parameters

Parameter	7-el	9-el	16-el	19-el
Diameter (cm)	71	71	111	111
3 dB BW (deg)	0.60	0.60	0.45	0.45
Peak Gain (dB)	43.6	42.8	46.7	46.0
Beam Spacing (deg)	0.65	0.57	0.45	0.45
Edge Taper (dB)	-5	-5	-10	-10

Table 2: Parameter space searched in the study

Component	Parameter	Range of Values
Jammer	Elevation	-90° to 90°
	Azimuth	0° to 180°
	JNR	-20 to +60 dB
	PRF	10^{-3} to 10^{3}
	Duty cycle	CW to 10^{-5}
	Bandwidth	CW
Receiver	Bandwidth	fixed
User	SNR	-40 to +20 dB

the pulses have become sufficiently short that little adaptation takes place while the jammer is on and the $\overline{P_e}$ is nearly that of the unadapted antenna.

Figure 4c shows how the response to the same jammer varies with jammer power. A low power jammer produces a $\overline{P_e}$ which is below the clipping limit of $\overline{P_e} = 10^{-6}$. A high power jammer produces a large $\overline{P_e}$ which approaches the unadapted value of $\overline{P_e}$ as a result of the null depth limitation of 30 dB imposed to simulate hardware errors. This limitation is also responsible for the cusp in the 10^{-5} duty cycle curve at a JNR of about 30 dB. There is an intermediate region from approximately 0 dBN to 25 dBN, however, for which $\overline{P_e}$ is considerably worse for pulse jammers than for CW jammers.

Figure 4d shows how the response to this jammer varies with signal power. At low signal powers, $\overline{P_e}$ approaches a value of 0.5 for all duty cycles. At signal powers above -20 dBN, $\overline{P_e}$ decreases rapidly for CW and higher duty cycle jammers, indicating the effectiveness of the nulling. For the lower duty cycle jammers, however, $\overline{P_e}$ does not differ considerably from the unadapted value until near 0 dBN as a consequence of the less effective nulling of these jammers.

9-element MBA. Figure 5 shows similar plots for the 9-element square pack MBA. Because of the higher sidelobe levels in this antenna, $\overline{P_e}$ values above the clipping level occur in the first sidelobe, as shown in Figure 5a. As with the coverage area flanks in the 7-element MBA, low duty cycle pulse jammers are more effective than CW jammers in this region, with $\overline{P_e}$ values approaching those of the unadapted antenna. Figures 5b-d are qualitatively similar to the comparable plots in Figure 4, indicating the 9-element MBA responds to pulse jammers in much the same manner as the 7-element MBA. Minor quantitative differences can be determined from the plots.

16-element and 19 element MBA's. Analysis of the 16-element square and 19-element hexagonal MBA's shows that the response of these larger aperture antennas to pulse jammers is qualitatively similar to that of the 7-element and 9-element arrays. Figure 6 shows $\overline{P_e}$ plotted as a function of elevation for both antennas, indicating the similarity to results for the smaller aperture antennas shown in Figures 4a and 5a. Only minor quantitative differences exist between all four antennas, suggesting that performance is not very sensitive to the number of elements, the packing geometry, or the aperture size.

General characterization. For these antennas, it is possible to provide a general characterization of the parameter space for which $\overline{P_e}$ is worse for pulse jammers than for CW jammers. This space is constrained by the following qualitative features: 1) jammer angular position in sidelobes or flanks of

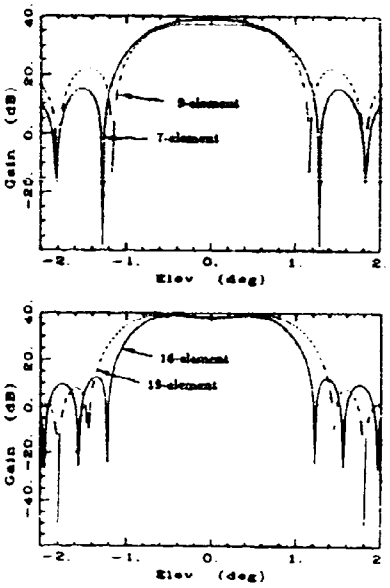

Figure 3: Antenna patterns for the four MBA's

the coverage area, 2) jammer period shorter than the adaptive system time constant, 3) jammer power approximately 0.25 dB above noise, 4) low jammer duty cycle, 5) user power greater than -15 dB above noise level. In addition, high PRF jammers have the valuable attribute that $\overline{P_e}$ is independent of PRF for certain duty cycles.

As was found in the study comparing the linear array with an MBA [5], there are a number of general rules which guide the choice of an optimal jammer for a particular antenna. First, pulse jammers can be more effective than CW jammers with the same peak power when the jammer is in the sidelobes or coverage area flanks. The primary exceptions are very low power users and very high power jammers. Second, for jammers in the flanks or sidelobes, the effectiveness of pulse jammers does not increase monotonically with jammer power. Pulse jammers of moderate power can thus be as effective as high power pulse or CW jammers. This result is in contrast to previous work, which suggested that null depth [2] or worst case $\overline{P_e}$ [4] is proportional to the average power of the pulse jammer. As is indicated by Figures 4a and 5a, $\log\overline{P_e}$ is proportional to average jammer power near the center of the area but not so in the flanks or sidelobes. Third, as has been shown previously [1,4], the optimal jammer period is generally comparable to the time constant of the adaptive antenna. However, near optimal performance can be obtained in particular cases if the jammer period is shorter than the adaptive time constant; such a pulse jammer is considerably more robust than one which is designed to reproduce the presumably unknown time constant of the adaptive antenna. Fourth, an optimal value of duty cycle can be identified for a particular antenna.

While it was assumed for this study that peak power is independent of duty cycle, microwave power devices are generally more efficient at low duty cycles. For a given input power, peak power at low duty cycles is typically 10 dB higher than for CW operation. This result provides an additional advantage to pulse jammers, particularly in light of the low duty cycles which were found to be most effective in this study.

V. MULTIPLE PULSE JAMMERS

To investigate antenna performance when multiple pulse jammers are present, a second jammer with fixed parameters was added to the simulation and the loop calculations were performed as with the single jammer. Multiple runs were

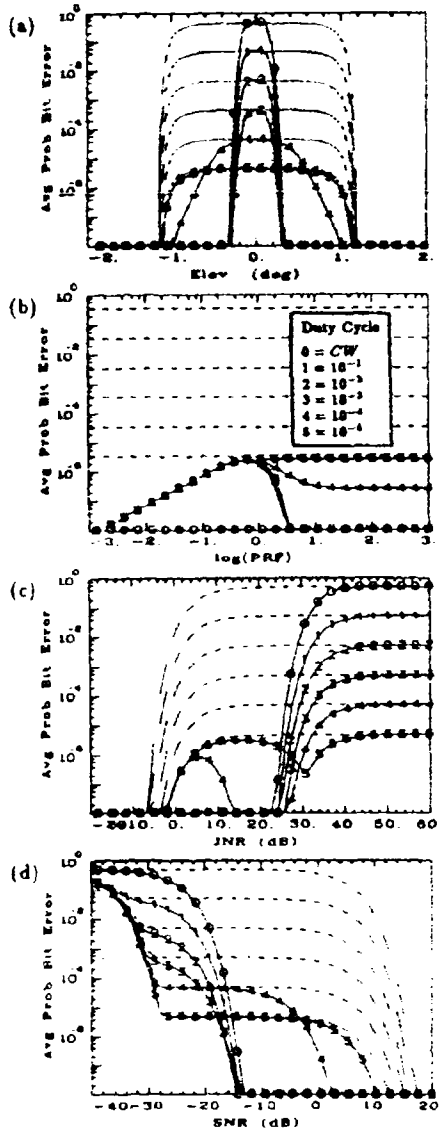

Figure 4: Adapted (solid) and unadapted (dashed) mean BER versus operating space parameters for the 7-element MBA with one jammer

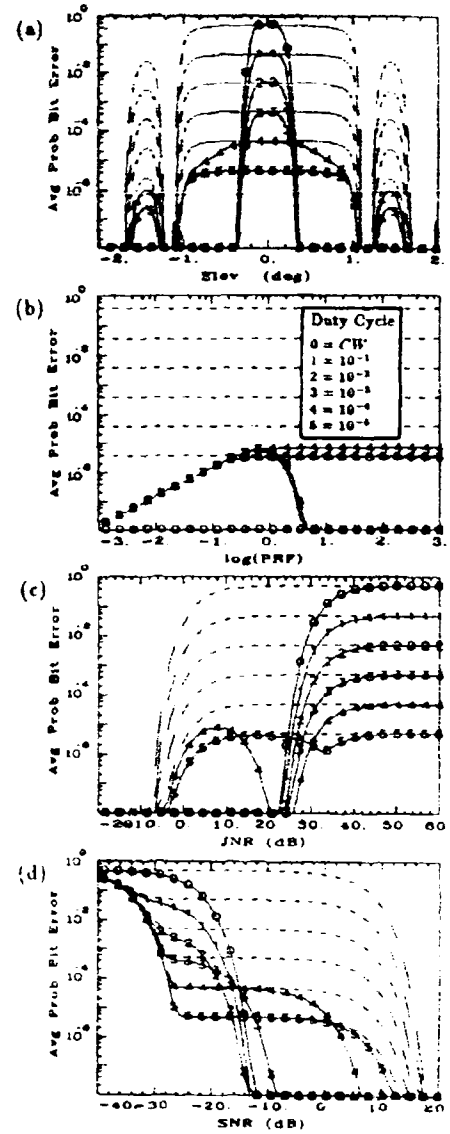

Figure 5: Adapted (solid) and unadapted (dashed) mean BER versus operating space parameters for the 9-element MBA with one jammer

made with different parameter values to determine parameter dependencies. To evaluate the impact of the second jammer, the "combined" bit error rate obtained by performing the calculation with both jammers operating simultaneously was compared with a "summed" bit error rate determined by calculating the SINR for each jammer separately and adding. Any difference between the combined and summed bit error rates indicates a coupling of the jammers or an inability of the antenna to simultaneously null the jammers to the level that each can be nulled separately.

A large number of cases were examined for all four MBA configurations. No cases were found for which the combined jammer performance differed from the summed performance by more than the computational error limits. Figure 7 shows two examples of two-jammer scenarios for which the "combined" $\overline{P_e}$ was compared with the "summed" $\overline{P_e}$ for the 7-element MBA. In both plots, $\overline{P_e}$ is plotted versus SNR with the "combined" $\overline{P_e}$ shown as a solid line and the "summed" $\overline{P_e}$ shown as a dashed line. In Figure 7a, the jammers were located at an elevation of 0.8° and azimuths of 30° and 0°, corresponding to one jammer midway between beams and the second near the center of the adjacent beam. The jammers operated in-phase with period 0.01. The first jammer had a fixed duty cycle of 0.1 and JNR=10 dBN. The second jammer had a variable duty cycle (corresponding to the four curves in the figure) and a JNR chosen to give the same average power as the first jammer. In Figure 7b, the jammers were located at an elevation of 0.8° and azimuths of 60° and 0°, corresponding to positions near the center of two adjacent beams. The jammers operated in anti-phase with period 1. The first jammer again had a duty cycle of 0.1 and JNR=10 dB. The second jammer had a variable duty cycle but a fixed power of JNR=10 dBN. In both figures, the small deviation of the "summed" $\overline{P_e}$ from the "combined" $\overline{P_e}$ can be accounted for by the inexact nature of calculating a "summed" $\overline{P_e}$.

While it is clear from temporal plots in these cases that the response to one jammer can affect the responses to other jammers, the equilibrium bit error rate appears to be unaffected by any coupling. Thus the null "pull-off" effect, which has been suggested as a potential problem for linear gradient adaptive systems [2], does not appear to affect the equilibrium nulling solution when evaluated in terms of $\overline{P_e}$.

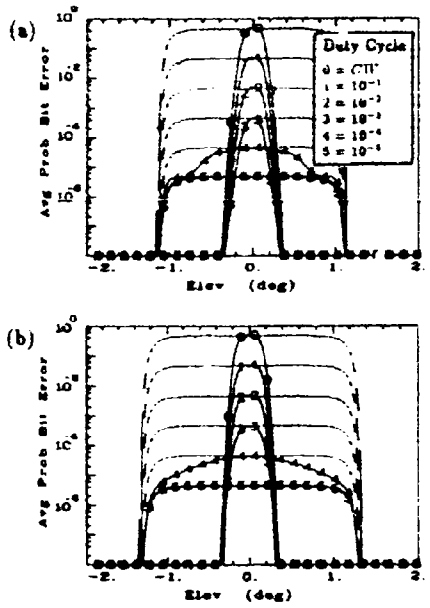

Figure 6: Adapted (solid) and unadapted (dashed) mean BER versus elevation for one jammer: a) 16-element MBA, b) 19-element MBA

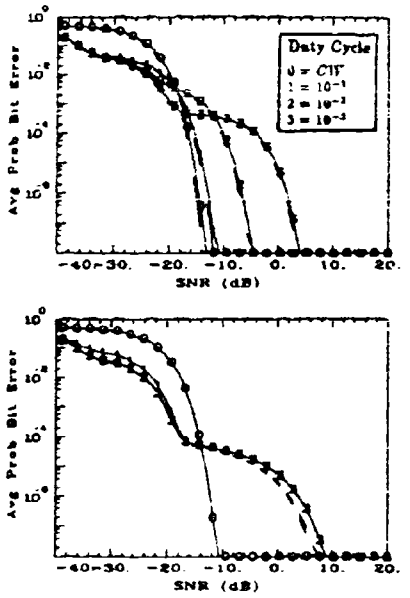

Figure 7: "Combined" (solid) and "summed" (dashed) mean BER versus SNR for the 7-element MBA for two two-jammer scenarios

VI. CONCLUSIONS

Four MBA antennas were investigated to determine the portion of the parameter space for which pulse jammers are more effective than CW jammers. This parameter sub-space was found to have well defined characteristics which are qualitatively similar for all four antennas. Antenna performance with one jammer present was found to be significantly worse for pulse jammers than for CW jammers under certain well-defined conditions. With multiple jammers present, performance was found to be the same as if the antenna adapted to each jammer independently. The results suggest that MBA performance in the presence of pulse jammers is relatively insensitive to aperture size, number of feed elements, and feed pack geometry for fixed area coverage dimensions.

REFERENCES

[1] R. T. Compton, "The effect of a pulsed interference signal on an adaptive array", *IEEE Trans. Aerospace Elect. Sys., AES-18*, 297, 1982.

[2] C. Zahm, "Pulsed and blinking jammer effects on adaptive arrays", *Proceed. Adaptive Antenna Sympos., RADC-TR-80-378*, Vol. 3, 2, 1980.

[3] J. L. Gleich and H. W. Hadley, "Adaptive antenna performance analysis against pulsed jammers", *Syracuse Research Corporation TR-85-1290*, 1985.

[4] A. A. Ksienski, "Effects of pulsed jammer on adaptive array performance", *IEEE Military Comm. Conf.*, 128, 1983.

[5] W. B. Gail and I. M. Weiss, "Adaptive antenna performance in a multiple pulse jammer environment", *IEEE Military Comm. Conf.*, 1990.

Discussion

Prof. Ince

The null depth is of the order of 30 dB. (Can you comment on that?)

Author's Reply

We artificially limited the null depth to 30 dB, essentially to simulate the effect of hardware errors which typically prevent the ultimate limit on the null depth from being obtainable.

Prof. Ince

(Do you assume) the receiver is linear? There are no capture effects, and so on?

Author's Reply

We simply solve that differential question: so various non-linear effects that come into a seal system were not included.

Prof. Ince

Do you intend to produce a prototype of this antenna?

Author's Reply

No, this is a computer analysis only. Directly, we're going to do more computer simulations with different sorts of jamming problems, that's all.

Performance Tradeoff of MILSATCOM Adaptive Multibeam Antennas

David H. Sensiba, Ira M. Weiss, Young S. Kim
The Aerospace Corporation
P.O. Box 92957
Los Angeles, CA 90009-2957
U.S.A.

Abstract - MILSATCOM satellite communication applications may require servicing a collection of users distributed over a localized geographical area in the presence of interfering noise sources. Recent interest in such applications has focused on the use of adaptive nulling antennas to counter interference by shaping the radiation pattern in response to the signal environment. This paper compares the nulling performance of gimballed multi-beam antennas (GMBAs) for hexagonal and square feed arrangements for two reflector diameters. Performance is characterized by the percent of the coverage area available for communication parameterized by data rate (area coverage mode) and by user / jammer separation resolution (spot beam mode).

I Introduction

MILSATCOM satellite communication applications may require servicing a collection of users distributed over a localized geographical area in the presence of interfering noise sources. In order to provide reliable area coverage performance, the receive antenna should reject interference outside of the coverage area while mitigating interference within the coverage area.

Spread spectrum techniques have been traditionally used to counter interference. To achieve further noise rejection, recent interest has focused on adaptive antenna processing. Adaptive antenna systems counter interference by shaping the antenna radiation pattern in response to the signal environment. An adaptive system consists of a multiple element antenna followed by an adaptive processor which measures the incoming signals and "cancels" an interfering signal by adapting the weights applied to each of the elements to place a pattern null in the direction of the undesired source.

For this study, a gimballed multi-beam antenna (GMBA) was selected for the antenna system. The GMBA is a mechanically steerable MBA based on simple technology and can be easily implemented on a spacecraft. The GMBA provides coverage to users dispersed over a fixed area against a variety of jammer threats. It generally has sidelobes that fall off rapidly outside the coverage area. The factors that most influence the GMBA design are the desired nulling resolution and coverage area. Resolution is a function of the antenna diameter and wavelength and coverage area is determined by these parameters and the number of beams.

The focus of this paper is a comparison of nulling performance for differing GMBA configurations. Two feed arrangement, hexagonal and square, are compared for reflector diameters of 71 and 111 centimeters. The EHF frequency band was selected to limit antenna size and improve nulling resolution within the chosen coverage area diameter of 1.5 degrees. Performance is evaluated in terms of the percent area coverage available for communication parameterized by data rate for the area coverage mode, and the user / jammer separation resolution for the spot beam mode.

II Antenna Configuration

Figure 1 illustrates the four antenna configurations studied in this report. The comparison configurations for the 71 cm. antenna consist of a 7-beam hexagonal lattice and a 9-beam square lattice. The comparison configurations for the 111 cm. antenna consist of a 19-beam hexagonal lattice and a 16-beam square lattice. The half power beamwidth is a function of the type of aperture, weighting, reflector diameter, wavelength, and edge taper [1,5]. The center-to-center beam spacing was chosen to produce a 1.5 degree diameter coverage area.

The 71 cm. antennas assume a circular aperture with uniform weighting giving a 3 dB beamwidth of 0.6 degrees in the EHF frequency band. The center-to-center beam spacing is 0.65 degrees for the hexagonal lattice and 0.57 degrees for the square lattice. The 111 cm. antennas assume a circular aperture with Bessel on a 10 dB pedestal weighting, giving a 3 dB beamwidth of 0.45 degrees at EHF. The center-to-center beam spacing is 0.45 degrees for both the hexagonal and square lattice.

The above parameters are listed in Table 1 along with the peak gain (assuming appropriate losses), double and triple / quadruple crossover points, and edge taper. The loss associated with the crossover points are with respect to the peak gain of each configuration. The apertures, weighting, and edge taper are chosen to be characteristic of current and future antenna systems and to produce sidelobe levels that reflect actual experience.

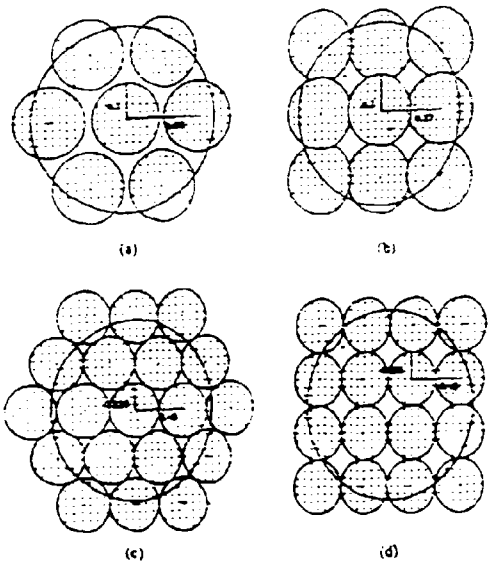

Figure 1. Antenna Configurations
(a) 7-beam hexagonal, (b) 9-beam square
(c) 19-beam hexagonal, (d) 16-beam square

	7 Beam	9 Beam	16 Beam	19 Beam
Aperture Weighting	Circular Uniform	Circular Uniform	Circular Bessel on pedestal	Circular Bessel on pedestal
Diameter	71 cm	71 cm	111 cm	111 cm
3 dB BW	0.60°	0.60°	0.45°	0.45°
Peak gain (dB)	43.6	42.8	46.7	46.0
Beam spacing	0.65°	0.57°	0.45°	0.45°
Double crossover	0.325°, -3.90 dB	0.285°, -2.65 dB	0.225°, -2.96 dB	0.225°, -2.96 dB
Triple/Quadruple crossover	0.375°, -4.78 dB	0.403°, -5.63 dB	0.260°, -4.05 dB	0.318°, -6.53 dB
Edge Taper (dB)	-5	-5	-10	-10

Table 1 Antenna Configurations

antennas is shown in Figure 2. The beams were weighted equally and the beam spacings were chosen to produce a uniform gain over the coverage area. As shown in Figure 2, the gain is fairly uniform out to 0.75 degrees for each of the four cases. The first sidelobe is approximately 25 dB down from peak gain for the 7-beam antenna, 20 dB down for the 9-beam antenna, 35 dB down for the 16-beam antenna and 33 dB down for the 19-beam antenna.

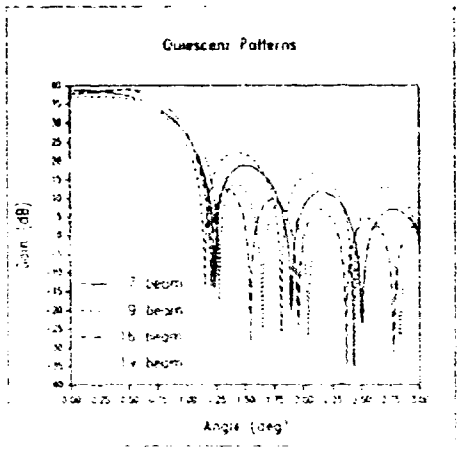

Figure 2 Area coverage quiescent antenna patterns

III Area Coverage

Area coverage performance assumes that the satellite is servicing a user at an unknown location within a specified area. The quiescent pattern consists of all the beams being "on" and equally weighted to produce a uniform coverage over the fixed area.

Three jammer scenarios are considered for the area coverage statistics. The first scenario consists of one mobile jammer within the coverage area. The second scenario consists of one mobile jammer within the coverage area and one fixed jammer outside of the area coverage. The third scenario consists of two mobile jammers within the coverage area and one fixed jammer outside of the coverage area. The mobile jammer signal is assumed to be 15 dB greater than that of the user signal at the receiver; the fixed jammer signal is assumed to be an additional 10 dB stronger. The statistics were generated by randomly selecting ten positions of the mobile jammer(s) within the area coverage. Two additional cases are included in the statistics in which the mobile jammer(s) is located at one of the double and one of the triple/quadruple crossovers to ensure that worst case jammers are properly considered. The addition of these cases may lead to somewhat more conservative results.

The antenna system "cancels" an interfering signal by measuring the incoming signals and adapting the weights applied to each of the elements to place a pattern null in the direction of the undesired source [4]. For an N-beam antenna, the steady state weights W are determined by the N x N correlation matrix C at the antenna elements and the initial pointing (weighting) vector P:

$$W = C^{-1}P$$

where

$$P = [1,1,\ldots,1]$$

Phasing has not been applied to the initial weights. Phasing would reduce the percent area coverage loss due to the narrowing of the null in the desired direction. This effect becomes less pronounced for multiple nulls [3]. System performance was measured by calculating the signal to interference plus noise ratio (SIR) and from that computing the energy per chip divided by the noise ($EChip/N_0$). This value was then compared to a threshold of 12.4 dB which was assumed for link closure.

function of data rate is shown in Figure 3 for each of the four antenna configurations and three jammer scenarios. As shown in this figure, the percent area coverage is a decreasing function of data rate. In the one jammer scenario, for example, the percent area coverage decreases from approximately 97% to 82% as the data rate increases from 1 MChips to 64 MChips for the smaller aperture antenna, and drops from 99% to 91% for the larger aperture antenna. The larger aperture antennas outperform the smaller aperture antennas for each of the three jammer scenarios, and performance for each of the antennas decreases as additional jammers are present. In general, the hexagonal configuration (7-beam, 19-beam) outperforms the comparable square configuration (9-beam, 16-beam), an effect which is more evident as the number of jammers increase.

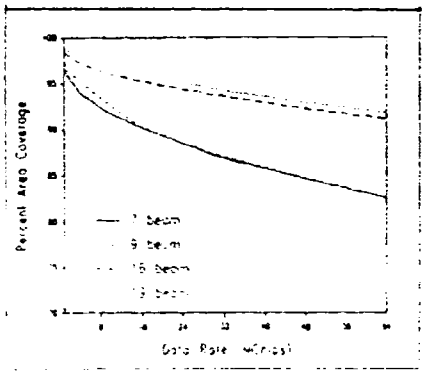

(a)

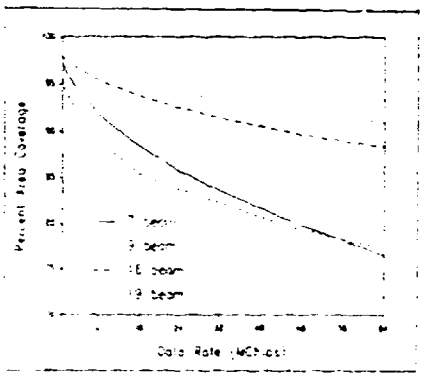

(b)

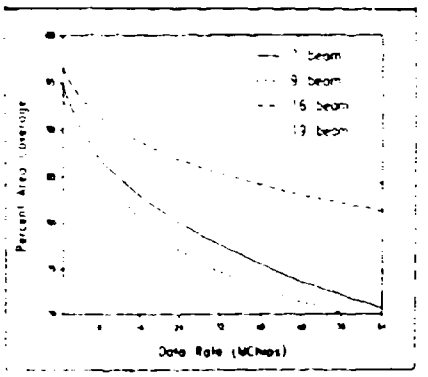

(c)

Figure 3 Coverage area availability for each of the four antennas
(a) One jammer scenario
(b) Two jammer scenario
(c) Three jammer scenario

Table 2 gives the percent area coverage for two important data rates, 8 MChips and 300 MChips, which correspond to multiplexed voice trunking and sensor data trunking. As Table 2 shows, the area coverage availability at the 8 MChips data rate is 92.4% for the 7-beam antenna with one jammer and 86.8% for the three jammer scenario. For the 19-beam antenna, the area coverage availability is 97.1% with one jammer and 92.1% for the three jammer scenario. At the 300 MChips data rate, the 7-beam antenna area coverage availability is 63.3% with one jammer and 53.7% for the three jammer scenario. For the 19-beam antenna, the area coverage availability is 81.0% with one jammer and 70.1% for the three jammer scenario.

Contour plots of SIR as a function of position within the beam are presented in Figure 4 for each of the four antenna configurations. The jammer scenario consists of a mobile jammer at an elevation of 0.12 degrees and an azimuth of 46 degrees and a fixed jammer at a elevation of 0.9 degrees (outside of the coverage area) and an azimuth of 90 degrees. These locations are denoted by an asterisk on each of the plots. The plots are of 1.0 degree radius to show the effects of both jammers.

The 19-beam antenna demonstrates the best performance with distinct nulls clearly placed at both jammer locations. In contrast, the smaller aperture antennas show difficulty resolving the jammers. The 7-beam antenna forms a "null ring" [2] passing through both jammers rather than distinct nulls at the jammers. The area inside the ring is not nulled and thus is available for communication. The null ring represents a deterioration of area coverage. The 9-beam antenna also forms a null ring, but it is narrower than for the 7-beam antenna. However, the area inside the ring is also nulled and thus is not available for communication. The 16-beam antenna produces similar results to the 9-beam antenna but with a further narrowing of the null ring area. Only in the 19-beam case are two distinct nulls produced. The area between the nulls, though of reduced SIR, is available for communication.

% Area Coverage for one jammer scenario

Data Rate	7 Beam	9 Beam	16 Beam	19 Beam
8 MChips	92.4	93.5	96.4	97.1
300 MChips	63.3	61.1	80.7	81.0

% Area Coverage for two jammer scenario

Data Rate	7 Beam	9 Beam	16 Beam	19 Beam
8 MChips	91.9	89.1	95.5	96.4
300 MChips	56.9	55.8	74.9	77.7

% Area Coverage for three jammer scenario

Data Rate	7 Beam	9 Beam	16 Beam	19 Beam
8 MChips	86.8	85.2	91.4	92.1
300 MChips	53.7	50.8	67.9	70.1

Table 2. Coverage area availability for voice multiplex trunking(8 MChips) and sensor trunking (300 MChips)

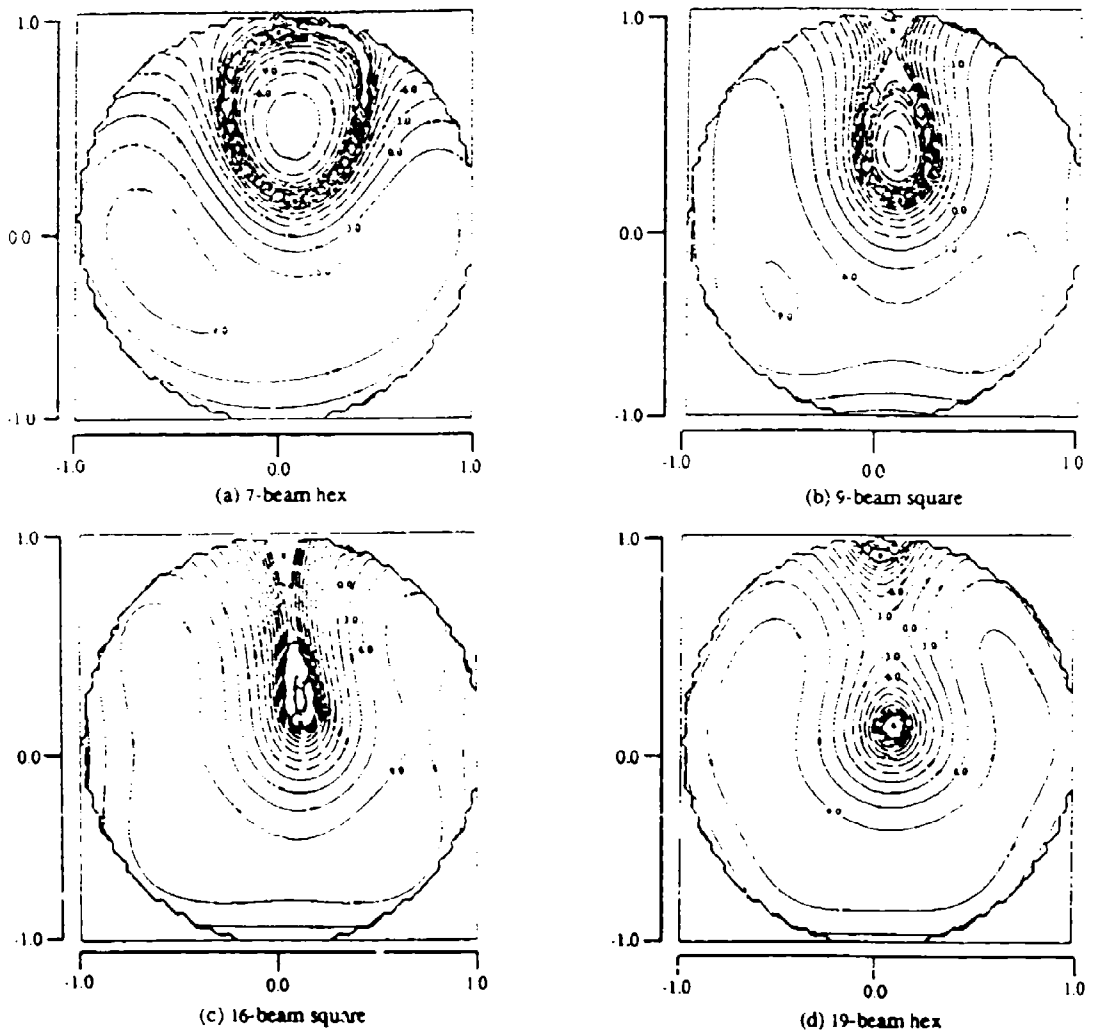

(a) 7-beam hex (b) 9-beam square

(c) 16-beam square (d) 19-beam hex

Figure 4. Contour plots for a two jammer scenario

IV Spot Beam

Spot beam performance assumes that the user location is known within a beam. The steady state weights are calculated as in the area coverage mode, but the initial pointing vector is chosen such that the beam covering the user is weighted unity and all other beams are weighted zero. User / jammer separation resolution is obtained by moving the jammer along a fixed path toward the user and calculating the SIR at each point along the path. As the jammer moves close to the user, the user signal falls into the null. Resolution is then a measure of the signal available from the user when a jammer is located at a given separation angle away from the user. In the following, the dedicated user signal is assumed to be 20 dB greater than that assumed in the area coverage analysis.

Figure 5 displays the SIR as a function of user / jammer separation angle for each of the four antenna configurations. For a typical detector, a SIR of 10 - 15 dB is needed for resolution. At a SIR of 12.5 dB, the separation angle for the 7, 16, 19-beam configurations vary from 0.045 degrees to 0.051 degrees (the 19-beam being best); the separation angle for the 9-beam configuration is 0.074 degrees. As expected, the 16 and 19-beam antenna outperform the 7 and 9-beam antennas at larger separation angles due to the larger aperture. There is no significant difference in performance between the hexagonal and square lattice for the larger aperture antenna, but for the smaller aperture antenna, the 7-beam hexagonal lattice clearly outperforms the 9-beam square lattice.

V. Conclusion

Area coverage and resolution performance were compared for differing GMBA configurations. Hexagonal and square lattices for both a small and a large antenna aperture were considered. The hexagonal lattice produced better area coverage performance than the square lattice for the same size aperture. The hexagonal lattice also produced better resolution performance for the smaller aperture; the resolution performance for the larger aperture was comparable for the two lattice types. The larger aperture antennas produced better performance for both area coverage and resolution than the smaller antenna. The tradeoff in choosing a larger aperture is size and number of feeds which is reflected in added complexity, weight, and cost.

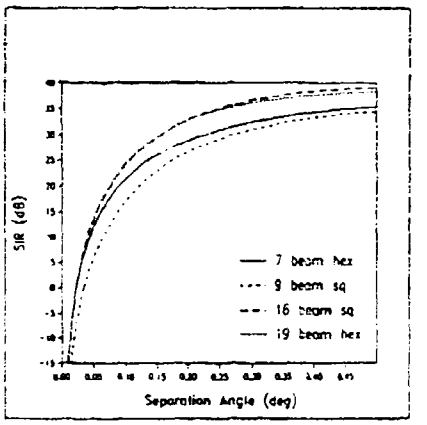

Figure 5. User / jammer resolution

References

[1] Imbriale, William A., et al: Antenna Design and Technology for Satellite Communications", Short Course, IEEE Military Communications Conference, 1984

[2] Mayhan, Joseph T.: "Adaptive antenna design considerations for satellite communication antennas", IEE Proc. Vol. 130 No. 1, Feb 1983

[3] Potts, B.M., Mayhan, J. T., Simmons, A.J.: "Some factors affecting angular resolution in an adaptive antenna", IEEE Conf. on Communication, June 1981

[4] Monzingo, Robert and Miller, Thomas: Introduction to Adaptive Arrays, Wiley & Sons, New York, NY 1980

[5] Ramsay, John F.: "Lambda Functions Describe Antenna /Diffraction Patterns", MICROWAVES, June 1967

Discussion

W.Hoekstra, SHAPE Technical Centre, NL.

I am a bit puzzled by the crossing of the contours in the 19-antenna configuration. Is this caused by the fact that the jammer was located north of the user? In other words, would the rectangular array exhibit the same behaviour if the jammer was turned through 45°?

Author's Reply

Because the antenna is not actually circularly symmetric, there will be some azimuth variation. Although in this case the results were not compared with those for other azimuths, work on other problems suggests that the difference should not be large.

Prof. Ince

Why did you consider MBA rather than phased array?

Author's Reply

Because this was the antenna that was of interest.... It was an antenna design that was being studied for future applications. It was not a matter of looking first at performance in a general sense and then deciding how different antennas were affected: the interest was in looking at MBAs.

PASSIVE DETECTION AND LOCATION OF NOISE JAMMERS

by

Dr E.Briemle
Telefunken System Technik
Sedanstrasse 10, 7900 Ulm
Germany

1. Introduction

Air surveillance by active radars can be obstructed by suitable ECM-measures. In the simplest case, noise jamming signals in the radar frequencies are emitted to disturb the operation of ground based radar.

On the other hand, the various electromagnetic emissions originating from hostile aircraft (ESM- and jamming emissions as well as unintended but unavoidable emission such as acoustic waves, IR, ...) can be used for locating them and thus compensate for lacking radar contributions to the air-picture.

Due to the different nature of these emissions, different technological concepts are necessary. In this paper, we present and discuss the highlights of the concept for a Passive Jammer Locator (PJL) developed at **Telefunken System Technik** in Ulm. At present it is designed to process CW-type jamming signals.

Results of several field trials carried out with an experimental system that was built on the base of this concept are given.

2. Operational Task

Ground based radars are mainly jammed by airborne jammers emitting specific signals in their operating frequencies. PJL-Sensors are designed to respond to this threat by locating the jamming aircraft by measuring and suitably processing the jamming emissions (broad band noise signals).

As passive sensors do not have control over the characteristics of the detected and processed signal, angular strobes are the only spatial information that can possibly be obtained. Actual location of jamming aircraft has to be carried out in a Sensor Fusion Post (SFP) by using simultaneous angular information from at least two sensors. The available strobes are simply intersected, a procedure commonly referred to as "Triangulation". Its principle for the simplest case of one emitter is illustrated in Figure 1.

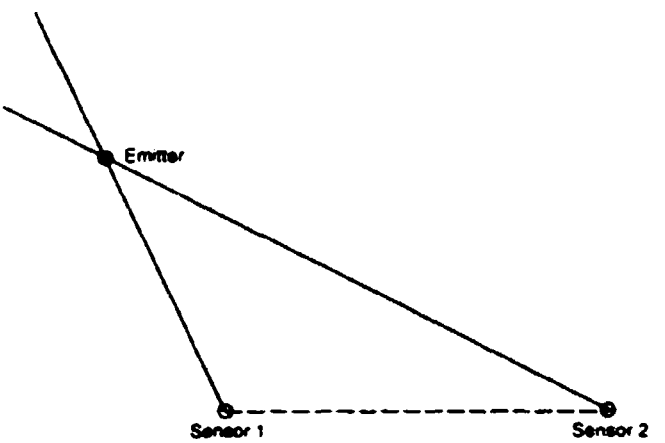

Figure 1 Principle of triangulation

In multiple emitter scenarios, triangulation displays considerable complexity as most of the resulting strobe to strobe intersections do not correspond to actual emitters. They are referred to as Triangulation-Ghosts.

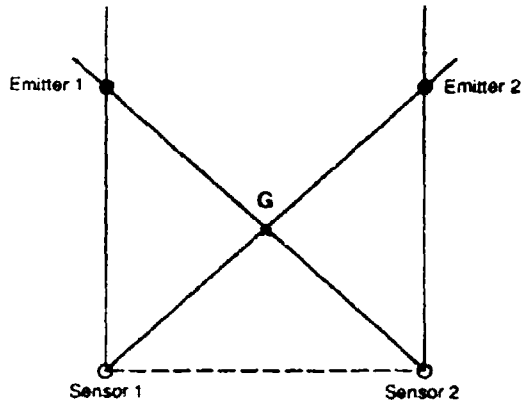

Figure 2 Problem of ghosts:
Intersection G could correspond to an emitter, the outer strobes could result from sidelobes or false alarms

There is usually a variety of combinations of the resulting intersections that could account for a given intersection pattern. The process of distinguishing true emitters from ghosts is called "deghosting". One way to approach it is by observing the kinematic behaviour of all appearing intersections (velocity, acceleration) and then suppressing intersections with nonrealistic motion. This clearly requires high precision of target location along with sufficiently high update-rates for strobe information.

Furthermore, only partial instead of omni spatial coverage, insufficient angular resolution and sidelobes complicate the triangulation procedure as can be seen in the following figures:

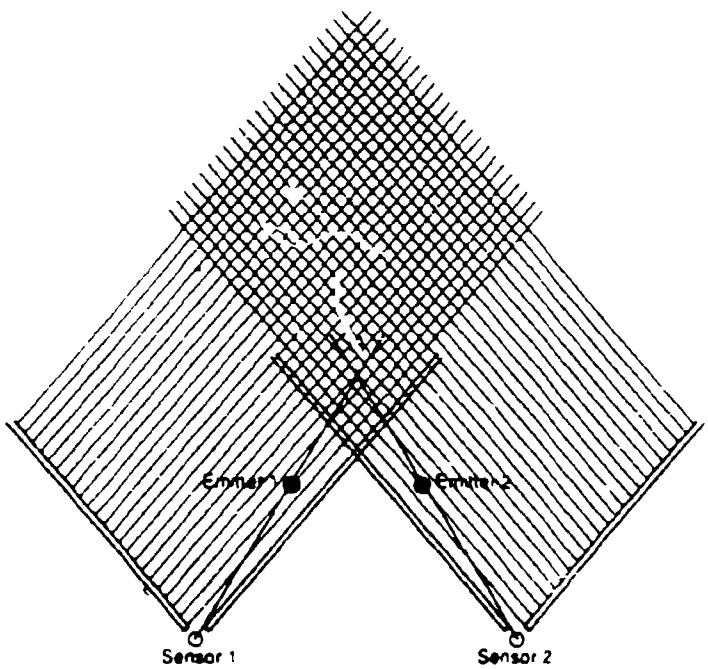

Figure 3 Due to limited spatial coverage of the two sensors, only the ghost is visible

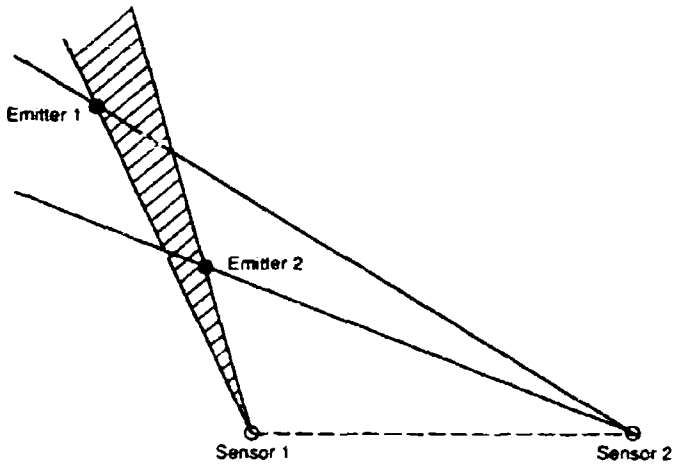

Figure 4 Insufficient resolution and false alarm. Two interpretations are possible:
1. There are two emitters, not resolved by Sensor 2
2. There is only one emitter, Sensor 2 reported a false alarm

We conclude that emitter location has to be precise, complete and unique.

But even when this is the case, kinematic deghosting won't remove all ambiguities. Therefore, additional significant correlation supporting object features (signatures) have to be extracted and reported to the SFP, preferably on request (for narrow band data link), to ensure their complete removal.

We summarize by stating the operational task for PJL-Sensors:

- Detection and location of airborne jammers
  - precise
  - complete
  - unique.
- Extraction of characteristic emitter features to support deghosting.

3. Proposed Concept, Functions and Entities

3.1 *Hardware*

In order to achieve completeness of jammer detection, full (simultaneous) spatial and frequency coverage is necessary.

To meet the former requirement, a circular array antenna is used for spatial sampling of the wavefield. Each element is equipped with a broadband superhet receiver and 2 AD-Converters (for I- and Q-channel) for digital processing of the received data.

The operational frequency range is covered by scanning through it at a rate determined by the needed update-rate.

3.2 *Software*

To ensure uniqueness, high spatial resolution is indispensable. In order to limit the size of receiving aperture (mobility), high resolution signal processing is to be used. Sidelobes should be recognized as well. In addition, an algorithm with high precision target parameter estimation is necessary. For that reason, PTMF algorithms (Parametric Target Model Fitting) are appropriate. Although being rather elaborate, they show high precision performance as the parameters to be estimated (source number, azimuth and elevation angles) appear explicitly in the mathematical description of the underlying signal model.

The best estimates for source number and location are gained by fitting rough initial estimates, extracted from conventional beamforming algorithm, to the measured data in an iterative manner.

Elevation and spectral signal power density, with a frequency resolution given by the scanning stepwidth, can be used as source characteristics to support the deghosting procedure. In addition, an internal strobe number is determined by a strobe tracking algorithm.

3.3 *Configuration and Function*

The major components, their function and their mutual interaction in a passive locating system based on the concept described above are illustrated below.

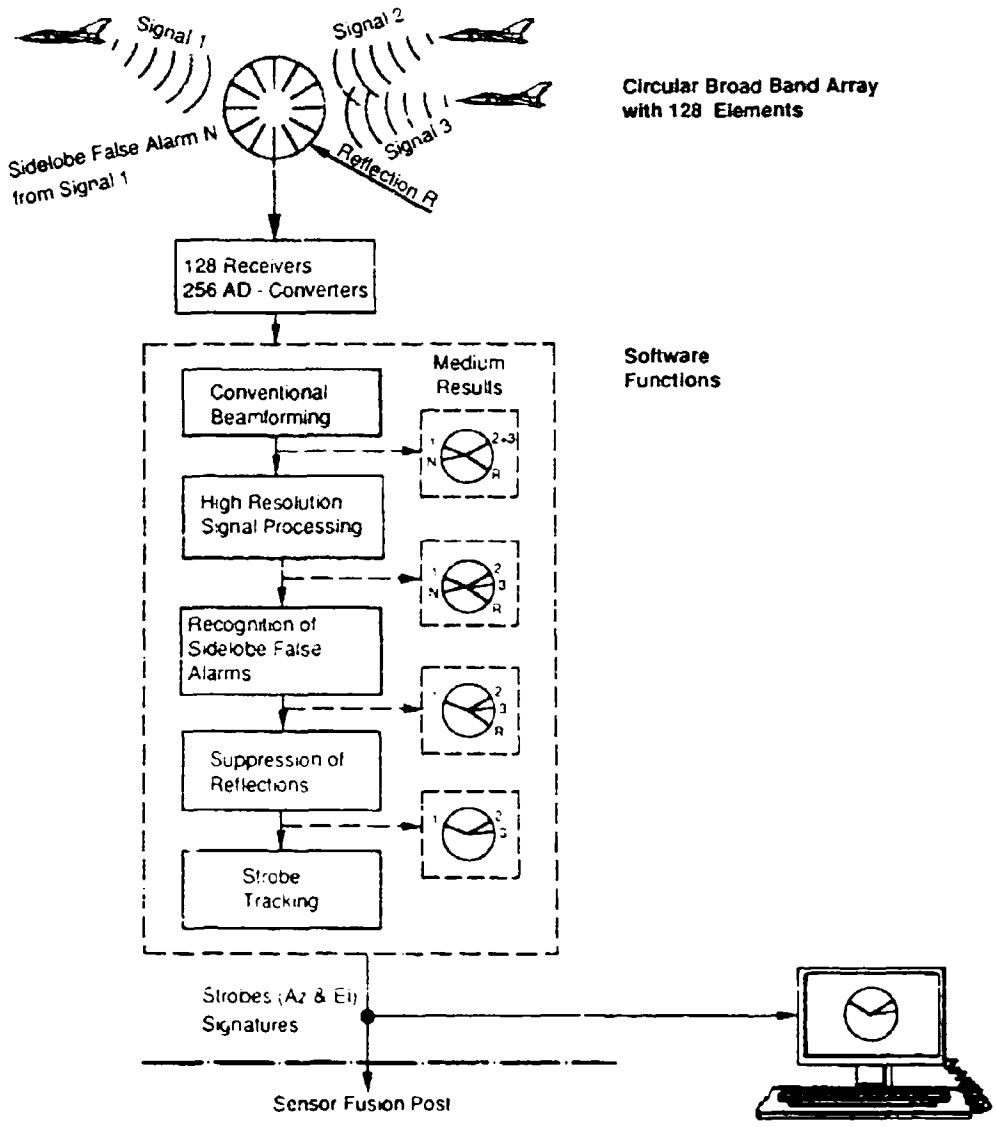

System configuration and functions

4. Features, Advantages and Growth Potential of the Concept

Without further comments, we list the properties, advantages and potential of **MASTER**:

- omnicoverage
- high spatial resolution with small antenna
- high accuracy in azimuth, elevation and power
- high update rate
- few and low sidelobes
- supression of reflexions
- scanning of frequency range (broad band)
- scenario-adaptivity
- extendibility to include ESM-functions
- optimal basis for use of trilateration
- modular configuration possible

5. Description of Experimental System

In 1984, the German BWB initiated and since then supported the development of a PJL-concept and the realization of an experimental sensor, with still limited performance, at Telefunken System Technik in Ulm. It became known under the name **MASTER** which stands for the German "**M**obiles **A**daptives **ST**örer-**ER**kennungssystem" (Mobile Adaptive Jammer Locating System).

In the first phase (until 1987), basic investigations to define the suitable hardware (antenna) and processing units were carried out. Following it, the hardware and software modules were developed and integrated.

The crucial HW-components are shown in the picture below.

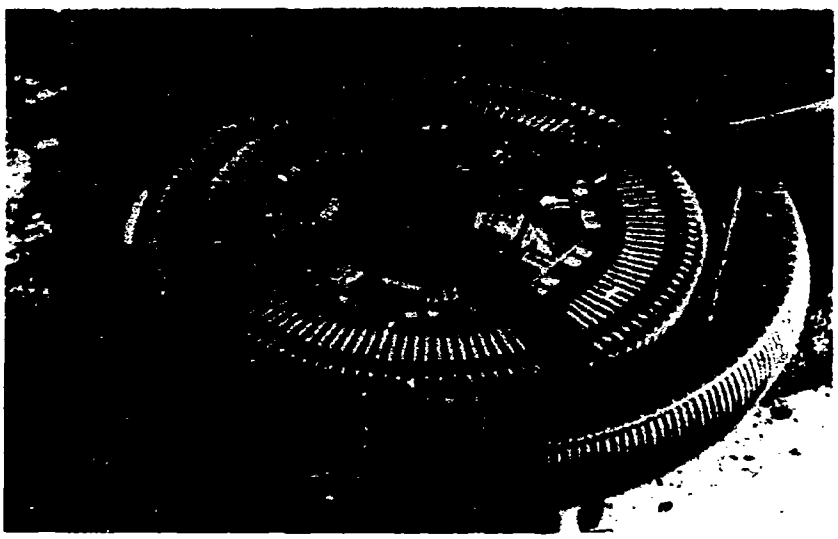

Antenna with receivers and AD-converters

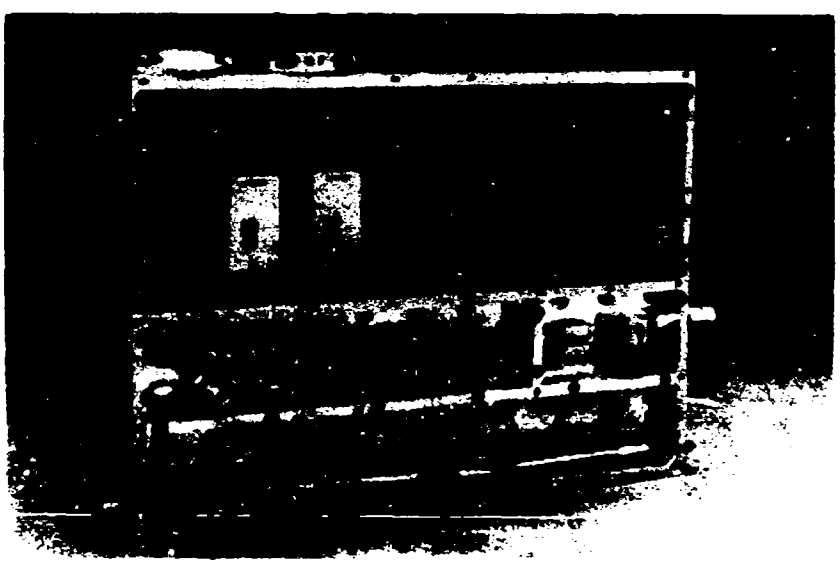

Single receiver and AD-converters

MASTER Experimental System

SW-Modules implemented include:

- SW for calibration of receiver array
- SW for sensor control
- Signal processing including strobe tracking

Sensor operation can be interrupted any time to renew sensor tuning (calibration). This is necessary because "high fidelity" signal detection is required (less than 10 deg phase and 15 percent amplitude deviation between channels) to ensure the desired performance. For that purpose, signal generation and distribution test measurement is incorporated. In the following section we present some results gained by processing the measured data.

6. Results with Experimental System

In order to prove that the required performance can be achieved with the experimental system in a real noise jammer environment, several field trials were carried out with the assistance of the German air force. The jamming aircraft (1-3) were tracked by two ground based radar for reference data: TRML in Ulm and CRC air surveillance radar in Freising.

In all time sections and frequency windows evaluated, resolution performance and accuracy were as expected. Figures 5 and 6 below illustrate the gain in angular resolution by use of superresolution processing of received data during time periods of lengths 15 and 50 minutes respectively. Two aircraft approach the passive sensor, cross each other's path and then turn into a circular pattern.

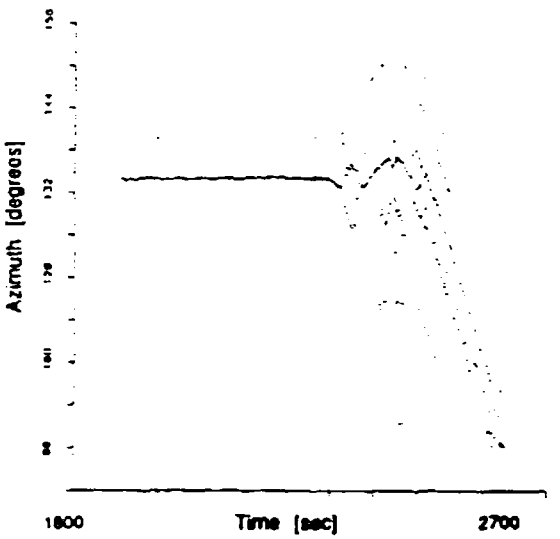

Figure 5a Angular strobes after beamforming

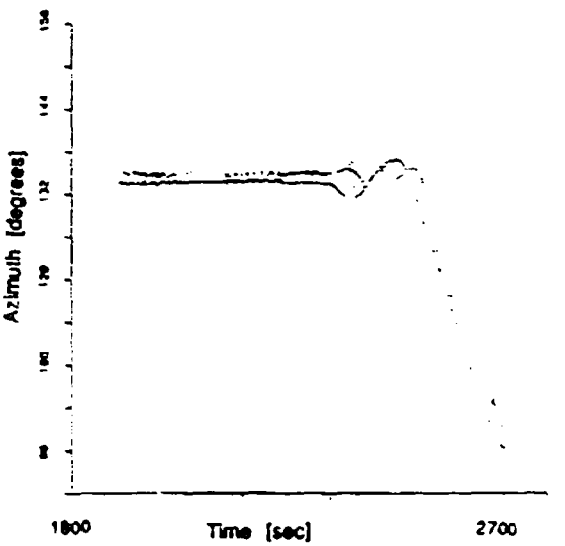

Figure 5b Angular strobes after superresolution

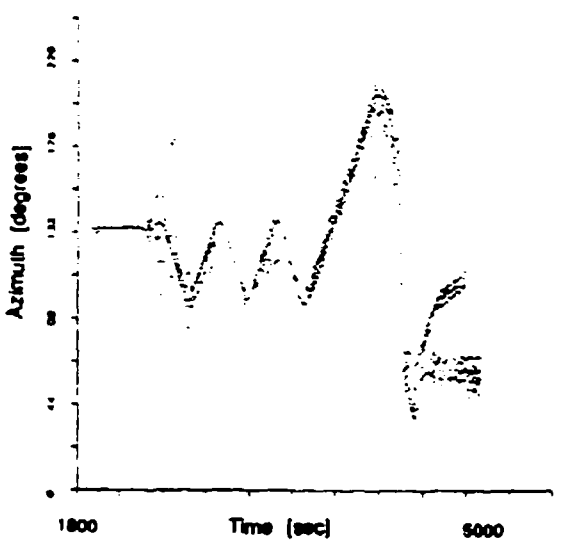

Figure 6a Angular strobes after beamforming

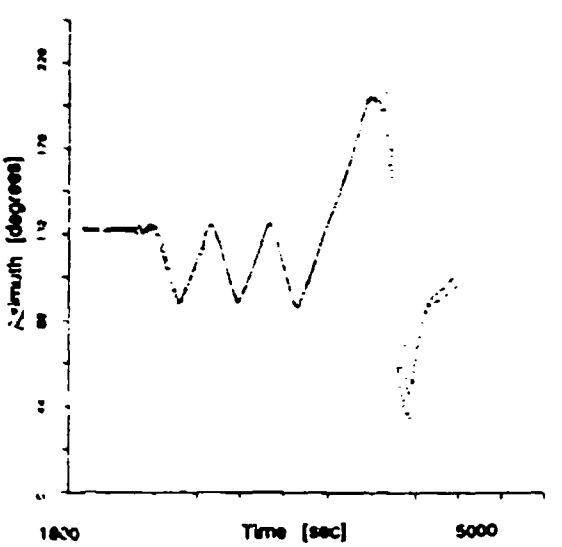

Figure 6b Angular strobes after superresolution

7. Bibliography

(1) U.Nickel: Winkelauflösung eng benachbarter Ziele mit Gruppenantennen (Angular resolution of closely spaced targets with array antenna), FFM-Bericht Nr. 329, 1983

(2) H.B.Driesen, H.J.Davies: Aspects of Jammer Strobe Triangulation, Tracking and Interception, STC-IN-342, 1975

(3) G.van Keuk: Ein Verfahren zur Korrelation von Peilungen vieler Ziele in einem rechnergestützten Triangulierungssystem (A method for correlation of strobes of many targets in a computer supported triangulation system), FFM-Bericht Nr. 307, 1981

(4) R.Baltes, G.van Keuk: Rechnergestütztes Verfahren der Triangulation vieler Ziele (Computer supported triangulation of many targets), VS-Diensterfindung vom 13.11.1987

Discussion

Mr Weis

What is the frequency range of the system?

Author's Reply

The antenna system range is from 2.4 GHz to 6 GHz. But (in the case of) the receivers we (made) to cost, we restricted their frequency range from 2.8 GHz to 3.1 GHz. But we have produced a few – I think three – receivers with the whole frequency range that the antenna is designed for and measured the accuracy of performance in that range for phase and amplitude to confirm that we would reach the same (system) performance (over the full) frequency range.

Mr D.Jennings

What techniques were used to remove jammer reflections and how did you ensure that genuine jammer signals were not inadvertently removed?

Author's Reply

They have different properties. We use the following features to identify reflections:

- They exhibit less motion than jammers
- Their power variation behaviour is different
- They are expected to show significant correlation (complex value) with candidates for reflection.

E.Balboni, Charles Stark Draper Laboratory, US

Please comment on the feasibility of real-time application of this tracking system from a hardware and software viewpoint.

Author's Reply

The operational frequency range is scanned in such a way that every frequency window of interest is processed at the required update rate (1 second). To do this, a reduction by a factor of 10,000 in the processing time is needed. Studies at Telefunken System Technik show that a factor of 1000 can be achieved via array processing and other techniques. The remaining factor of 10 will be achieved through algorithmic simplifications, selective use of high resolution, and exploitation of future processing speeds. Present development shows that this is possible.

A MODULATION QUALITY FACTOR FOR LOW PROBABILITY OF INTERCEPT (LPI) COMMUNICATION SYSTEMS

by

Glenn Prescott*, Lawrence Gutman* and Dan Connolly*
Wright Research and Development Center
Wright-Patterson AFB, Dayton, OH 45433-6543
United States

Abstract

LPI system quality factors were developed in a previous effort [1] in order to provide a quantitative analysis tool for the system engineer to employ in evaluating the effectiveness of LPI techniques in the presence of jammers and intercept receivers. These LPI system quality factors were derived from the system link equations which describe the signal power gains and losses as a function of system link parameters. In this paper, we focus on the issue of LPI modulation by defining the modulation quality factor. The LPI modulation quality factor is a measure of the covertness of a particular type of modulation when detection is attempted by a particular type of intercept receiver. The utility of this quality factor is illustrated by examples and performance curves which demonstrate the concept.

Introduction

A typical LPI scenario is illustrated in Figure 1, representing any situation in which a cooperative transmitter and receiver are targeted by jammers - which disrupt the communications receiver; and intercept receivers - which attempt to detect and exploit the transmitted signal. Since all players are likely to be present in any realistic situation, both the communications receiver and the intercept receiver must be able to function in the presence of jamming.

The purpose of any LPI communication system is to successfully conduct communications between a cooperative transmitter and receiver in such a manner as to minimize the probability of interception by an unauthorized receiver. The communications system is assumed to have a variety of techniques available for reducing the probability of interception. For example, the transmitter may employ steerable high gain antennas and emit a signal with low power density and large time bandwidth product. The communications receiver may have null steering antennas, adaptive interference suppression filters, and employ coherent processing. On the other hand, the intercept receiver has similar available technologies - steerable antennas with low side lobes for eliminating inadvertent (or intentional) jamming, and adaptive filters for excising narrowband interference, for example.

The principle players in the LPI scenario each have critical characteristics which can be easily evaluated and compared. For example, the communications transmitter is characterized by its transmission power, type of modulation and antenna characteristics. The communications receiver characteristics are defined based on some minimum received bit energy per noise power density ratio, E_b/N_o at the receiver input required to provide some acceptable bit error performance, P_e. Antenna gain characteristics, receiver bandwidth and noise figure are also important parameters to be considered.

The adversaries to the transmitter and receiver are the interceptor and jammer, respectively. The intercept receiver is typically a non-coherent energy detector whose performance is established

*Glenn Prescott is with the University of Kansas, Lawrence Gutman and Dan Connolly are with the Wright Research & Development Center, Wright-Patterson AFB, OH

by its probability of detection, P_d and probability of false alarm, P_{fa}. Its performance will also be influenced by intercept antenna characteristics, intercept receiver bandwidth and noise figure. The jammer targets the receiver, therefore the essential parameter in this case is the jammer power spectral density – that is, the amount of power that can be distributed over the operating frequency range of the receiver. Therefore, both power and antenna gain play a major role in determining jammer effectiveness.

We previously analyzed the relationships among these players by performing a simple link analysis [1]. From this link analysis we were able to develop a set of metrics for evaluating the effectiveness of a variety of LPI technologies. We called these metrics the *LPI System Quality Factors*, since they revealed strengths and vulnerabilities, and provided the system designer the insight to determine how to most effectively concentrate system resources.

The Communications/Interceptor Link

The signal power available at both the communications receiver and the intercept receiver is perhaps the most important parameter in determining the performance of the two systems. We naturally assume that there is some performance requirement imposed upon the communications receiver, expressed in terms of bit error probability. This requirement will dictate some minimum required signal energy necessary to provide the specified performance level. The signal power available at the detector input of the communications receiver, S_c can be expressed as:

$$S_c = \frac{P_t G_{tc} G_{ct}}{(4\pi R_c/\lambda)^2 L_c} \qquad (1)$$

In the numerator, P_t is the transmitter power; G_{tc} is the gain of transmitter antenna in the direction of the comm receiver; and G_{ct} is the gain of comm receiver in the direction of the transmitter.

The carrier power available to the intercept receiver is:

$$S_i = \frac{P_t G_{ti} G_{it}}{(4\pi R_i/\lambda)^2 L_i} \qquad (2)$$

G_{it} and G_{ti} account for the gain of the transmitter antenna in the interceptor direction, and the gain of the interceptor receiver in the transmitter direction, respectively. The denominator terms in both expressions represent losses, where $(4\pi R/\lambda)^2$ is free space propagation loss, relatively dependent on the propagations path lengths, R_c and R_i. L_i and L_c account for atmospheric losses due to rain, water vapor and oxygen absorption along each respective path.

LPI System Quality Factors

The relative merit of the LPI system with respect to the interceptor can be observed by comparing the received signal-to-noise ratios at the communications receiver and the intercept receiver [2,3]. S_c/N_{oc} is the signal-to-noise density ratio required to achieve some minimum error performance at the communications receiver, while S_i/N_{oi} is the signal-to-noise density ratio available to the intercept receiver. Taking the ratio of these,

$$\frac{S_c/N_{oc}}{S_i/N_{oi}} = \frac{P_t G_{ct} G_{tc} (4\pi R_i/\lambda)^2 L_i N_i}{P_t G_{it} G_{ti} (4\pi R_c/\lambda)^2 L_c N_c} \qquad (3)$$

Cancelling common terms and rearranging

$$\left(\frac{R_c}{R_i}\right)^2 = \frac{G_{tc} G_{ct}}{G_{ti} G_{it}} \cdot \frac{L_i}{L_c} \cdot \frac{N_i}{N_c} \cdot \frac{S_i/N_{oi}}{S_c/N_{oc}} \qquad (4)$$

Where we define the overall LPI quality factor in terms of R_c and R_i

$$Q_{LPI} = 20 \log\left(\frac{R_c}{R_i}\right) \qquad (5)$$

which indicates that any improvement in LPI effectiveness will either allow the communications system to operate over a longer range, or will require the intercept receiver to move closer to the transmitter in order to achieve some specified level of performance.

We have expressed the link equations in terms of groups of parameters which we previously identified [1] as quality factors relating to the antenna, path loss, interference and modulation. In this paper we will restrict our attention to

the modulation quality factor which is defined in decibels as:

$$Q_{MOD} = 10\log\left(\frac{S_i/N_{oi}}{S_c/N_{oc}}\right) \qquad (6)$$

and for simplicity we can express the modulation quality factor in terms of a ratio of parameters as:

$$\tilde{Q}_M = \frac{S_i/N_{oi}}{S_c/N_{oc}} \qquad (7)$$

The modulation quality factor contains the detectability parameters which describe the quality of communications based upon some acceptable bit error rate P_e, and the performance of the intercept receiver based upon some acceptable probability of detection, P_d and probability of false alarm, P_{fa}. Only the parameters of the signal and the method used to detect the signal are important. Any factors causing the intercept receiver to require a larger signal to noise ratio to achieve a specified performance level increases the modulation quality factor.

The LPI Modulation Quality Factor

The LPI modulation quality factor is seen to be a function of the ratios of the incident signal to noise ratios at the communications receiver and the intercept receiver. In order to use the modulation quality factor to analyze the performance of a particular type of communication signal we need to express S_i/N_{oi} and S_c/N_{oc} in terms of meaningful signal and system parameters.

For the communications receiver, we need to relate S_c/N_{oc} to a performance specification, P_e. We will examine a general class of binary modulation techniques, focusing specifically on direct sequence (pseudonoise) coded BPSK modulation; and on frequency hopped BFSK modulation.

It is well known that for a spread spectrum system operating with some specified processing gain, the input SNR can be expressed as:

$$\frac{S_c}{N_c} = \frac{E_b B_d}{N_{oc} B_i} \qquad (8)$$

where B_d is the data bandwidth, which for binary communications is equal to the bit rate; and B_i/B_d is the spread spectrum processing gain. We can further relate E_b/N_{oc} to the performance of the communication receiver using the following [4]:

$$P_e = Q\left\{\sqrt{\frac{E_b}{N_{oc}}(1-\rho_c)}\right\} \qquad (9)$$

where ρ is the binary symbol correlation coefficient. Solving this equation for E_b/N_{oc} and including the spread spectrum processing gain yields,

$$\frac{S_c}{N_c} = \frac{B_d}{B_i(1-\rho_c)}\left[Q^{-1}(P_e)\right]^2 \qquad (10)$$

For the intercept receiver, we need to relate its performance to the input SNR available from the communication signal. There are numerous models which accomplish this. The model we will use here is attributed to Engler and Howard [5], and it expresses the predetection SNR required to achieve some user specified P_{fa} and P_d,

$$\frac{S_i}{N_i} = \frac{\chi_o + \sqrt{\chi_o^2 + 16T_iB_i\chi_o}}{4T_iB_i}\rho_T\rho_B \qquad (11)$$

where χ_o is the intercept receiver post detection SNR and $\chi_o = \{Q^{-1}(P_{fa}) - Q^{-1}(P_d)\}^2$, and

- B_i - intercept receiver bandwidth
- T_i - intercept receiver integration time
- ρ_T - reciprocal of signal duty cycle
- ρ_B - maximum of $[B_i, B_{si}] \div B_i$

and B_{si} is the signal instantaneous bandwidth.

Finally, combining (8), (10) and (11), we have the expression for the modulation quality factor:

$$\tilde{Q}_M = \frac{\chi_o + \sqrt{\chi_o^2 + 16T_iB_i\chi_o}}{4T_iB_d(E_b/N_{oc})}\rho_T\rho_B \qquad (12)$$

which, for a binary modulation format can be expressed as,

$$\tilde{Q}_M = \frac{\chi_o + \sqrt{\chi_o^2 + 16T_iB_i\chi_o}}{4T_iB_d[Q^{-1}(P_e)]^2}\rho_T\rho_B(1-\rho_c) \qquad (13)$$

We can define the type of modulation being evaluated by selecting the appropriate parameters. For example, the underlying narrowband modulation is selected by choosing ρ_c; where $\rho_c = -1$ is BPSK, and $\rho_c = 0$ is BFSK. Pure PN modulation is indicated by choosing $B_d > B_i$ as shown in (8). Frequency hopping is indicated by choosing the appropriate values of ρ_B and B_i; while time hopping is indicated via ρ_T.

To demonstate the use of the modulation quality factor, Q_{MOD} is plotted versus several parameters of interest. In Figure 2, the modulation quality factor is expressed as a function of the probability of detection for a BPSK system. Figure 3 shows the behavior of the modulation quality factor versus the comm system probability of error. Figures 4 demonstrates the behavior of the modulation quality factor versus communication receiver bandwidth for two different information bandwidths.

Conclusions

The object of defining quality factors for LPI communication systems is to provide a tool for the evaluation of the effectiveness of various LPI techniques. LPI system quality factors were developed in a previous effort. In this paper we have concentrated on defining a modulation quality factor which can be used to evaluate the relative detectability of various types of LPI modulation. The expression for modulation quality factor accounts for the type of modulation, including PN, freqeuncy hopping, and hybrid PN/FH techniques, as well as the type of underlying digital modulation (BPSK and BFSK in the case demonstrated here). The expression given in (13) can be modified to apply to QPSK or any other form of modulation.

References

[1]. Gutman, L. L., and Prescott, G. E., "System Quality Factors for Low Probability of Intercept Communications," *Proceedings of the 1989 International Conference on Systems Engineering*, pp. 475-478, Dayton, Ohio, 24-26 August 1989.

[2]. J. D. Edell, "Wideband, Non-coherent, Frequency-Hopped Waveforms and Their Hybrids in Low-Probability of Intercept Communications," Naval Research Laboratory Report 8025, November 8, 1976.

[3]. Paul Crepeau, "LPI and AJ Modulation Quality Factors," Naval Research Laboratory Report 3436, January 1977.

[4]. Cooper, G. R. and McGillem, C. D., *Modern Communications and Spread Spectrum*, McGraw-Hill Book Co.,1986.

[5]. H. F. Engler, Jr., and D. H. Howard, "A Compendium of Analytic Models for Coherent and Non-coherent Receivers," Air Force Wright Aeronautical Laboratories Technical Report, AFWAL-TR-85-1118, September 1985.

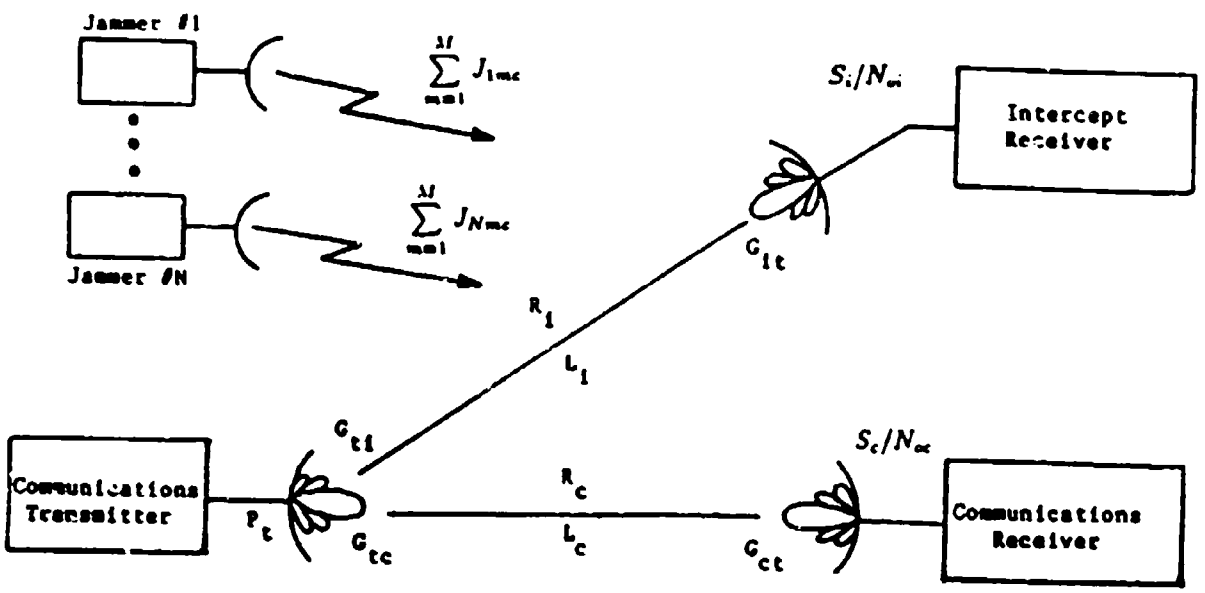

Figure 1 – LPI Scenario

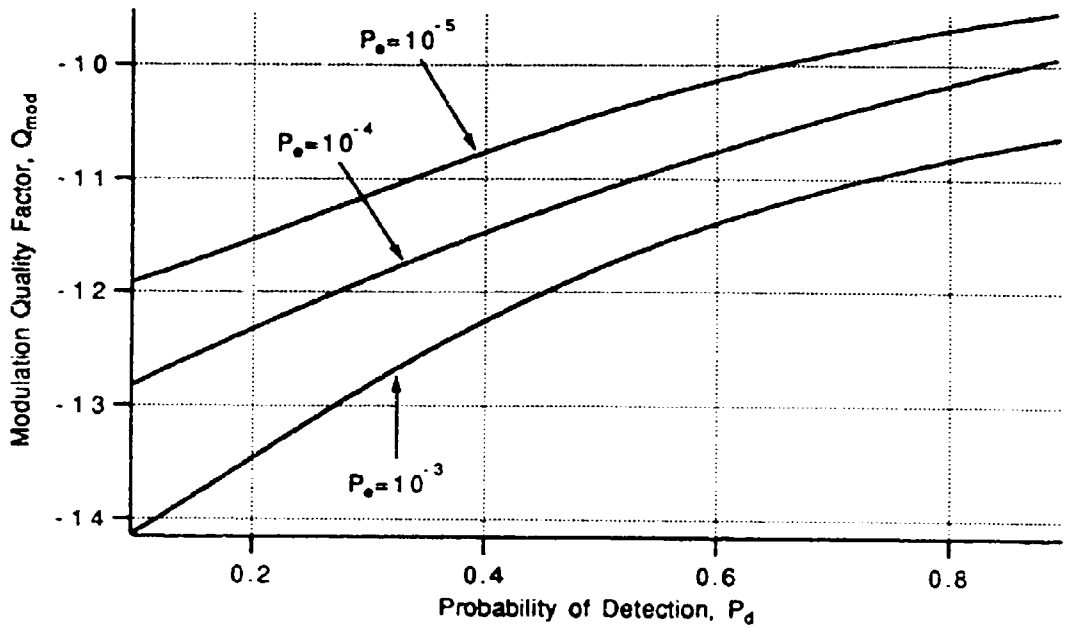

Figure 2 - Q_{mod} with $P_e=10^{-3}$, B_d=10 KHz, B_i=1 MHz, T_i=1 sec.

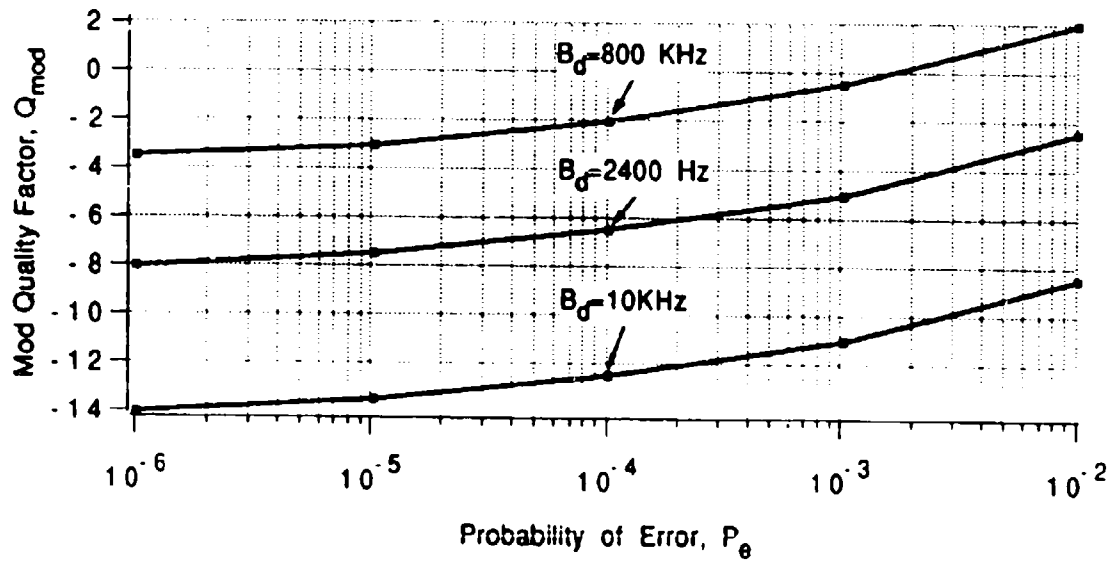

Figure 3 - Q_{mod} versus P_e for P_d=0.5, $P_{fa}=10^{-4}$, $B_c=B_i$=1MHz, T_i=1 sec

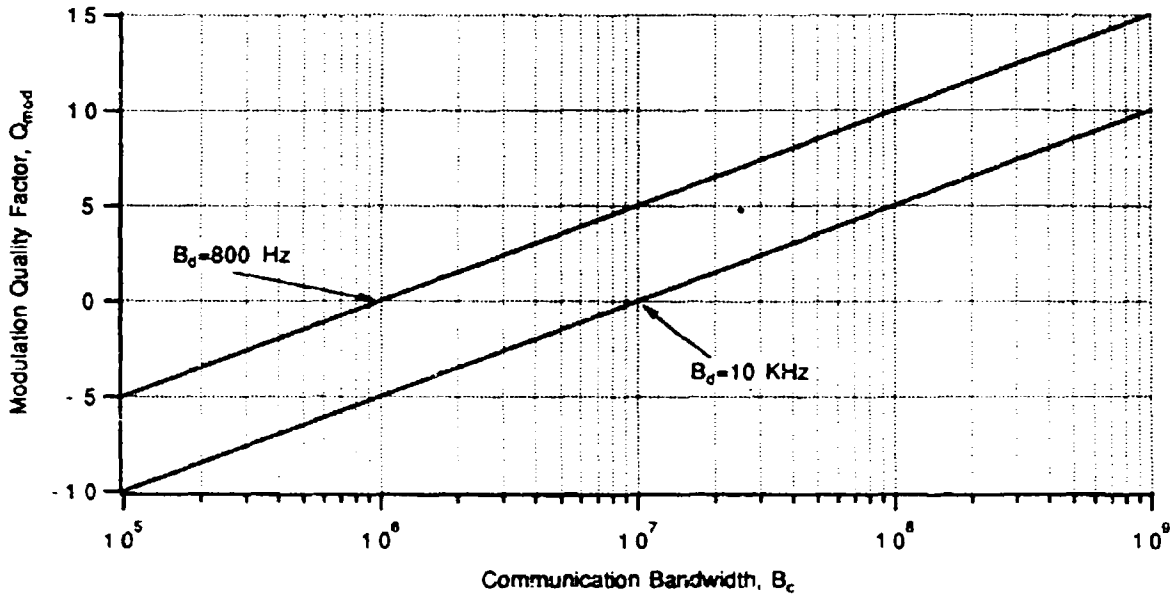

Figure 4 - Q_{mod} versus Comm Bandwidth for P_d=0.5, $P_e = 10^{-3}$, $B_i = B_c$, T_i=1 sec, $P_{fe} = 10^{-4}$

REPORT DOCUMENTATION PAGE

1. Recipient's Reference	2. Originator's Reference	3. Further Reference	4. Security Classification of Document
	AGARD-CP-488	ISBN 92-835-0605-7	UNCLASSIFIED

5. Originator Advisory Group for Aerospace Research and Development
North Atlantic Treaty Organization
7 rue Ancelle, 92200 Neuilly sur Seine, France

6. Title ELECTRONIC COUNTER-COUNTER MEASURES FOR AVIONICS SENSORS AND COMMUNICATION SYSTEMS

7. Presented at the Avionics Panel Symposium held in Ottobrunn, Germany, from 1st to 5th October 1990.

8. Author(s)/Editor(s)	9. Date
Various	February 1991
10. Author's/Editor's Address	**11. Pages**
Various	116

12. Distribution Statement This document is distributed in accordance with AGARD policies and regulations, which are outlined on the Outside Back Covers of all AGARD publications.

13. Keywords/Descriptors

ECCM
Avionics sensors
Communication systems
Electronic counter-counter measures
Jammers
Electronic warfare
Radar
Electronic warfare simulation

14. Abstract

The performance of sensor and communication systems can be limited significantly by hostile Electronic Counter Measures (ECM). These include passive measures such as radar and laser warning receivers, interception, emitter location systems as well as active measures such as jammers in various roles using different techniques and deception devices.

The symposium covered ECCM ranging from frequency agility to spread spectrum and data fusion techniques for both sensor and communications systems.

AGARD Conference Proceedings No.488 Advisory Group for Aerospace Research and Development, NATO ELECTRONIC COUNTER-COUNTER MEASURES FOR AVIONICS SENSORS AND COMMUNICATION SYSTEMS Published February 1991 116 pages The performance of sensor and communication systems can be limited significantly by hostile Electronic Counter Measures (ECM). These include passive measures such as radar and laser warning receivers, interception, emitter location systems as well as active measures such as jammers in various roles using different techniques and deception devices. P.T.O.	AGARD-CP-488 ECCM Avionics sensors Communication systems Electronic counter-counter measures Jammers Electronic warfare Radar Electronic warfare simulation	AGARD Conference Proceedings No.488 Advisory Group for Aerospace Research and Development, NATO ELECTRONIC COUNTER-COUNTER MEASURES FOR AVIONICS SENSORS AND COMMUNICATION SYSTEMS Published February 1991 116 pages The performance of sensor and communication systems can be limited significantly by hostile Electronic Counter Measures (ECM). These include passive measures such as radar and laser warning receivers, interception, emitter location systems as well as active measures such as jammers in various roles using different techniques and deception devices. P.T.O.	AGARD-CP-488 ECCM Avionics sensors Communication systems Electronic counter-counter measures Jammers Electronic warfare Radar Electronic warfare simulation
AGARD Conference Proceedings No.488 Advisory Group for Aerospace Research and Development, NATO ELECTRONIC COUNTER-COUNTER MEASURES FOR AVIONICS SENSORS AND COMMUNICATION SYSTEMS Published February 1991 116 pages The performance of sensor and communication systems can be limited significantly by hostile Electronic Counter Measures (ECM). These include passive measures such as radar and laser warning receivers, interception, emitter location systems as well as active measures such as jammers in various roles using different techniques and deception devices. P.T.O.	AGARD-CP-488 ECCM Avionics sensors Communication systems Electronic counter-counter measures Jammers Electronic warfare Radar Electronic warfare simulation	AGARD Conference Proceedings No.488 Advisory Group for Aerospace Research and Development, NATO ELECTRONIC COUNTER-COUNTER MEASURES FOR AVIONICS SENSORS AND COMMUNICATION SYSTEMS Published February 1991 116 pages The performance of sensor and communication systems can be limited significantly by hostile Electronic Counter Measures (ECM). These include passive measures such as radar and laser warning receivers, interception, emitter location systems as well as active measures such as jammers in various roles using different techniques and deception devices. P.T.O.	AGARD-CP-488 ECCM Avionics sensors Communication systems Electronic counter-counter measures Jammers Electronic warfare Radar Electronic warfare simulation

The symposium covered ECCM ranging from frequency agility to spread spectrum and data fusion techniques for both sensor and communications systems. ISBN 92-835-0605-7	The symposium covered ECCM ranging from frequency agility to spread spectrum and data fusion techniques for both sensor and communications systems. ISBN 92-835-0605-7
The symposium covered ECCM ranging from frequency agility to spread spectrum and data fusion techniques for both sensor and communications systems. ISBN 92-835-0605-7	The symposium covered ECCM ranging from frequency agility to spread spectrum and data fusion techniques for both sensor and communications systems. ISBN 92-835-0605-7

AGARD

NATO OTAN

7 RUE ANCELLE · 92200 NEUILLY-SUR-SEINE

FRANCE

Téléphone (1)47.38.57.00 · Télex 610 176
Télécopie (1)47.38.57.99

DIFFUSION DES PUBLICATIONS
AGARD NON CLASSIFIEES

L'AGARD ne détient pas de stocks de ses publications dans un but de distribution générale à l'adresse ci-dessus. La diffusion initiale des publications de l'AGARD est effectuée auprès des pays membres de cette organisation par l'intermédiaire des Centres Nationaux de Distribution suivants. A l'exception des Etats-Unis, ces centres disposent parfois d'exemplaires additionnels; dans les cas contraire, on peut se procurer ces exemplaires sous forme de microfiches ou de microcopies auprès des Agences de Vente dont la liste suite.

CENTRES DE DIFFUSION NATIONAUX

ALLEMAGNE
Fachinformationszentrum,
Karlsruhe
D-7514 Eggenstein-Leopoldshafen 2

BELGIQUE
Coordonnateur AGARD-VSL
Etat-Major de la Force Aérienne
Quartier Reine Elisabeth
Rue d'Evere, 1140 Bruxelles

CANADA
Directeur du Service des Renseignements Scientifiques
Ministère de la Défense Nationale
Ottawa, Ontario K1A 0K2

DANEMARK
Danish Defence Research Board
Ved Idraetsparken 4
2100 Copenhagen Ø

ESPAGNE
INTA (AGARD Publications)
Pintor Rosales 34
28008 Madrid

ETATS-UNIS
National Aeronautics and Space Administration
Langley Research Center
M/S 180
Hampton, Virginia 23665

FRANCE
O.N.E.R.A. (Direction)
29, Avenue de la Division Leclerc
92320, Châtillon sous Bagneux

GRECE
Hellenic Air Force
Air War College
Scientific and Technical Library
Dekelia Air Force Base
Dekelia, Athens TGA 1010

ISLANDE
Director of Aviation
c/o Flugrad
Reykjavik

ITALIE
Aeronautica Militare
Ufficio del Delegato Nazionale all'AGARD
3 Piazzale Adenauer
00144 Roma EUR

LUXEMBOURG
Voir Belgique

NORVEGE
Norwegian Defence Research Establishment
Attn: Biblioteket
P.O. Box 25
N-2007 Kjeller

PAYS-BAS
Netherlands Delegation to AGARD
National Aerospace Laboratory NLR
Kluyverweg 1
2629 HS Delft

PORTUGAL
Portuguese National Coordinator to AGARD
Gabinete de Estudos e Programas
CLAFA
Base de Alfragide
Alfragide
2700 Amadora

ROYAUME UNI
Defence Research Information Centre
Kentigern House
65 Brown Street
Glasgow G2 8EX

TURQUIE
Milli Savunma Başkanlığı (MSB)
ARGE Daire Başkanlığı (ARGE)
Ankara

LE CENTRE NATIONAL DE DISTRIBUTION DES ETATS-UNIS (NASA) NE DETIENT PAS DE STOCKS DES PUBLICATIONS AGARD ET LES DEMANDES D'EXEMPLAIRES DOIVENT ETRE ADRESSEES DIRECTEMENT AU SERVICE NATIONAL TECHNIQUE DE L'INFORMATION (NTIS) DONT L'ADRESSE SUIT.

AGENCES DE VENTE

National Technical Information Service
(NTIS)
5285 Port Royal Road
Springfield, Virginia 22161
Etats-Unis

ESA/Information Retrieval Service
European Space Agency
10, rue Mario Nikis
75015 Paris
France

The British Library
Document Supply Division
Boston Spa, Wetherby
West Yorkshire LS23 7BQ
Royaume Uni

Les demandes de microfiches ou de photocopies de documents AGARD (y compris les demandes faites auprès du NTIS) doivent comporter la dénomination AGARD, ainsi que le numéro de série de l'AGARD (par exemple AGARD-AG-315). Des informations analogues, telles que le titre et la date de publication sont souhaitables. Veuiller noter qu'il y a lieu de spécifier AGARD-R-nnn et AGARD-AR-nnn lors de la commande de rapports AGARD et des rapports consultatifs AGARD respectivement. Des références bibliographiques complètes ainsi que des résumés des publications AGARD figurent dans les journaux suivants:

Scientifique and Technical Aerospace Reports (STAR)
publié par la NASA Scientific and Technical
Information Division
NASA Headquarters (NTT)
Washington D.C. 20546
Etats-Unis

Government Reports Announcements and Index (GRA&I)
publié par le National Technical Information Service
Springfield
Virginia 22161
Etats-Unis

(accessible également en mode interactif dans la base de données bibliographiques en ligne du NTIS, et sur CD-ROM)

Imprimé par Specialised Printing Services Limited